Afdelingen for Bærende Konstruktioner
Department of Structural Engineering
Danmarks Tekniske Højskole · Technical University of Denmark

Membrane Action Tests of Reinforced Concrete Square Slabs

Chen Ganwei

Bent S. Andreasen

M.P. Nielsen

Serie R No 273 1991

MEMBRANE ACTION TESTS OF REINFORCED CONCRETE SQUARE SLABS

CHEN GANWEI
BENT S. ANDREASEN
M. P. NIELSEN

Membrane Action Tests of Reinforced Concrete Square Slabs

Tryk:
Afdelingen for Bærende Konstruktioner
Danmarks Tekniske Højskole
Lyngby
ISBN 87-7740-074-7

Resumé

Denne rapport beskriver 22 forsøg vedr. kuppelvirkning i armerede betonplader. Pladerne havde såkaldt normal hindring af randenes flytning i vandret plan. Belastningen var to enkeltkræfter.

Forsøgsidéen, prøvelegemerne, materialerne, forsøgsopstillingen, måleinstrumenterne og forsøgsresultaterne beskrives i detaljer. Endelig sammenlignes forsøgsresultaterne med de teoretiske, plastiske løsninger.

Summary

This report describes compressive membrane action tests of 22 reinforced concrete square slabs with normal horizontal restraint and subjected to two concentrated loads.

The test design, the test specimens, the materials, the test set–up, the measuring instruments and the test results are reported in details. The test results are finally compared with the theoretical plastic solutions.

Contents

Notations

a:	Distance
b:	Distance
c_v:	Coefficient of variation
d:	Effective depth for the reinforcement at bottom side
d':	Effective depth for the reinforcement on top side
f_c:	Uniaxial compressive strength of concrete
f_c^*:	Plastic compressive strength of concrete, defined as $f_c^*=\nu f_c$
f_{su}:	Ultimate tensile strength of reinforcement
f_y:	Yield strength of tensile reinforcement
f_y':	Yield strength of compressive reinforcement
$f_{0.2}$:	0.2% offset strength of reinforcement
f_{max}:	Maximum deflection of slab
f_{umax}:	Maximum deflection corresponding to ultimate loads of slab
h:	Depth of slab
m:	Dimensionless moment of slab
m_m:	Dimensionless membrane moment
n:	Number of tests
$\dot{u}$:	Increment of the deflection
x:	Variable length
$\bar{x}$:	Mean value

A_1, A_2: Areas in the "area rule"

A_s: Cross–sectional area of the reinforcement at bottom per unit length

A_s': Cross–sectional area of the reinforcement on top per unit length

H: Horizontal membrane force per unit length

I: Instantaneous center of rotation

M_j: Moment capacity of normal slab, defined as $M_j=\phi(\frac{d}{h}-\frac{\phi}{2\nu_b})\cdot h^2 f_c$

M_{jm}: Moment, the sum of M_j and M_m

M_j': Moment capacity of compressive reinforcement, defined as $M_j'=\phi'(\frac{d'}{h}-\frac{\phi'}{2\nu_b})\cdot h^2 f_c$

M_m: Membrane moment, defined as $M_m=m_m h^2 \nu_m f_c$

P: Concentrated load

P_u: Ultimate concentrated load in test

P_{theory}: Theoretical concentrated load

S: Work parameter

T_m: Total membrane tensile forces at surroundings

T_{um}: Ultimate total membrane forces at surroundings

W_e: External work

W_i: Internal work

γ: Relative effective depth for the bottom reinforcement, $\gamma=d/h$

γ': Relative effective depth for the top reinforcement, $\gamma'=d'/h$

δ: Relative deflection, $\delta=f_{umax}/h$

δ': parameter, $\delta'=\delta/k$

κ: Load and geometrical factor

λ: Slenderness of slab

ν: Effectiveness factor

ν_b: Effectiveness factor for bending

ν_m: Effectiveness factor for membrane action

ξ: Compressive zone depth factor

ρ: Reinforcement ratio, $\rho = As/h$

σ: Standard deviation

ϕ: Mechanical degree of bottom reinforcement, $\phi = \frac{A_s f_y}{h f_c}$

ϕ^*: Effective mechanical degree of bottom reinforcement, $\phi^* = \phi/\nu_b$

ϕ': Mechanical degree of top reinforcement, $\phi' = \frac{A'_s f'_y}{h f_c}$,

$\phi^{*\prime}$: Effective mechanical degree of top reinforcement, $\phi^{*\prime} = \phi'/\nu_b$

Introduction

It has been well–known that due to arch or dome action, the ultimate flexural capacity of a horizontally restrained concrete slab may be calculated by the classical yield line methods.

In the literature, most of the membrane action tests have been done with uniform or almost uniform load. Flexural tests of two–way reinforced concrete slabs with normal restraint and subjected to concentrated loads have not been carried out yet, as far as it is known.

This report describes compressive membrane action tests of 22 reinforced concrete square slabs with the so–called normal horizontal restraint, i.e., a restraint met for instance in slab systems, where the internal slabs are surrounded by the neighbour slabs. This restraint does not fully prevent horizontal displacements, but can still offer a significant resistance to the displacement. The test slabs are subjected to two concentrated loads.

The test slabs were carried out in the Structural Research Laboratory of Technical University of Denmark, in 1988. The project was accomplished under grants to Professor M. P. Nielsen sponsored by the Danish Council for Scientific and Technical Research (STVF).

The main purpose of these tests is to provide information for the effects of various parameters such as concrete strength, reinforcement percentage and loading position on the compressive membrane behavior and load carrying capacity of two–way reinforced concrete slabs with normal restraint and subjected to two concentrated loads.

The report analyzes the tests in general. In addition, the test design, the specimens, the materials, the test set–up, the measuring instruments and the test results are also stateded in details.

The test results are compared with the theoretical plastic solutions firstly derived and proposed by Bent Andreasen and M. P. Nielsen [86.1].

Chapter 1. Theoretical Background

The theoretical solutions based on the theory of plasticity are derived in this chapter. The expressions of the theoretical solutions are the same as those found by Bent Andreasen and M. P. Nielsen for rectangular slabs with horizontal restraints at all edges and subjected to uniform loads [86.1]. Only the expressions for the load and the geometrical factor κ are different.

1.1 Basic Assumptions

The theory of plasticity is applied. The concrete is assumed to be a rigid plastic material. The yield condition for concrete is taken to be the modified Coulomb failure criterion with a zero tension cut–off.

The well–known fact that the concrete is not perfectly plastic is taken into account by reducing the uniaxial compression strength f_c by means of the effectiveness factor ν, where $\nu \leq 1.0$.

The reinforcement is assumed to be rigid–plastic with the yield stress f_y. Reinforcement bars are assumed to carry only stresses in their longitudinal direction, i.e., dowel effects are neglected.

It is certainly assumed that punching failure does not occur before final failure. Concerning the "area rule" which is a part of Calladine's method, the reader is referred to Calladine [68.1], Bent Andreasen and M. P. Nielsen [86.1].

1.2 Solutions for Reinforced Concrete Square Slabs with Horizontal Restraints at All Edges and Subjected to Two Concentrated Loads.

The slab and the used yield line pattern are shown in Fig. 1.1.

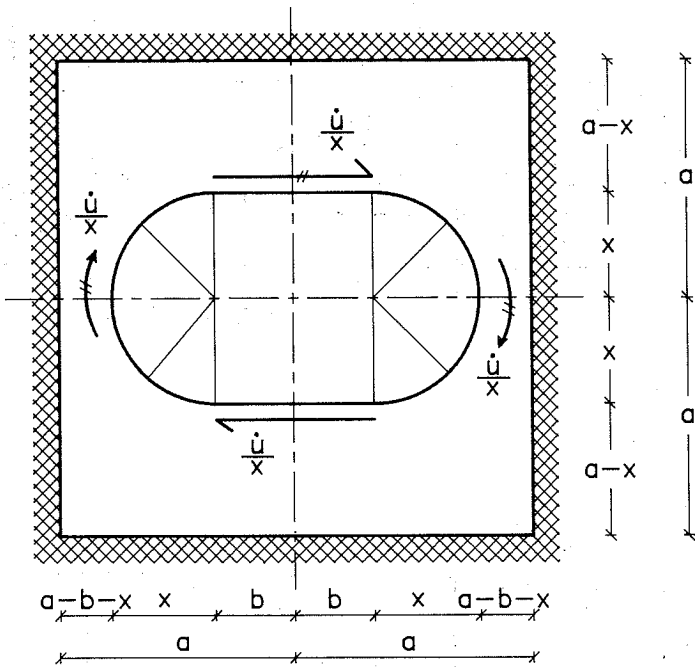

Figure 1.1 Square slab with horizontal restraints along all edges and subjected to two concentrated loads.

The cross sections in one quarter of the yield lines are shown in Fig. 1.2.

The internal and external work can then be written as

$$W_i = 4S \cdot f_c^* \tag{1.1}$$

$$W_e = 2P \cdot \dot{u} \tag{1.2}$$

Here, S is the work from one quarter of the cross section.

a.) Small deflection

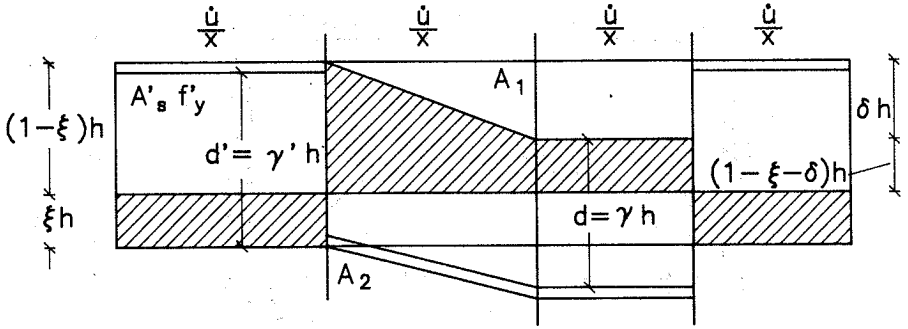

b.) Large deflection

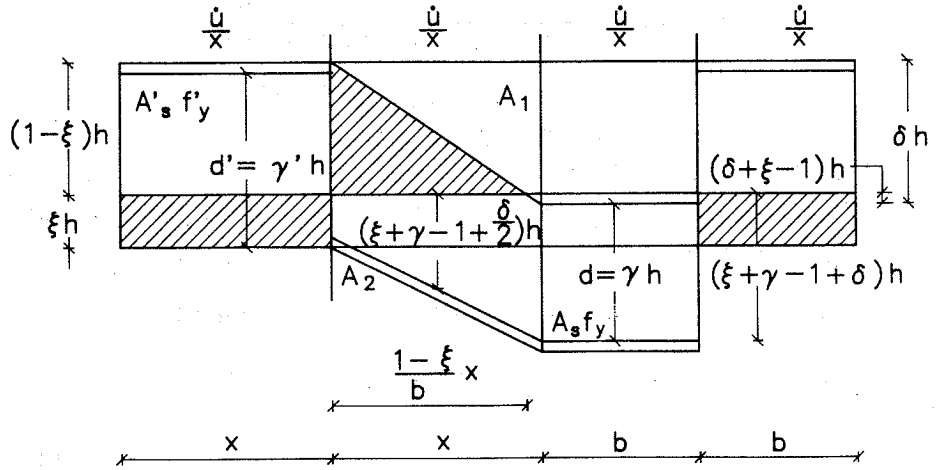

Figure 1.2 Cross sections in one quarter of the yield lines of a deflected square slab for a small and a large deflection, respectively.

Using the upper bound theorem, the total dimensionless load carrying capacity can be written as

$$\frac{2P}{h^2 f_c^*} = \frac{4S}{\dot{u}h^2} \tag{1.3}$$

The expression for S in the slab with a small deflection is given first.

The areas A_1 and A_2 in the area rule are

$$A_1 = h\cdot\left[\frac{\pi}{2}\cdot x\cdot[(1-\xi-\delta)+\frac{\delta}{2}+\phi^{*'}]+b[(1-\xi-\delta)+\phi^{*'}]\right] \tag{1.4}$$

$$A_2 = h\cdot\{\frac{\pi}{2}\cdot x\cdot[\xi+\phi^*]+b[\xi+\phi^*]\} \tag{1.5}$$

Using the area rule, ξ can be found to be

$$\xi = \frac{1}{2}[1-(\phi^*-\phi^{*'})-\frac{\delta}{2}(2-\kappa)] \tag{1.6}$$

Here,

$$\kappa = \frac{\frac{\pi}{2}\cdot x}{b+\frac{\pi}{2}\cdot x} = \frac{1}{1+\frac{2b}{\pi x}} \tag{1.7}$$

The work parameter S can be written

$$S = \frac{\dot{u}}{x}\cdot\frac{h^2}{2}\{\frac{\pi x}{2}[\xi^2+(1-\xi-\delta)^2+\delta(1-\xi-\frac{2}{3}\delta)+2\phi^*(\gamma'-\xi)+2\phi^*(\gamma-$$
$$(1-\xi-\frac{\delta}{2}))]+b[\xi^2+(1-\xi-\delta)^2+2\phi^{*'}(\gamma'-\xi)+2\phi^*[\gamma-(1-\xi)-\delta)]]\} \tag{1.8}$$

The condition for the equations above to be valid is

$$1-\xi-\delta \geq 0 \tag{1.9}$$

It gives rise to the condition

$$\delta < \frac{2}{2+\kappa}[\,1 + (\phi^{*} - \phi^{*\prime})\,] \tag{1.10}$$

If equation (1.10) can not be satisfied, the large deflection solution must be used. ξ in this case is determined by

$$\xi = 1 + \delta' - \sqrt{\delta'[\delta' + 2 + 2(\phi^{*} - \phi^{*})]} \tag{1.11}$$

where,

$$\delta' = \delta/\kappa \tag{1.12}$$

The work parameter S for a large deflection is given by

$$S = \frac{\dot{u}}{x}\cdot\frac{h^2}{2}\Big\{ \frac{\pi x}{2}[\xi^2 + \frac{1}{3}\frac{(1-\xi)^3}{\delta} + 2\phi^{*\prime}(\gamma' - \xi) + 2\phi^{*}(\gamma + \xi + \frac{\delta}{2} - 1)] +$$

$$b[\xi^2 + 2\phi^{*\prime}(\gamma' - \xi) + 2\phi^{*}(\gamma + \xi + \delta - 1)]\Big\} \tag{1.13}$$

Inserting (1.6) into (1.8), (1.11) into (1.13) and these expressions for S into (1.3), the total load carrying capacity can be found as

$$\frac{2P}{h^2 f_c^{*}} = \frac{2\pi}{\kappa}(m + m_m) = \frac{2\pi}{1 + \frac{2b}{\pi x}}(m + m_m) \tag{1.14}$$

where for $\delta \le \frac{2}{2+\kappa}[1 + (\phi^{*} - \phi^{*\prime})]$

$$m = \phi^{*}(\gamma - \frac{\phi^{*}}{2}) + \phi^{*\prime}(\gamma' - \frac{\phi^{*\prime}}{2}) \tag{1.15}$$

$$m_m = \frac{1}{4}[\,1 - (2-\kappa)\delta + \frac{1}{12}(12 - 4\kappa - 3\kappa^2)\delta^2\,] + \frac{1}{2}\phi^{*}\cdot\phi^{*\prime} +$$

$$\frac{\delta}{4}(2-\kappa)(\phi^{*}+\phi^{*'})-\frac{\phi^{*}}{2}(1-\frac{\phi^{*}}{2})-\frac{\phi^{*'}}{2}(1-\frac{\phi^{*'}}{2}) \tag{1.16}$$

and for $\delta > \frac{2}{2+\kappa}[1+(\phi^{*}-\phi^{*'})]$

$$m=\phi^{*}(\gamma-\frac{\phi^{*}}{2})+\phi^{*'}(\gamma'-\frac{\phi^{*'}}{2}) \tag{1.17}$$

$$m_m=\frac{1}{6}(3+6\delta'+2\delta'^{2})-\frac{1}{3}\sqrt{\delta'[\delta'+2+2(\phi^{*}-\phi^{*'})]^{3}}+\frac{1}{2}(\phi^{*2}+\phi^{*'2})$$

$$+\frac{1}{2}\{\phi^{*}[2+\kappa(2-\kappa)]\delta'-2\phi^{*'}(1+\delta')]\} \tag{1.18}$$

Here, m is the normal ultimate bending moment and m_m stands for the so–called membrane moment.

For concrete slabs without reinforcement, the theoretical solutions of the load carrying capacity are much simpler. They may be found inserting $\phi^{*}=\phi^{*'}=0$ into the above equations. We find for

$$\delta \le \frac{2}{2+\kappa} \tag{1.19}$$

$$m_m=\frac{1}{4}[1-(2-\kappa)\delta+\frac{1}{12}(12-4\kappa-3\kappa^{2})\delta^{2}] \tag{1.20}$$

and for

$$\delta > \frac{2}{2+\kappa} \tag{1.21}$$

$$m_m=\frac{1}{6}(3+6\delta'+2\delta'^{2})-\frac{1}{3}\sqrt{\sigma'(\sigma'+2)^{3}} \tag{1.22}$$

The load carrying capacity is a function of the variable parameter x. For the simple case of a plain concrete slab, it is easy to find that

$$\frac{\partial\left[\frac{2P}{h^2 f_c^*}\right]}{\partial x} < 0$$

for both the small deflection and the large deflection cases.

The lowest upper bound can be reached only when x takes the possibly largest value, i.e.

$$x = a - b \tag{1.23}$$

Inserting equation (1.23) into (1.7), we get

$$\kappa = \frac{1}{1 + \frac{2b}{\pi(a - b)}} \tag{1.24}$$

The yield line pattern and the moment factor $\frac{2\pi}{\kappa}$ are the same as found by a normal yield line calculation.

For slabs with reinforcement, the theoretically minimizing the equations with respect to x is possible, but the expressions obtained are rather complicated. It has been found that in normal cases of reinforced concrete slabs, the lowest upper bound will be reached only when x takes the possibly largest value, just as those of plain concrete slabs. For slabs with normal reinforcement degrees, equation (1.24) is a theoretically correct solution.

In Fig. 1.3, the dimensionless membrane moment m_m is plotted against the relative maximum deflection δ in slabs for differemt values of the effective mechanical reinforcement degree ϕ^*, while in Fig. 1.4, the curves of dimensionless total moment capacity ($m+m_m$) versus δ for different ϕ^* are shown.

The relationships between the dimensionless total moment capacity ($m+m_m$) and ϕ^* are depicted for different values of δ in Fig. 1.5.

These figures are plotted for the parameter $\kappa=\frac{\pi}{\pi+1}$, i.e., the distance between the two concentrated loads is one third of the span and for $\phi^{*'}=0$.

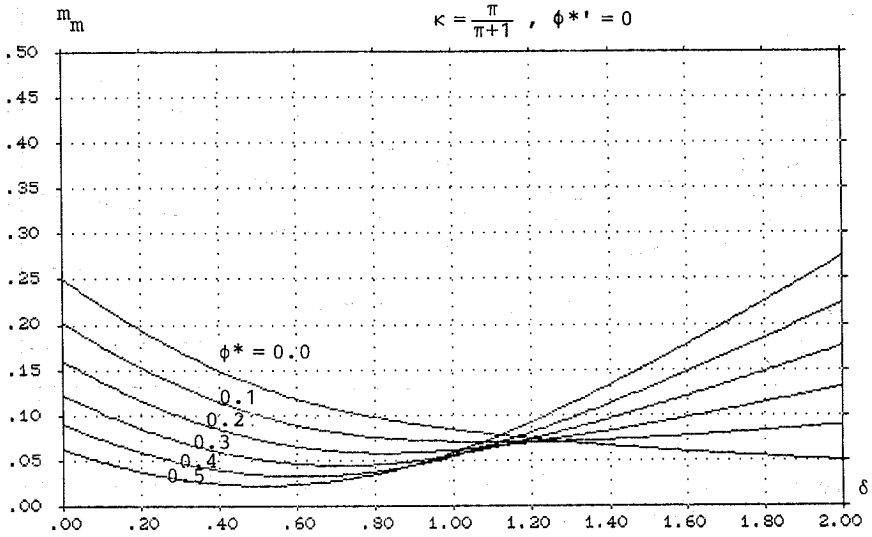

Figure 1.3 Membrane moment versus relative deflection for various reinforcement degrees.

From these three figures, it appears that the membrane moment m_m is decreasing with increasing value of ϕ^* in the important part of the δ region, while the total moment capacity $(m+m_m)$ is increasing with increasing values of ϕ^*. It must also be noticed that in the practical range, i.e. for relatively small reinforcement degrees ϕ^*, both the membrane moment m_m and the total moment $(m+m_m)$ have a flat part in the curves for δ lying between 0.7 and 1.50.

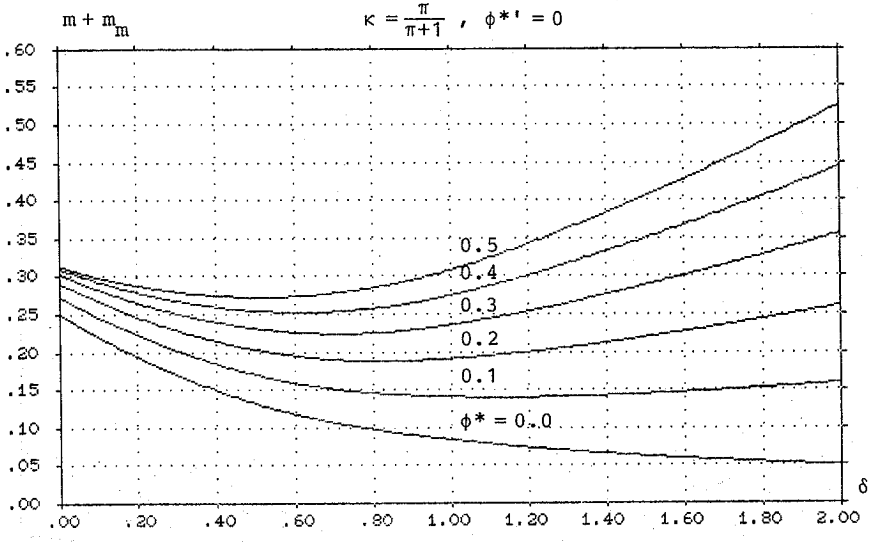

Figure 1.4 The total moment capacity versus relative deflection for various reinforcement degrees.

Based on the analysis above, we may simplify the complicated theoretical solutions for relatively small reinforcement degrees by putting the dimentionless membrane moment at a constant value, say 0.11. The calculation of moment carrying capacity of reinforced concrete slabs with membrane action is then carried out as a normal yield line calculation. The yield line pattern is determined for a slab without membrane action. When the yield line pattern is found, the positive bending moment M_j is replaced by M_{jm}, the sum of the positive bending moment M_j and the membrane moment M_m, $M_{jm}=M_j+M_m$. The sum M_{jm} is used everywhere in the expressions for the load carrying capacity where M_j is placed. The normal negative bending moment, M_j', is unchanged.

The moments are given by

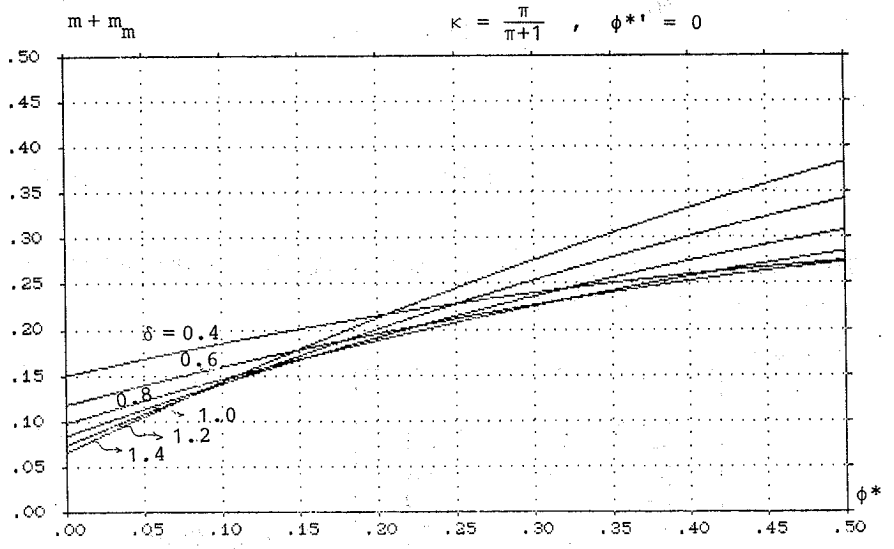

Figure 1.5 Total moment capacity versus reinforcement degree for various relative deflections.

$$M_{jm} = M_j + M_m \tag{1.25}$$

$$M_j = \phi(\frac{d}{h} - \frac{\phi}{2\nu_b}) \cdot h^2 f_c \tag{1.26}$$

$$M_m = 0.11 \nu_m h^2 f_c \tag{1.27}$$

$$M_j' = \phi'(\frac{d'}{h} - \frac{\phi'}{2\nu_b}) \cdot h^2 f_c \tag{1.28}$$

The effectiveness factors ν_b and ν_m can be determined by

$$\nu_b = 0.97 - \frac{f_c}{300} - \frac{f_y}{5000} \qquad \text{for} \begin{cases} f_y < 900 \text{ MPa} \\ f_c < 60 \text{ MPa} \end{cases} \tag{1.29}$$

and

$$\nu_m = \frac{2}{\sqrt{f_c}} \qquad (f_c \text{ in MPa}) \tag{1.30}$$

The surroundings, which provide the restraints to the slab, are subjected to the horizontal forces from the slab, see Fig. 1.6.

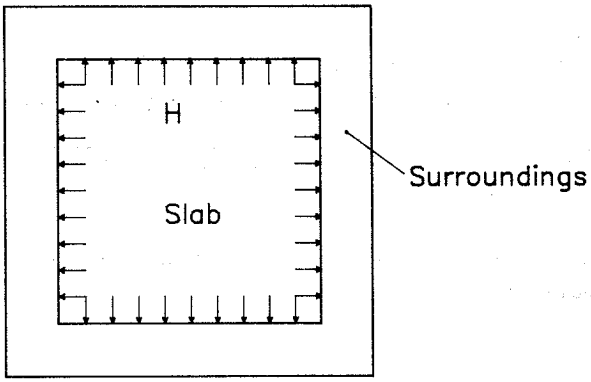

Figure 1.6 Forces on surroundings from a slab with membrane action.

If we want to utilize the membrane action to enhance the bending carrying capacity of the slab, we must control the surroundings to make sure that they can offer such a restraint.

The horizontal membrane line load H per unit length can be determined by

$$H = \xi h \cdot \nu_m f_c$$

Here, the relative compression zone, ξ, is determined by equations (1.6) and (1.11).

The theoretical relations for ξ versus δ for different ϕ^* values are shown in Fig. 1.7 and 1.8.

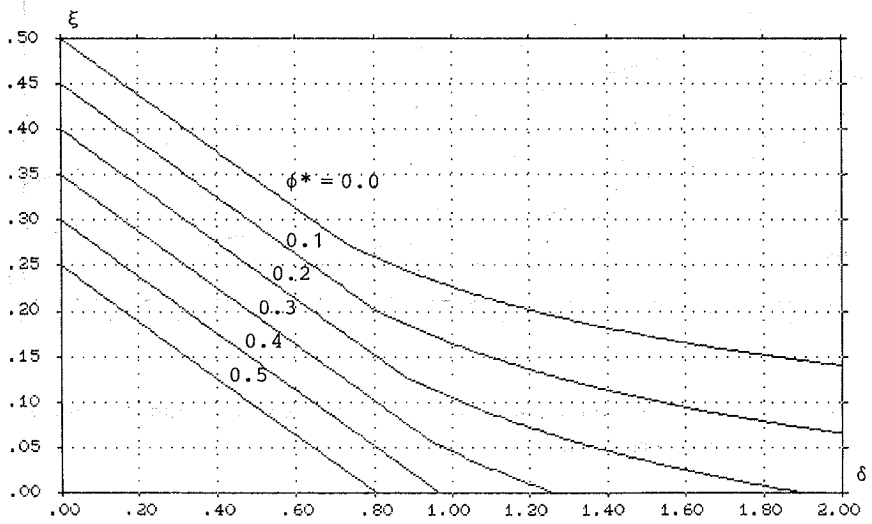

Figure 1.7 The relative compression zone versus the relative deflection for various reinforcement degrees.

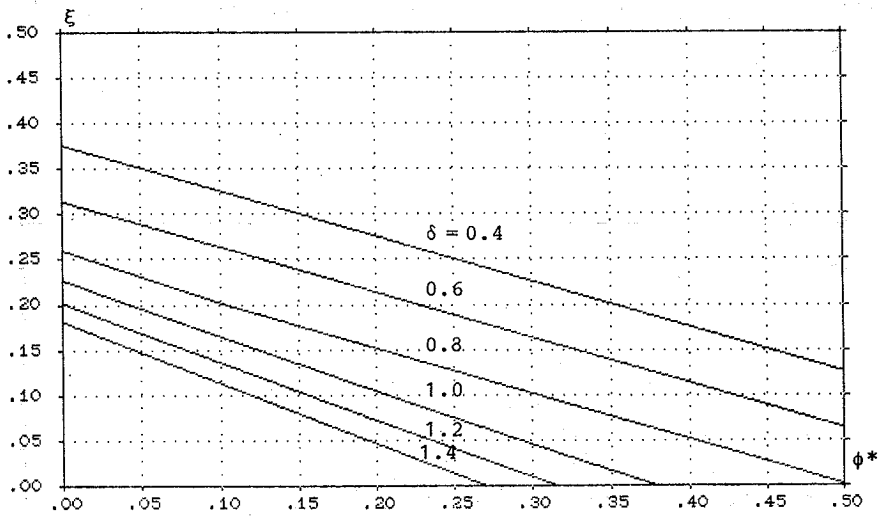

Figure 1.8 Relative compression zone depth versus reinforcement degree for various relative deflections.

Chapter 2. Test Plan

The main object of the tests, the geometrical forms of the test specimens and the test program are given in this chapter.

2.1 Main Object

The tests are conducted to provide information for the effects of various parameters such as concrete strength, reinforcement percentage, loading position on the

compressive membrane behavior and bending carrying capacity of two way orthogonally reinforced concrete slabs with normal lateral restraint and subjected to two concentrated loads.

2.2 Test Specimen

As shown in Fig. 2.1, all tested slabs were 1900 × 1900 × 60mm with effective span 1800 mm. The span / thickness ratio was 30. In order to get a bending failure, all slabs had continuous same amount of reinforcement on the bottom faces in both directions, however, none of the slabs had stirrups. For transportation purpose, four hangers were placed near the corners. The cover was 10 mm. In order to fix the reinforcement grid in a plywood mould, plastic tongs with 10 mm net height was used.

2.3 Test Program

The total number of tests carried out in this project is 22, which has been divided into 3 groups according to the different reinforcements. Group 1 has 3 tests with $\phi 4$ mm bars in a 150×150 mm^2 reinforcement net while group 2 has 14 tests with $\phi 6$ mm bars in a 300×300 mm^2 reinforcement net and group 3 has 5 tests with $\phi 6$ mm bars in a 200×200 mm^2 reinforcement net.

Each test consists of one slab and 6 150×300 mm cylinders. For detailed descriptions of materials, see Chapter 3.

All the slabs are tested in the test set–up described in Chapter 4.

The main mechanical and material parameters and test results for each slab are provided in Table 8.1.

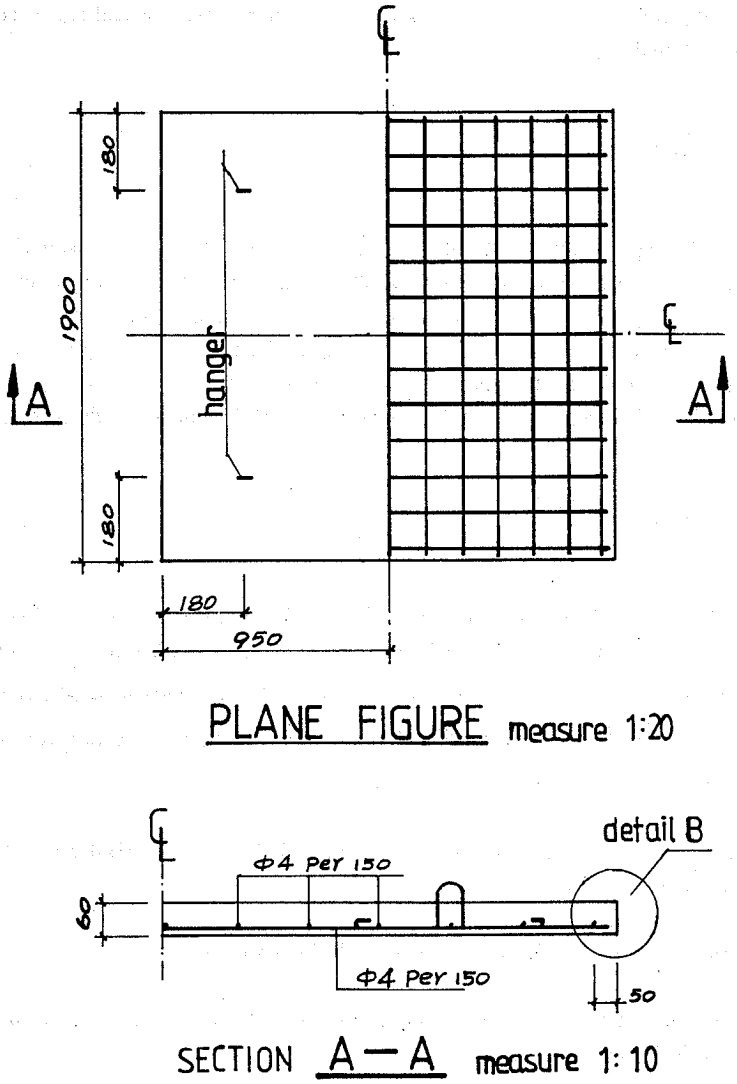

Figure 2.1 Plane of tested slabs.

Chapter 3. Materials

The different materials, the manufacturing and curing, and the determination of material properties are described in this chapter.

3.1 Concrete

As compressive strength of concrete is the most important parameter for determining the behavior and the load carrying capacity of slabs with compressive membrane action, 5 grades of concrete with compressive strength varying from 10–50 MPa were used in the tests. The recipe for each grade of concrete is listed in Appendix A.

The cement was a kind of rapid hardening portland cement. The fine aggregates were sea materials and the coarse aggregates were crushed stones.

Each slab was cast in a plywood mould by two batches of concrete together with 3 companion cylinders for each batch cast in steel moulds.

The slabs and cylinders were cast and compacted by compressed air vibrators at the same time. The top face of the slabs was trowelled by a steel rail. After casting, the slabs were covered by plastic and wet burlap sacks and held at a temperature of approximately 20^{0}C for about 24 hours. Then the formwork was removed and the slabs were placed in a plastic water bag. The cylinders were immersed in a water basin for one week. After this, the slabs and cylinders were stored in the testing hall (20^{0}C, and 45% relative humidity) until they were tested. On the day when one slab was tested, the 6 corresponding cylinders were tested in a 200 Mp MFL (Prüf und Mess MFL System) compression test machine. The machine was servo–controlled by a Wather & Bai SRG 5000. The cylinders which were tested up to failure were loaded at a rate of about 8 MPa per minute.

The average compressive strength of 6 cylinders in 2 batches was taken as the compressive strength of the concrete for the slab in question.

3.2 Reinforcement

In group 1 of the tests, a 4 mm cold–drawn indented steel net was used, while in the groups 2 and 3, 6 mm deformed bars of Swedish fabrication were used. Then bars were welded into a steel net with 300 mm and 200 mm grids respectively.

The tensile test specimens with length of 500 mm were taken from the delivered steel, amounting to a total of 8 specimens for group 1 and 15 specimens for group 2 and 3.

For every tensile test specimen, the ultimate force, the uniform elongation after failure and the force–strain relationship were obtained by tension tests. The tests were carried out in a 60 Mp Mohr & Federhaff AG universal test machine, shown in Fig. 3.1. The strains of the bars were determined by an Amsler Extensometer, type EUL 1133/22, using a measurement amplifier, type Amsler MUL 1147, as seen in Fig. 3.2. The force–strain curve was drawn directly by an x–y plotter.

Typical curves of force and strain for the 4 mm indented bars and for the 6 mm deformed bars are shown in Fig. 3.3 and Fig. 3.4 respectively.

The test results are summarized in Table 8.1. For both 4 mm indented bars and 6 mm deformed bars, no definite yield points could be detected, hence the yield strength is defined as 0.2% offset strength measured on the force–strain graph.

For the 8 specimens of the 4 mm indented bars, the average 0.2% offset tensile strength $f_{0.2}$ was 684.9 MPa with a standard deviation of σ=13.51 MPa and a coefficient of variation c_v of only 1.97 %. The average ultimate tensile strength f_p was 727.7 MPa, with σ=9.86 MPa and c_v=1.35%.

From the tests of the 15 specimens of 6 mm deformed bars, the mean value of $f_{0.2}$ was 539.7 MPa with σ=5.674 MPa, c_v=1.05% and the average f_p was 640.3 MPa with σ=7.426 and c_v = 1.16%. The mean value of the uniform elongation after failure was 12.9%.

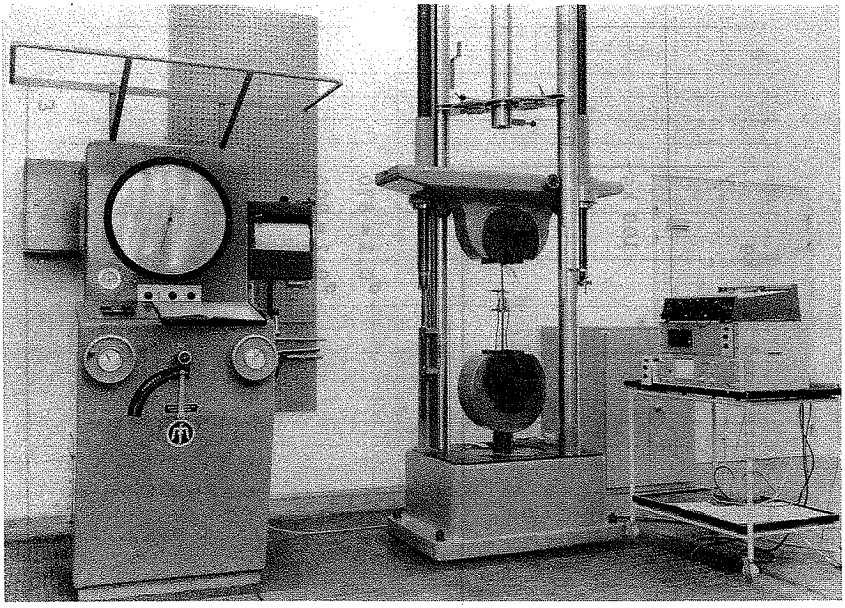

Figure 3.1 Tension test of reinforcement.

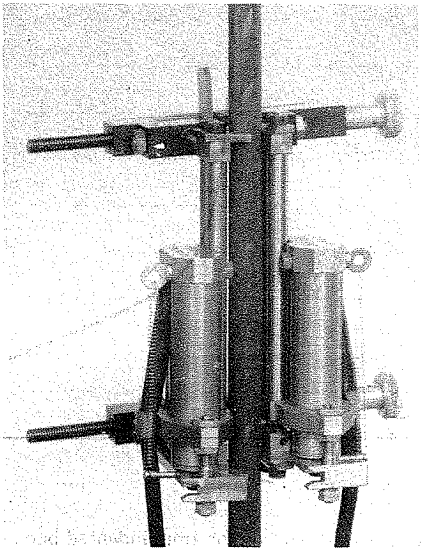

Figure 3.2 Extensometer clamped to test specimen.

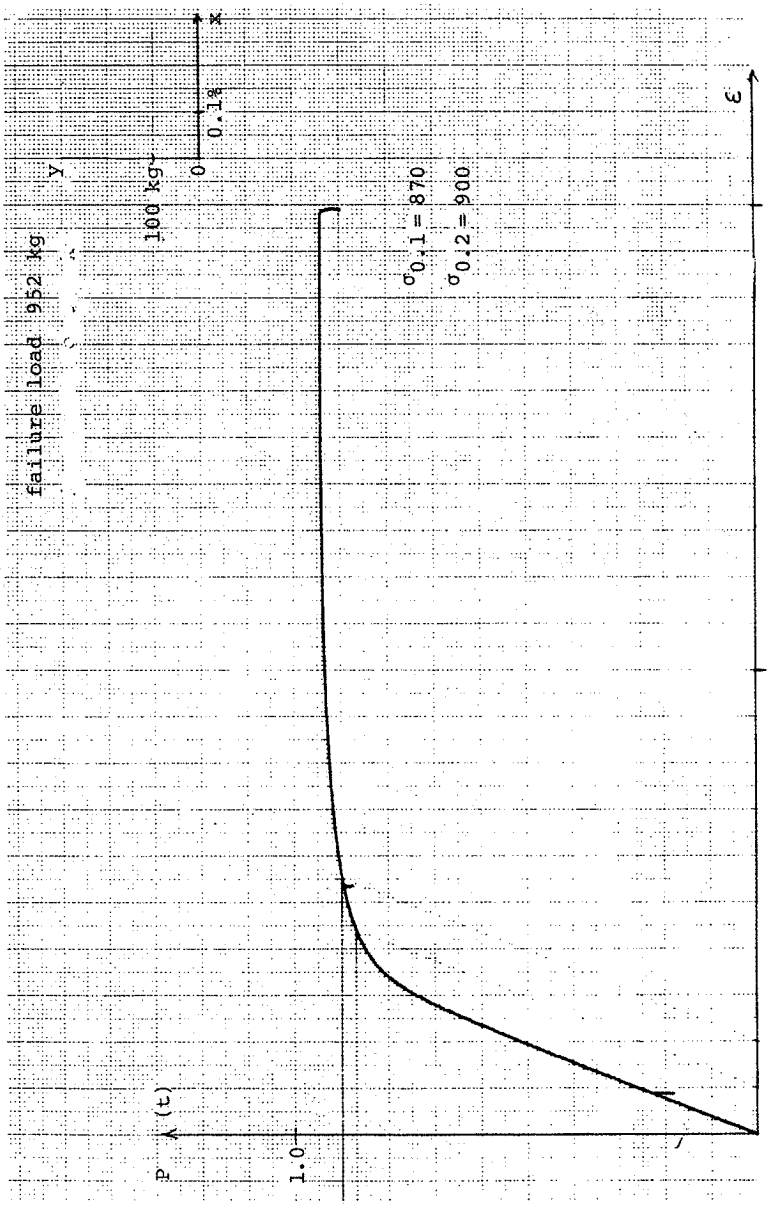

Figure 3.3 Typical force strain relation for 4mm indented bars.

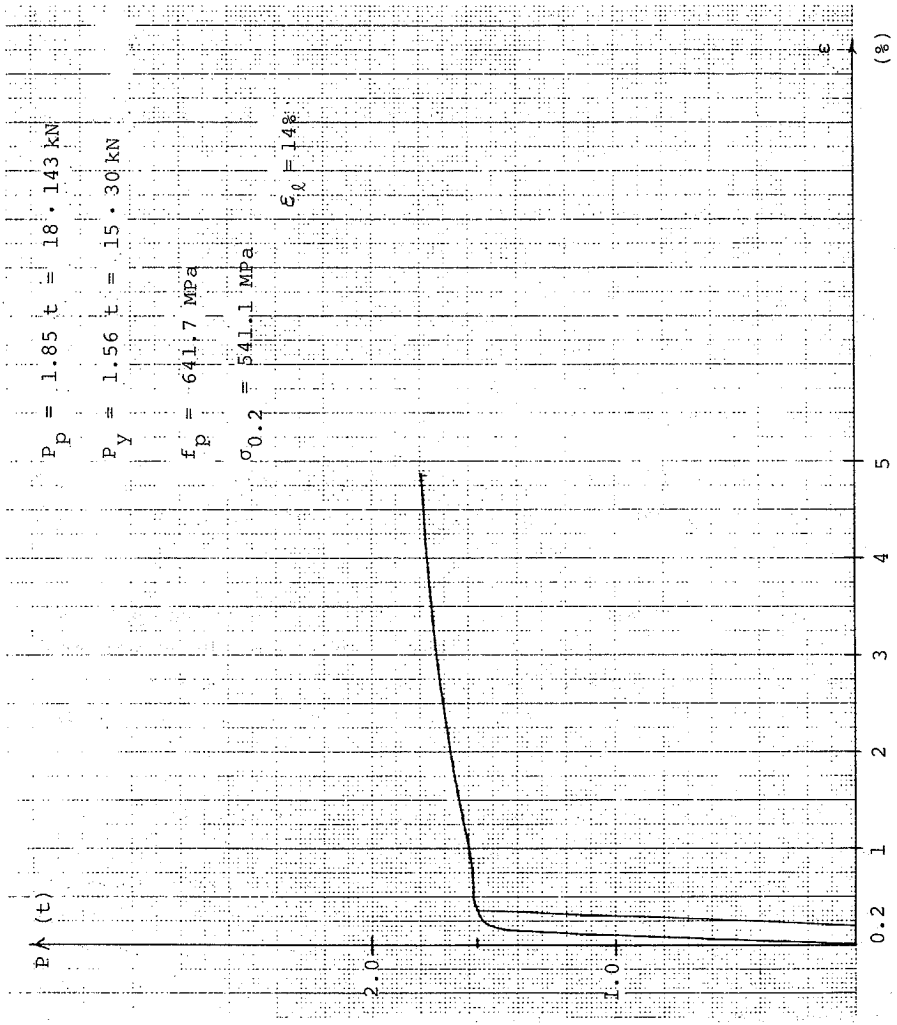

Figure 3.4 Typical force strain relation for 6mm deformed bars.

Chapter 4. Test Set–up

The main principle of these tests is sketched in Fig. 4.1 whereas Fig. 4.2 and Fig. 4.3 show the tests plan.

With regard to the concentrated loading positions, there were two types of loading as shown in Fig. 4.2 and Fig. 4.3.

For type 2, the two concentrated loads were placed at the two one–third points of the span in E–W direction and in the middle of the span in S–N diredtion.

For type 1, the two forces were placed in the same way as for type A in E–W direction but at the one–third point near south in S–N direction.

The test set–up for type 1 is shown in Fig. 4.4.

Before installation, the concrete slab was whitewashed and lined out with a 100 × 100 mm black grid in order to facilitate the observing and recording of the crack formations.

The loads were supplied by two 5 MP one way hydraulic oil pressure jacks, type Amsler EPZ 20/10. At loading, a 25 mm thick steel platen and a 10 mm weak wood fibre board both with diameter of 150 mm, were placed between jack and slab. In order to get uniform reactions along all edges, 40 mm diameter hard rubbers were used as supports.

The lateral restraint was obtained by four separate IPE 270 profiles surrounding the slab and connected to a stiffener. In the middle of each steel rod, there was a dynamometer, by which the horizontal lateral movements of the slab was recorded and the membrane forces were measured. In order to ensure that there was no clearances between the edges of the slab and the surrounding steel profiles, expansion cement grouts were filled into the 10 mm gaps after the installation of the steel frame, which was made of steel profiles and connected by 8 steel rods.

During the installation of the steel frame, four special corner devices shown in Fig. 4.5

were used just to adjust the profiles into proper position. The completed steel frame was loaded on the top side of the slab in the supporting positions through 8 adjustable bolts. Between the slab and the adjustable bolts, steel platens and weak fibre wood boards were used to reduce the local compressive stresses.

The design of the surrounding steel profiles and the locations of the connecting steel rods were based on the requirement that the deflections of the surrounding steel profiles in the middle of the side span should be similar to that of a surrounding concrete slab with the same thickness as the tested slab and having one meter width and the reinforcement with the same amount of magnitude as the connecting tensile steel rods used in the tests.

The connecting steel rods which were designed to take the induced membrane forces were made so that they would not yield at the failure loads of these tests.

In order to measure the deflections of the slabs and the lateral deformations of the surrounding steel profiles, an independent measuring system was set up, see Fig. 4.6, (with loading type 2).

Regarding the measurements of the loads, the corresponding membrane forces and the deflections, the readers are referred to Chapter 5.

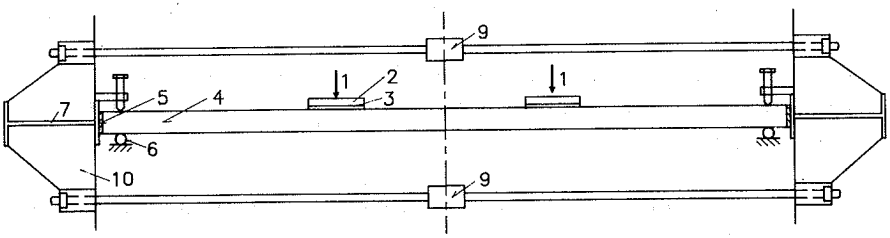

1. loads
2. loading platen
3. 10 mm weak wood fibre board
4. reinforced concrete slab
5. 10 mm grout filler made of expanding cement
6. 40 mm hard rubber support
7. IPE 270 profile
8. 20 mm steel rod
9. dynamometer
10. stiffener

Figure 4.1 The main principle of the membrane action tests.

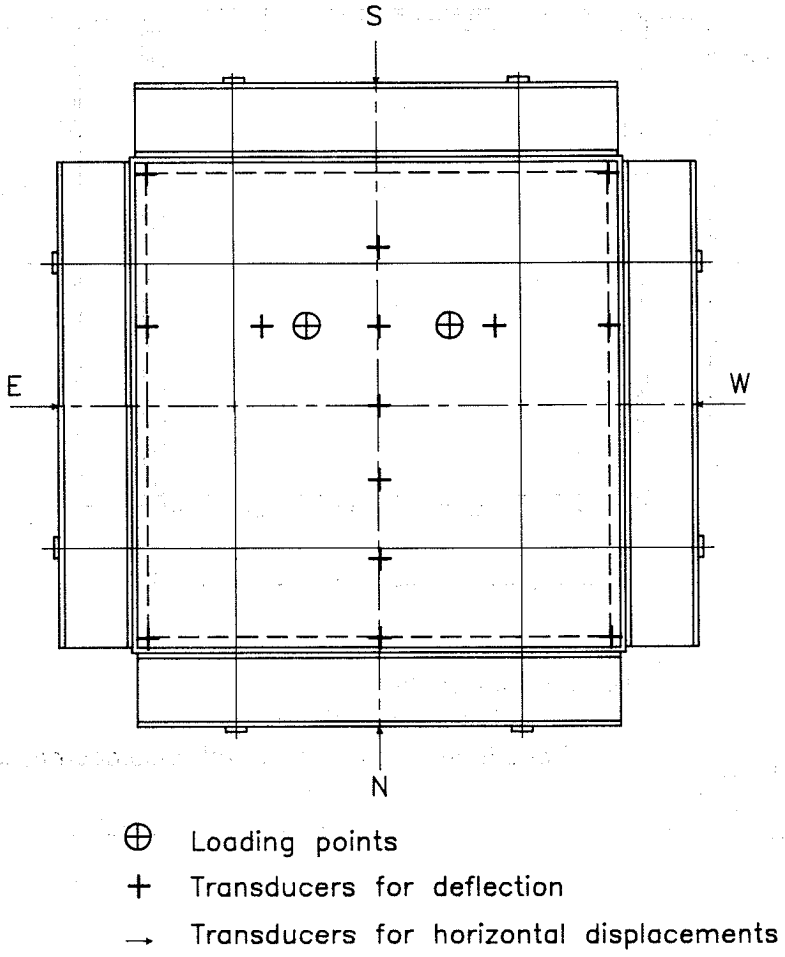

Figure 4.2 The plan of the slabs and the steel surroundings for load pattern 1.

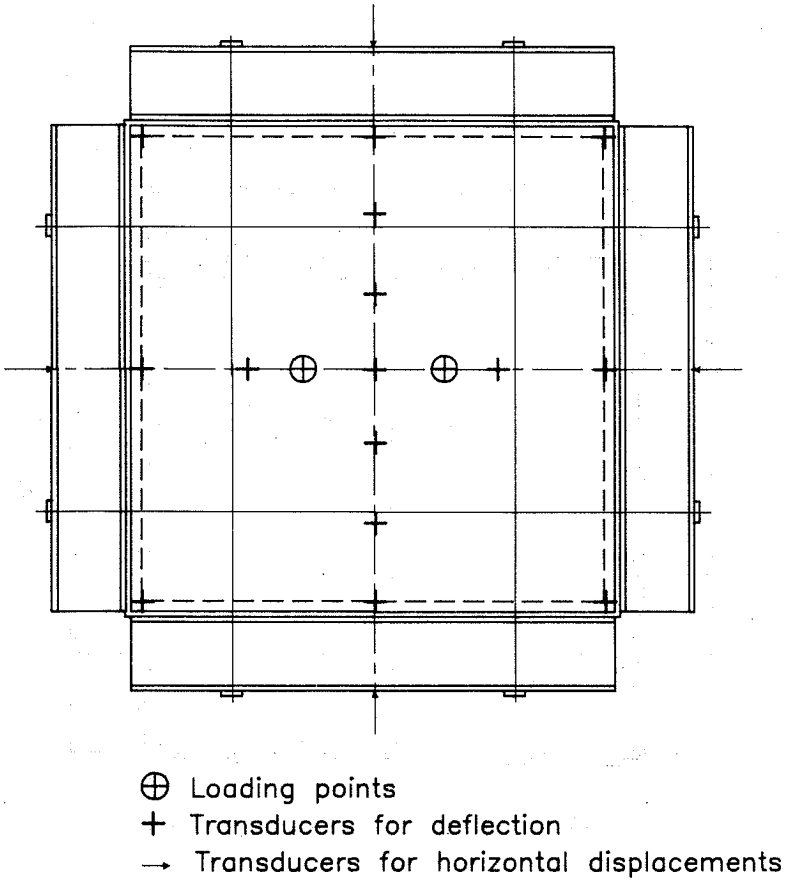

Figure 4.3 The plan of the slabs and the steel surroundings for load pattern 2.

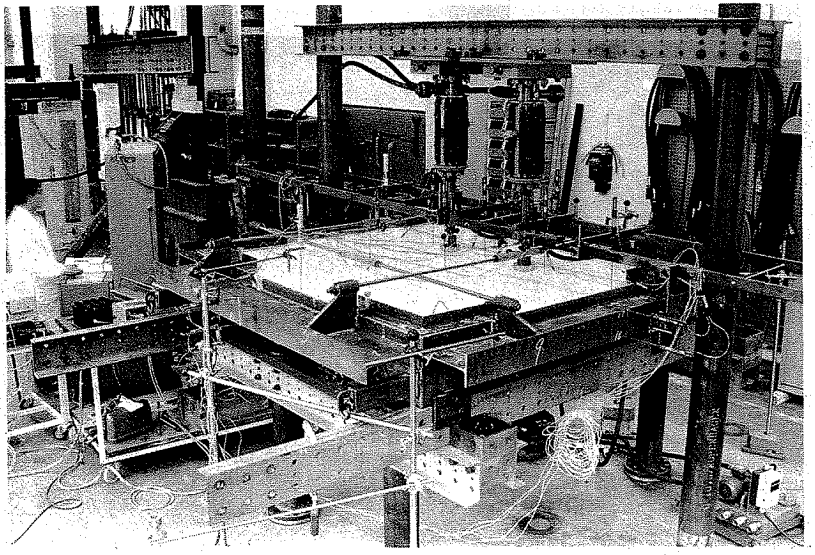

Figure 4.4 Test set–up for the membrane tests.

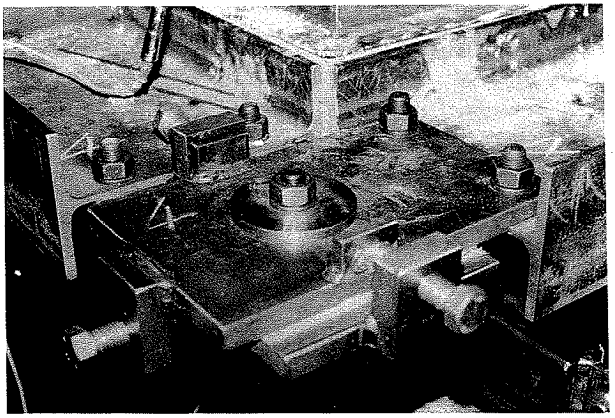

Figure 4.5 The special corner devices designed for installing and adjusting the steel surroundings.

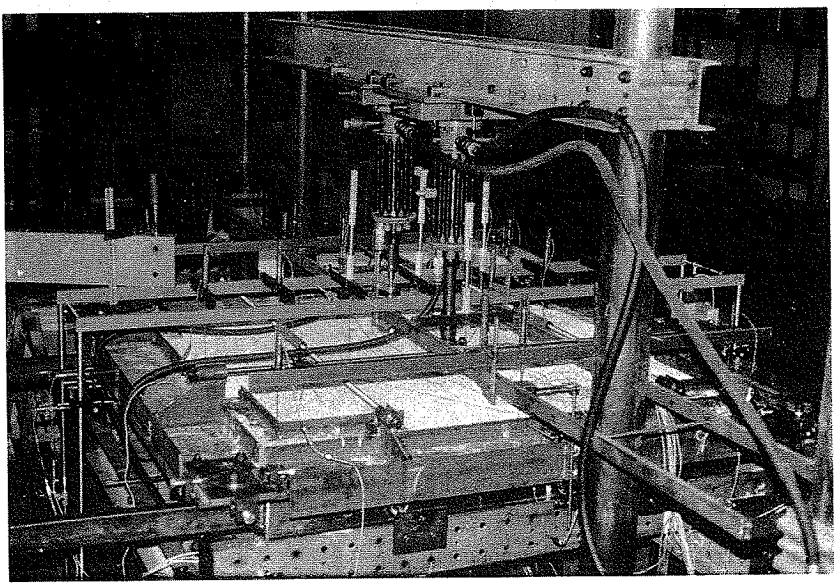

Figure 4.6 The test set–up and the measuring arrangements for the membrane tests.

Chapter 5. Measuring Instruments and Technique

This chapter contains the descriptions of all measurements taken in these tests and how they are taken.

In all tests, the load on the jacks was measured by an Amsler spring manometer with pressostate (seen to the left in Fig. 5.1). The magnitude was read visually on the scale of the manometer and recorded by electrical means, i.e. datalogger etc. with a device connected to the scale hand.

A small inconsistency between the values read from the spring manometer and the values registered by the datalogger was found as a result of a spring manometer reading inaccuracy. In later analyses, the load magnitude registered by electrical means was used.

The corresponding membrane forces in each connecting tensile steel rod were measured by means of 8 dynamometers, which were calibrated before and after the tests.

Furthermore, the deflections of the slab and the displacements of the surrounding steel profiles were measured by means of calibrated Hewlett Packard Displacement Transducers, type 7–DCDT–1000, for which the maximum working range was 50 mm, and Trans–Tek Displacement Transducers, model DC–DC–0246–00002, for which the maximum working range was 150 mm. The transducers were fixed to the specimens by means of the metal gadgets shown in Fig. 5.1. The position of transducers placed on the specimens is sketched in Fig. 4.2 and Fig. 4.3, and can also be seen in Fig. 4.4 and Fig. 4.6.

Using these measurements, it is possible to calculate the relative deflections of the slabs and the translations and rotations of the surrounding steel profiles during the tests.

All the electrical measurements were taken and recorded automatically with the aid of a datalogger, which was controlled by a computer.

In addition to the time, each scan covers 33 channels, viz.:

—— The voltage of the Wheatstone's bridge.
—— The load at the start of the scan.
—— 8 dynamometer readings.
—— 22 transducer readings (14 for deflections of the slab and 8 for translations and rotations of the surroundings).
—— The load at the end of the scan.

Each scan took approximately one minute.

All the readings were also printed in test site for visual inspection and stored on discs by means of the computer for later analysis.

The system and the electrical instruments are shown schematically in Fig. 5.2. It can also be seen in Fig. 5.1.

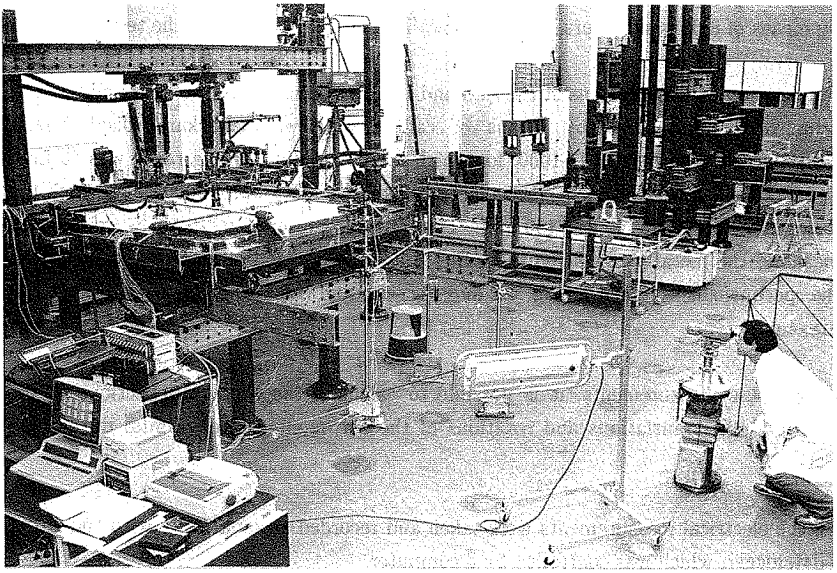

Figure 5.1 The test set–up and the measuring instruments.

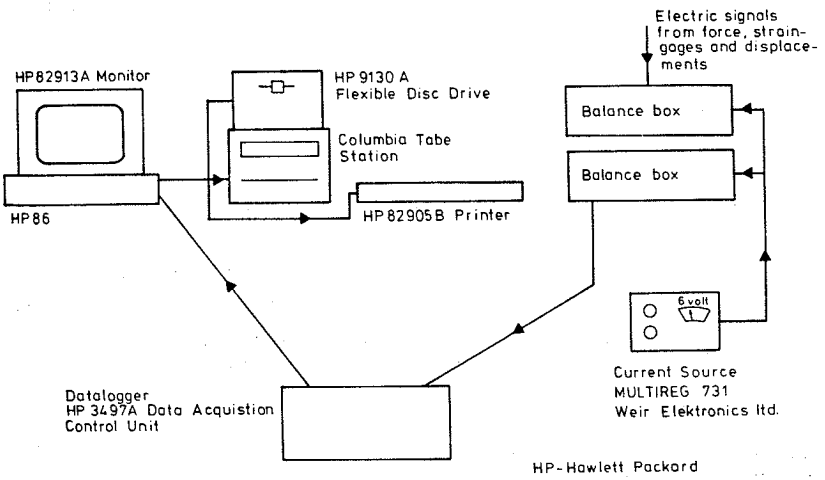

Figure 5.2 The different electrical instruments and the data picking up system.

Chapter 6. Test Procedure

Just before the starting of a test, a zero measurement was taken.

The slab was then loaded in steps of 0.25 ton (per jack), apart from the first step of 0.1 ton each. Up to the first visiable cracking, the load was applied during 5 minutes, including 1 minute for the actual loading. Then all measurements (including the time and loads) were taken automatically by the system described in Chapter 5. At least two scans were used. After the visiable cracking (which may also be detected through the increment of the dynamometers attached on the tensile steel rods, which jumped to a higher value at crack occurrence and by the load–deflection curve of the slab drawn by an x–y plotter), the load was applied during 20 minutes and the measurements

were taken at 5 minutes interval.

When the slab was near failure, i.e. when considerable deformations were taking place at constant load, the slab was loaded in steps of 0.05 ton per jack and the measurements were taken at 0.5 minute interval.

A typical loading history is shown in Fig. 6.1, which was recorded by an x–y plotter for slab MAT–17.

During the test, the crack formations and deformations were observed.

The first visiable cracking load at which the critical cracking pattern forms and the ultimate load were especially noted. After failure, the cracking pattern was inked and close photographs were taken for both up and down faces of the failed slabs.

The photographs are shown in Chapter 7.

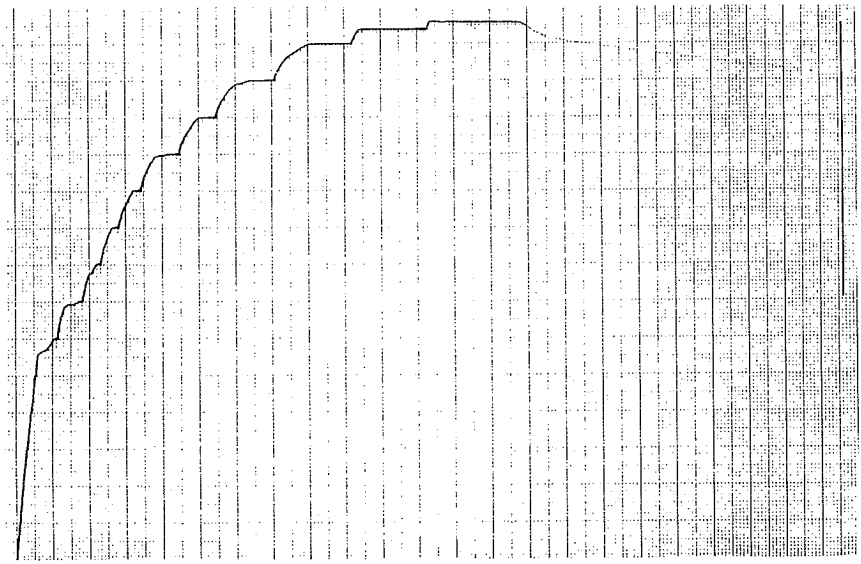

Figure 6.1 MAT–17.

Chapter 7. Observations

In this Chapter, some observations made during the tests are described. Firstly, some general phenomena are emphasised and then some differences between the individual tests are discussed. Photographs which show the cracking models and failure patterns for both top and bottom faces of tested slabs are also shown in this Chapter, Fig. 7.1 and 7.2.

In general, before slabs cracking, the corresponding membrane forces are rather small and the deflections are almost linearly varying with the loads. After cracking, both the deflections and corresponding membrane forces suddenly increase and nonlinear behaviour appears.

In all the tests, the first cracking was found at the bottom face of the slab at a load of about 22–30% of the failure load.

It appeared along the line connecting the two loading points and the lines connecting a loading point with two corners at the same side. When increasing the loads, the radial cracks emerging from the loading points gradually occurred and propagated.

At a load of about 85–90% of the failure load, a large circular or elliptical crack formed on the top face of the slabs accompanied by large deflections.

It seems that in all tests, the reinforcement in the middle of the span yielded. In group 1 in the tests, the reinforcement even broke in the middle span before final failure because of the very limited elongation capacity.

At the supports, the deformations were about 4–6 mm in all tests. The maximum net deflection varied from 26.5 mm – 74.2 mm. Before the slabs reached failure, the crack width in E–W direction was at least 8–10 mm in all tests. The concrete crushed along the edges in most of the tests, see photographs in Fig. 7.1 and Fig. 7.2.

Two kinds of failure patterns, a bending failure and a punching–like bending failure were observed in these tests.

In the bending failure, the concrete crushes along the line connecting two loading points on top and along a small ellipsoid at the bottom. At failure, a cone formed.

Half of the tests had this kind of bending failure.

In the punching–like bending failure, only the concrete around one loading platen was pushed down, but the reinforcement seemed to be yielding and the failure loads were compared with the slabs loads which failed in bending.

Half of the tests got this punching–like bending failure.

After one loading point was punched off, the test still continueed. Some of the slabs then got the same failure pattern as the slabs with bending failure at the same or a little higher load. But a few of the slabs failed with another loading point punched off at a 20% higher load.

The reasons for the punching–like bending failure may be one of the followings or a combination of them.

1. The small ductility of the reinforcement.
As mentioned before, in group 1, a 4 mm cold–drawn indented steel grid was used as reinforcement. The tensile tests of these bars showed an elongation at failure less than 5%.
In the membrane tests, all 3 slabs (Mat–1, Mat–2 and,Mat–3) with this type of reinforcement got the punching–like failure. Before final failure, the reinforcement bars in the middle area of the slabs were broken.

2. Non–uniform reactions along the edges.
Even that hard rubber rods were used as supports, the difference between deformations around the four edges were detected during the tests. In some tests, the difference reached 1 mm at high loads, which gave rise to non–uniform reactions along the edges.

3. Imperfections of the slabs.
Because of the limited mixing capacity, all slabs were, as mentioned earlier, cast in two batches. The interval between two batches was 10–15 minutes, which has led to the differences in compressive strengths of the cylinders in the two batches in a few tests.

When two loading points were located in different batches, it may cause one load point to fail first. In most of the tests, the lines of the two batches could be distinguished and the slab was installed in such a way that the two loading points were located in the concrete of the same batch.

The crackings at both top and bottom sides of the tested slabs and the failure patterns can be seen clearly from photographs shown in Fig. 7.1 and Fig. 7.2.

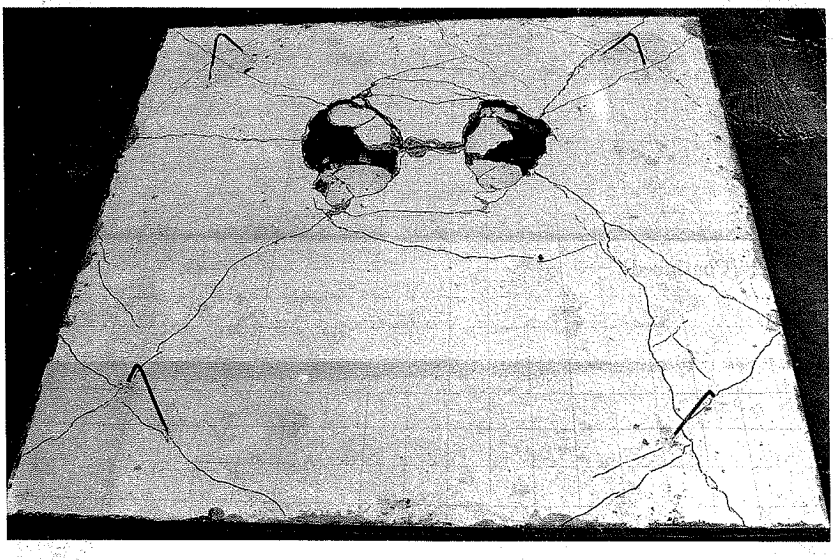

Figure 7.1 Photos of the top of the tested slabs.

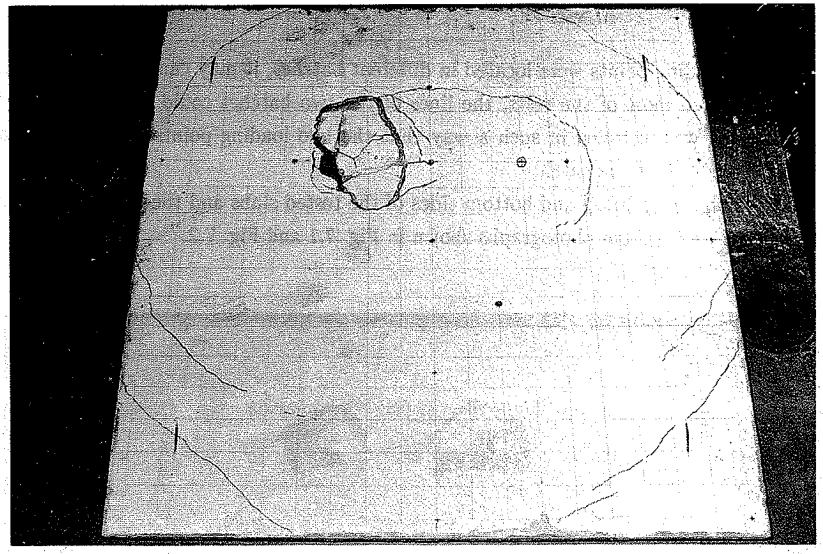

Figure 7.2 (Continued).

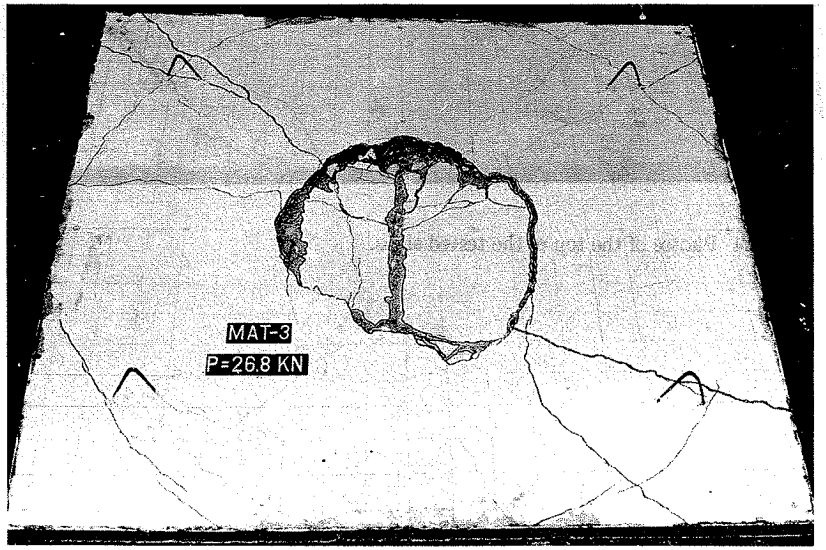

Figure 7.3 (Continued).

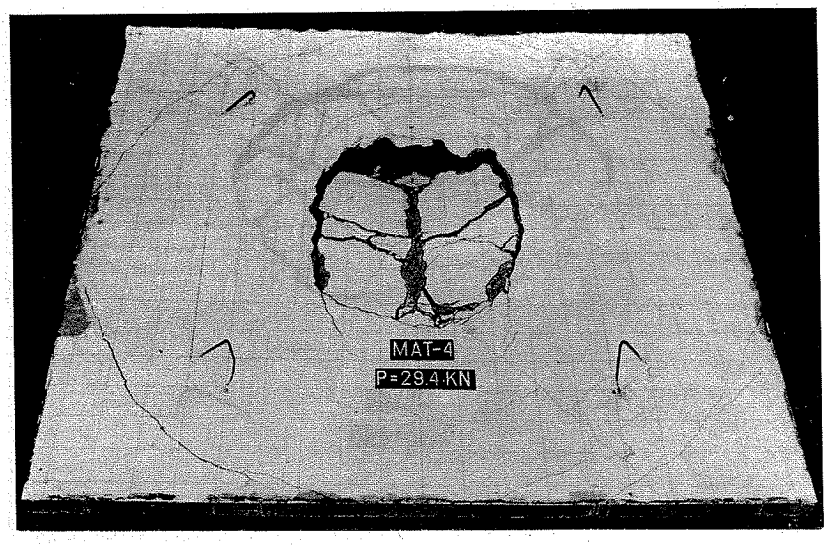

Figure 7.4 (Continued).

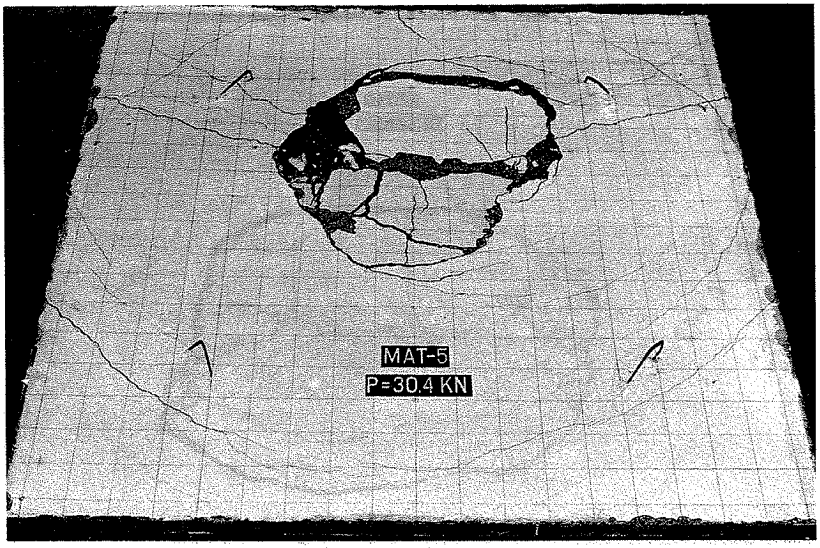

Figure 7.5 (Continued).)

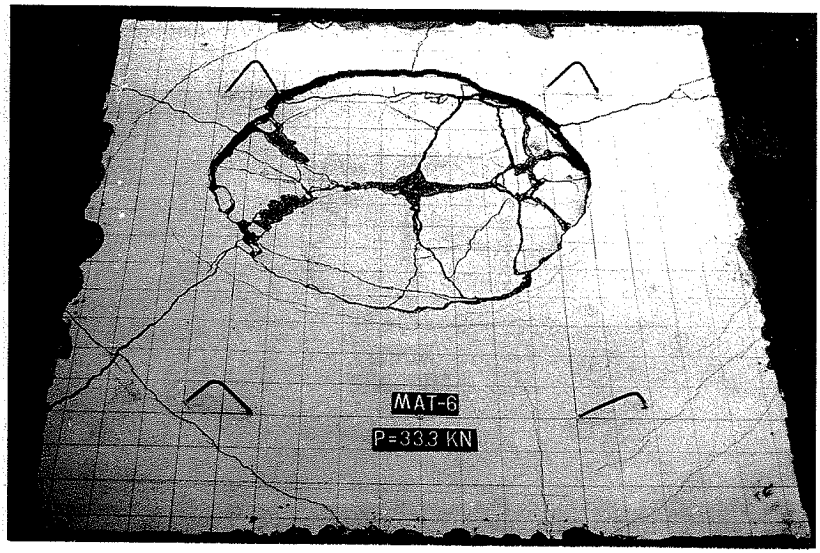

Figure 7.6 (Continued).

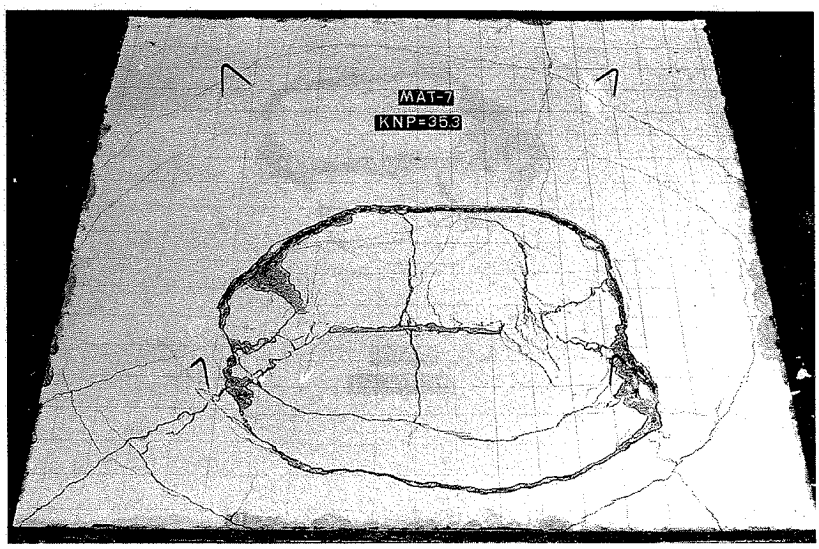

Figure 7.7 (Continued).

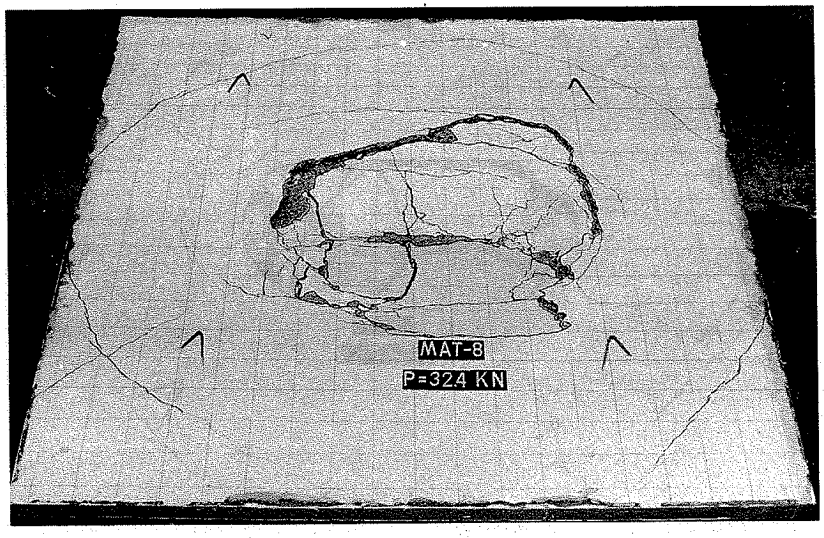

Figure 7.8 (Continued).

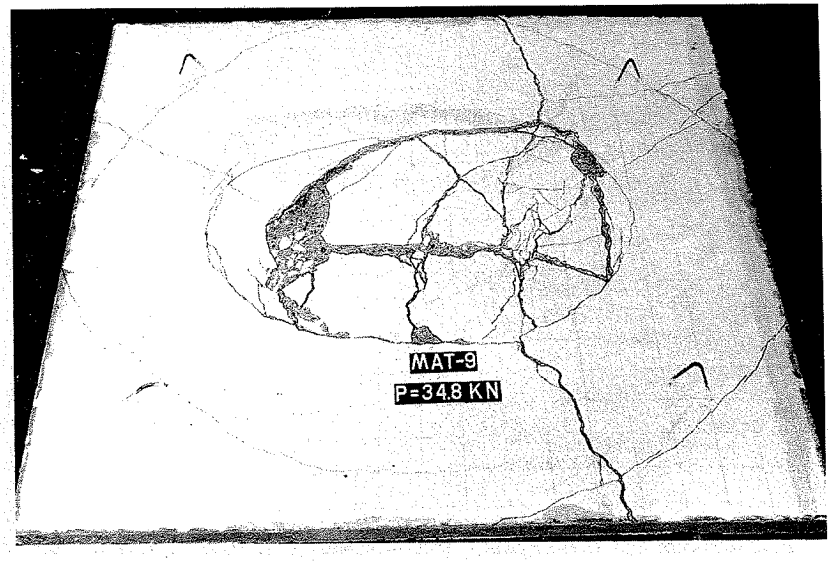

Figure 7.9 (Continued).

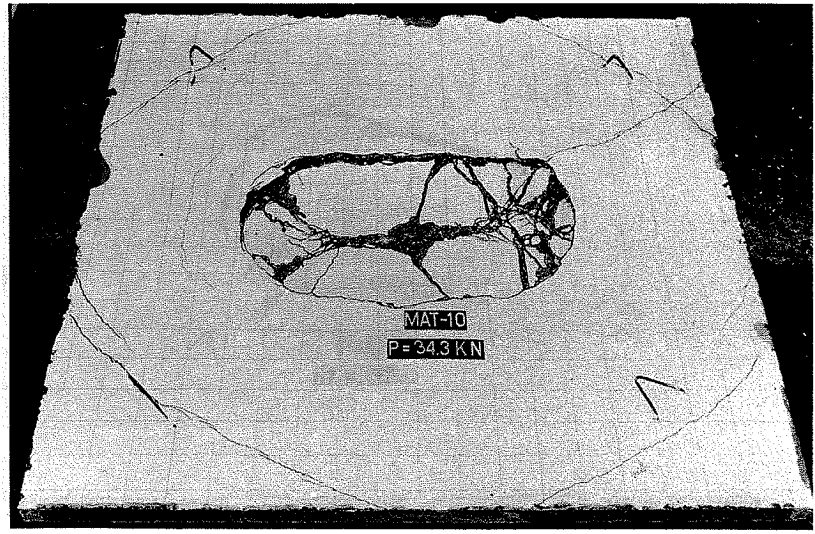

Figure 7.10 (Continued).

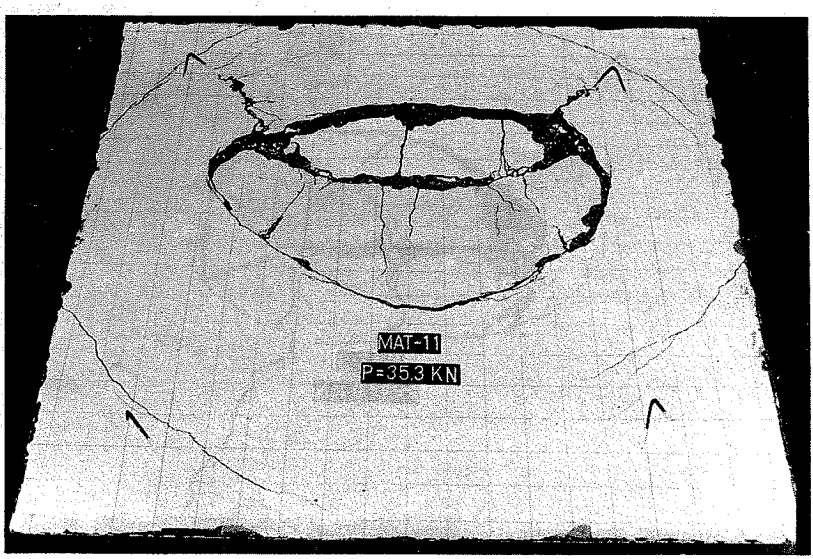

Figure 7.11 (Continued).

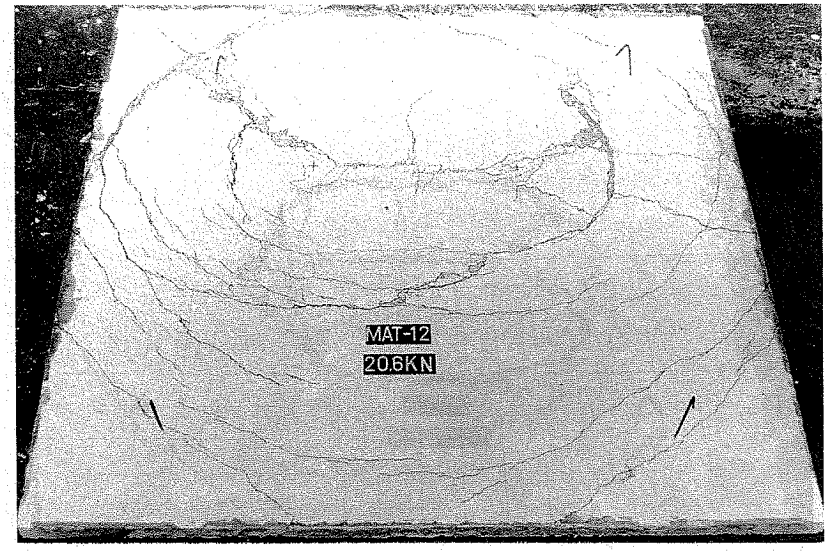

Figure 7.12 (Continued).

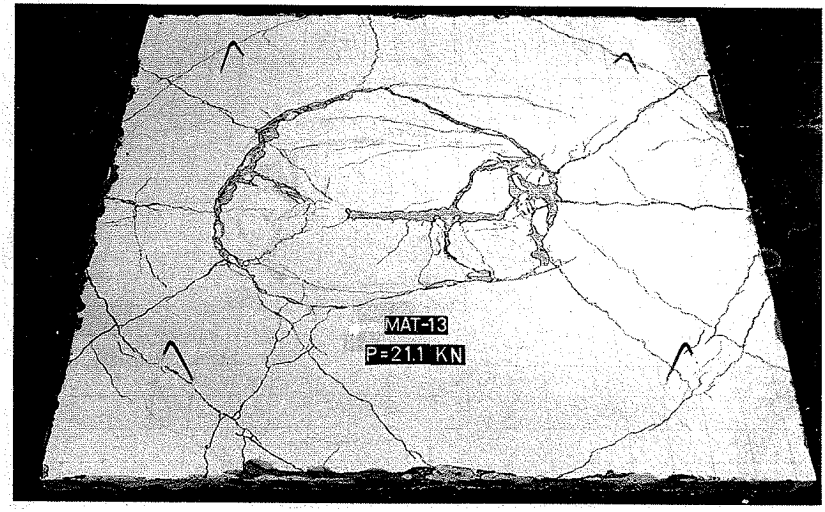

Figure 7.13 (Continued).

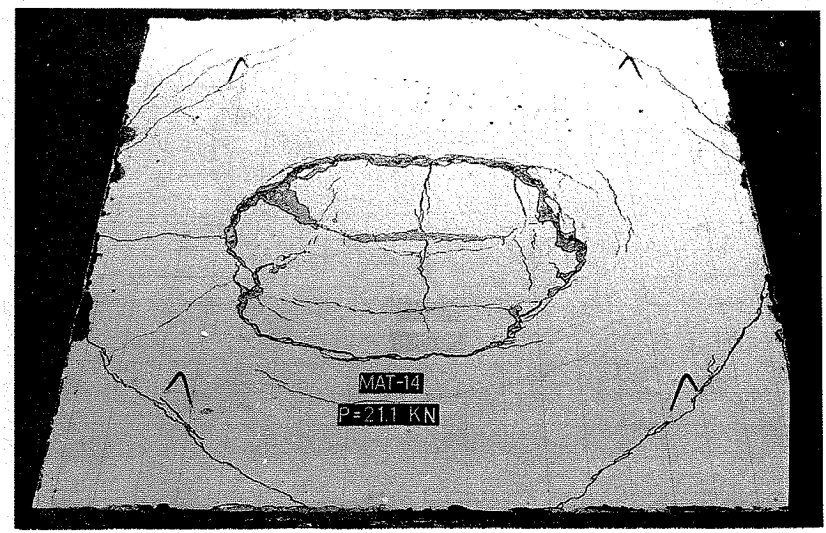

Figure 7.14 (Continued).

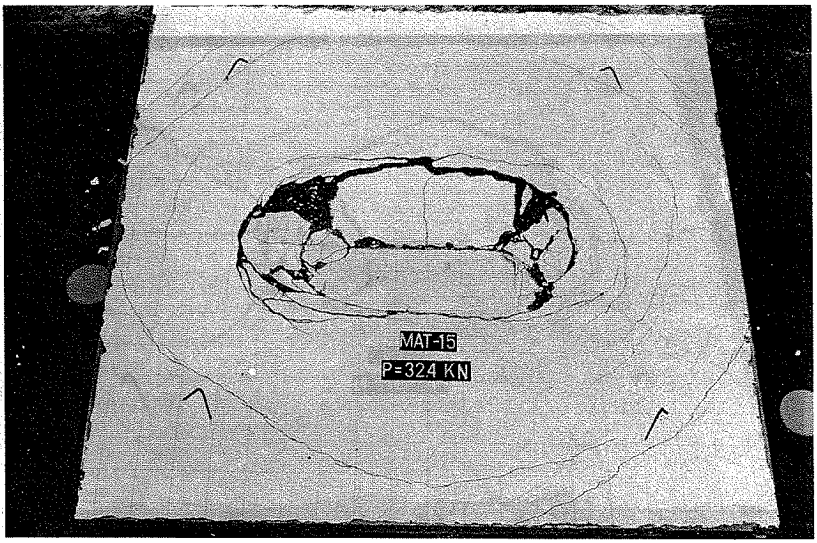

Figure 7.15 (Continued).

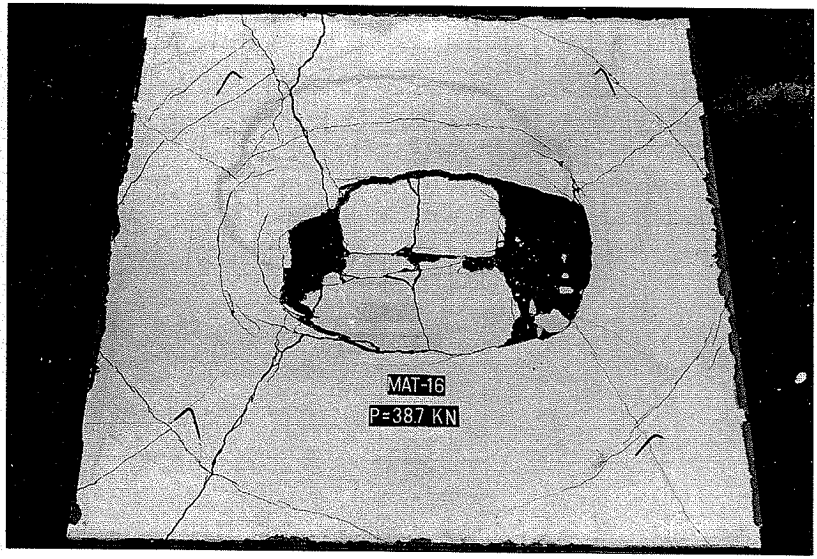

Figure 7.16 (Continued).

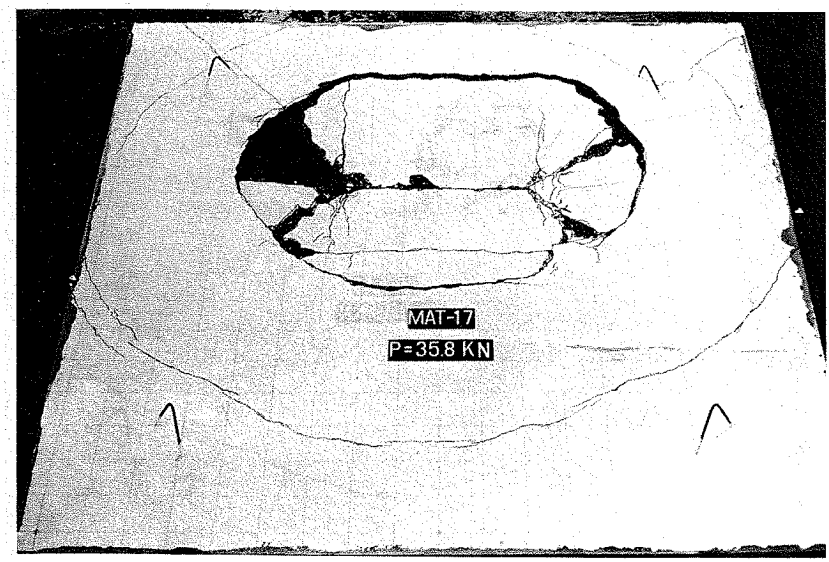

Figure 7.17 (Continued).

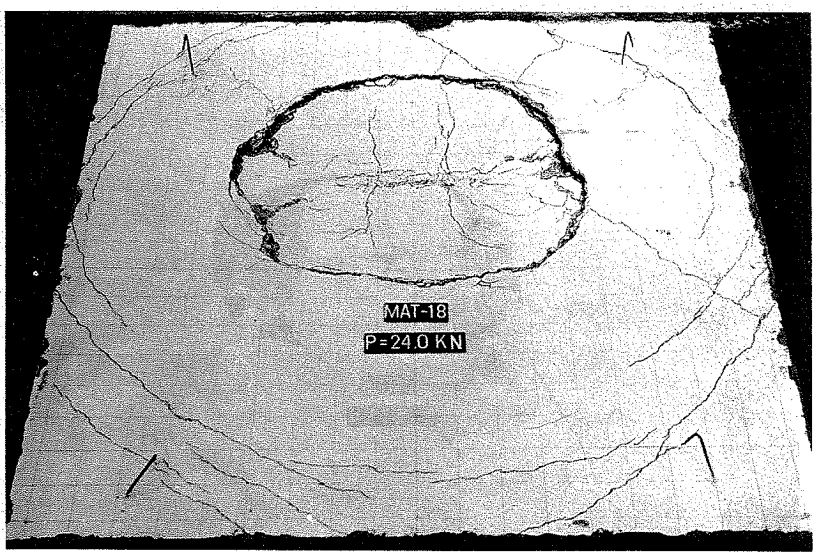

Figure 7.18 (Continued).

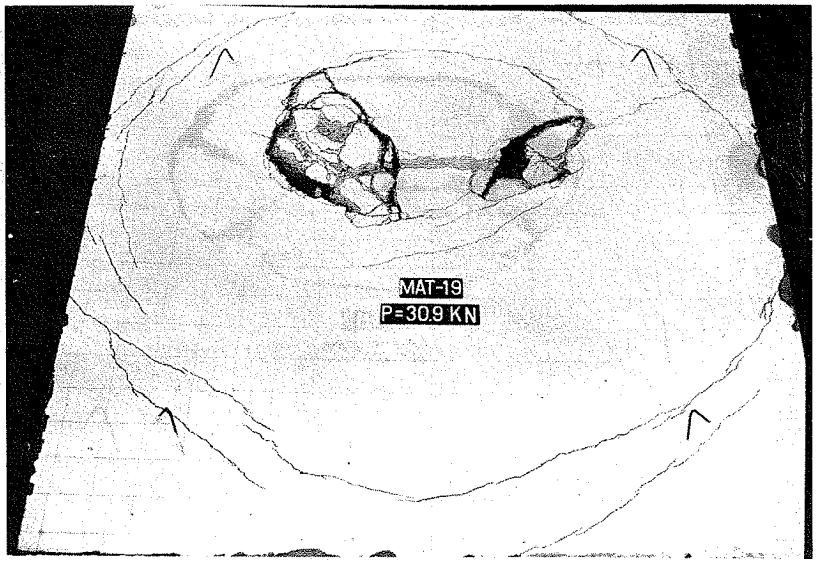

Figure 7.19 (Continued).

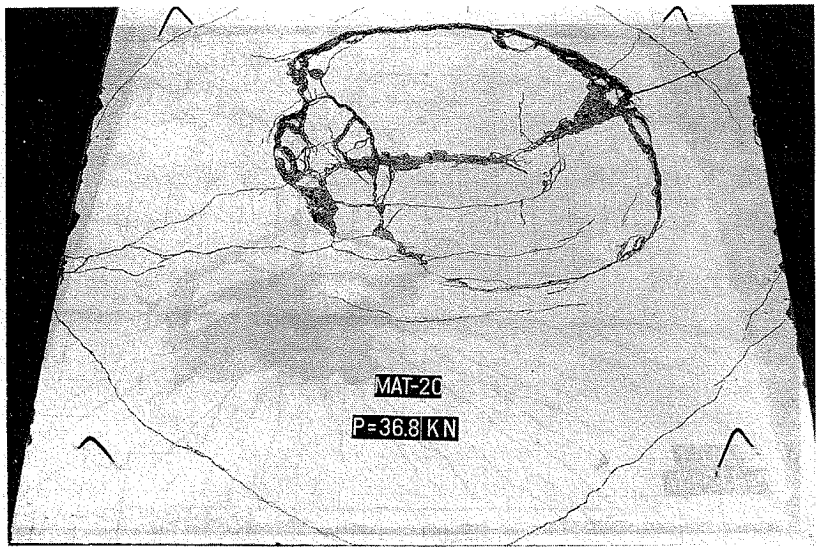

Figure 7.20 (Continued).

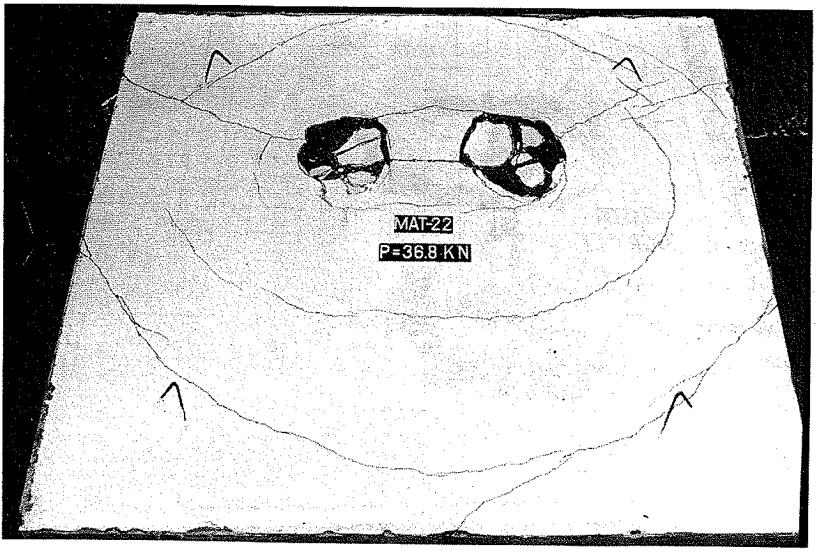

Figure 7.21 (Continued).

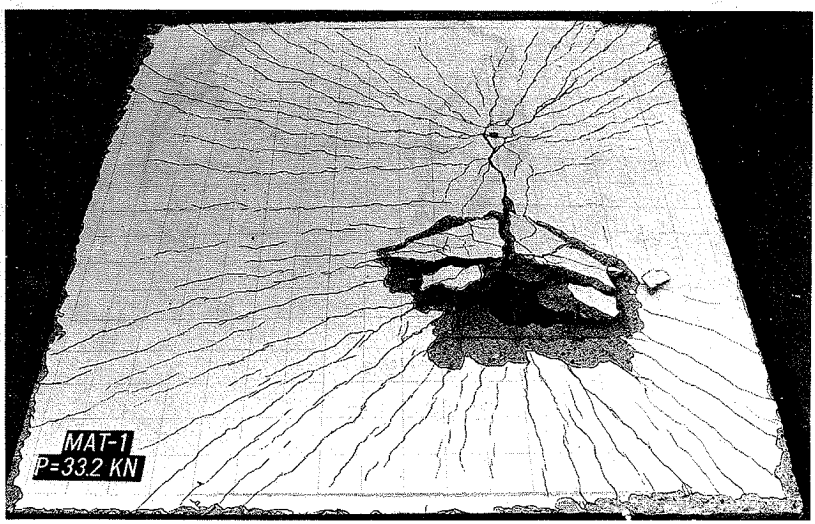

Figure 7.22 Photos of the bottom sides of the tested slabs.

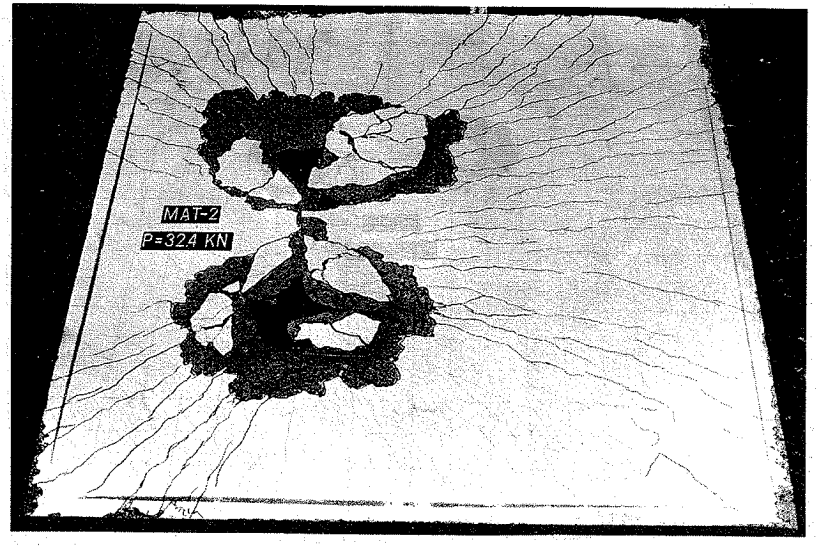

Figure 7.23 (Continued).

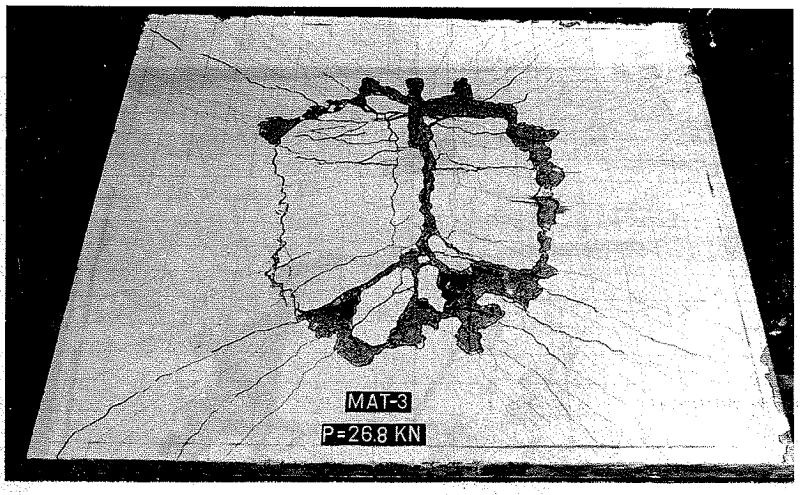

Figure 7.24 (Continued).

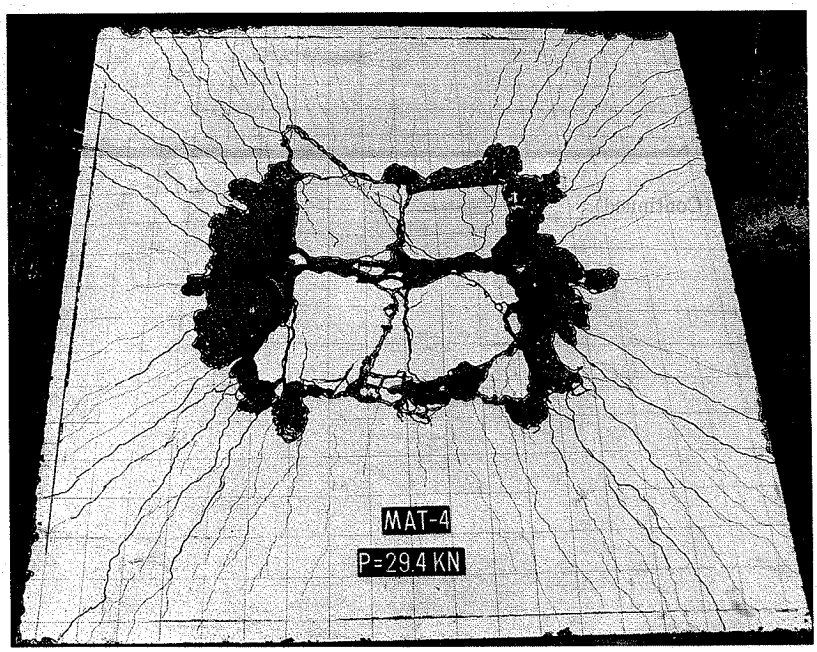

Figure 7.25 (Continued).

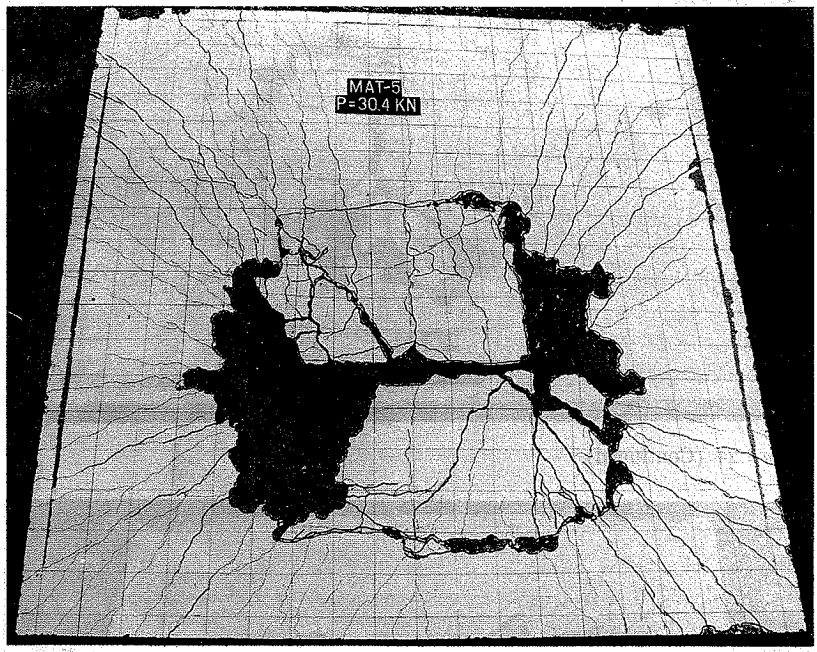

Figure 7.26 (Continued).

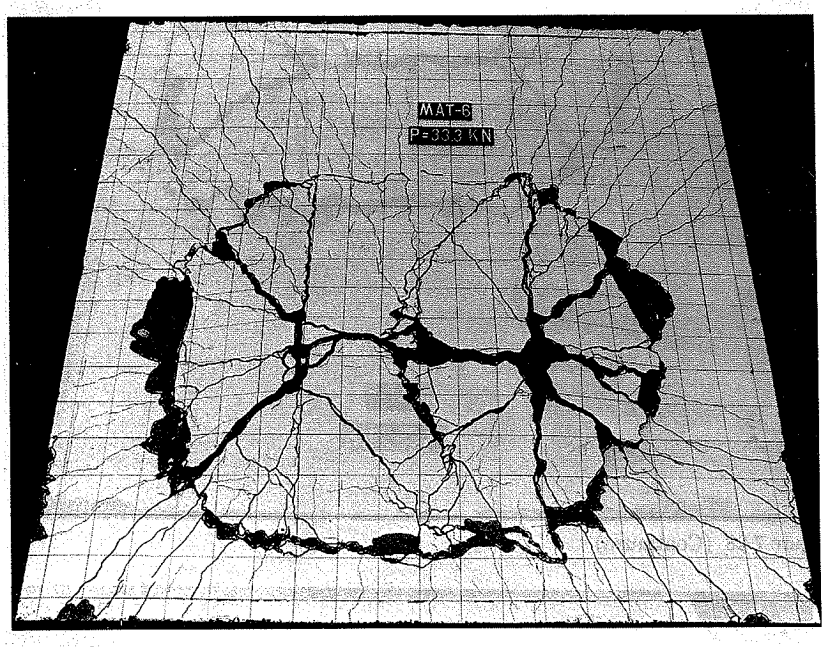

Figure 7.27 (Continued).

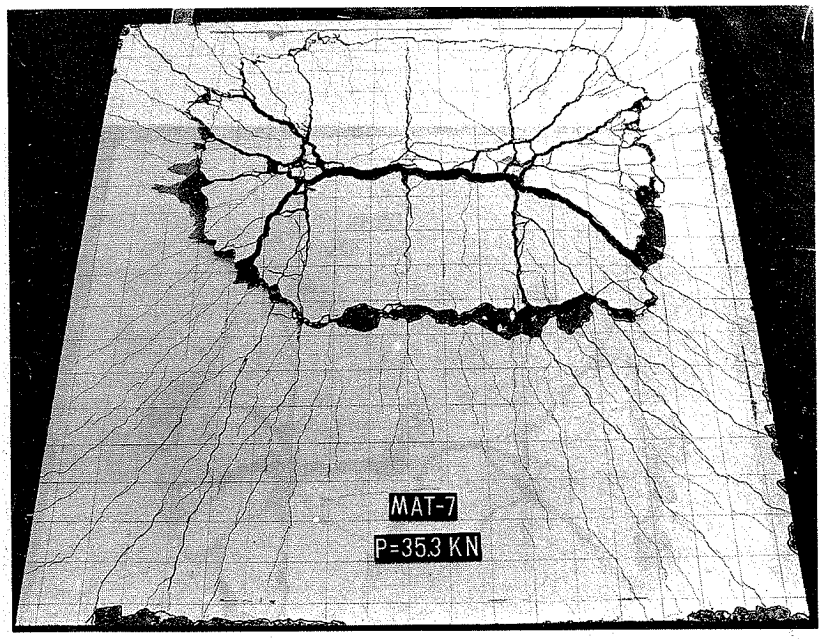

Figure 7.28 (Continued).

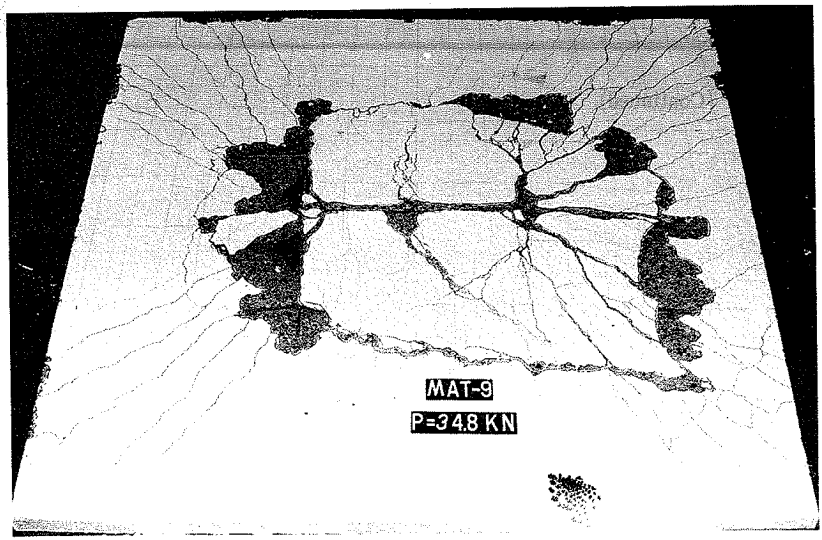

Figure 7.29 (Continued).

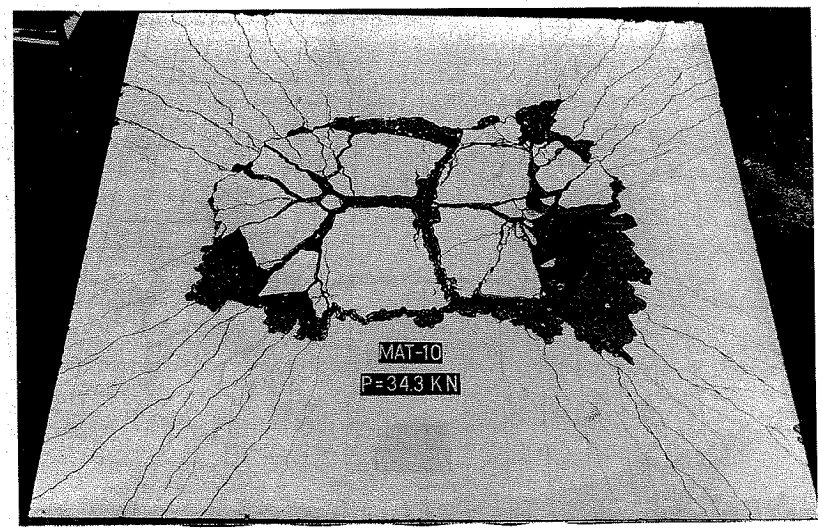

Figure 7.30 (Continued).

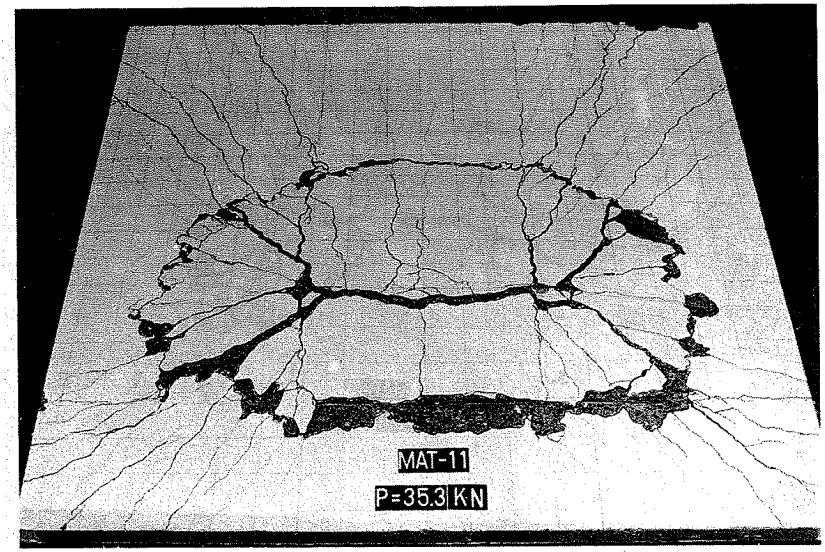

Figure 7.31 (Continued).

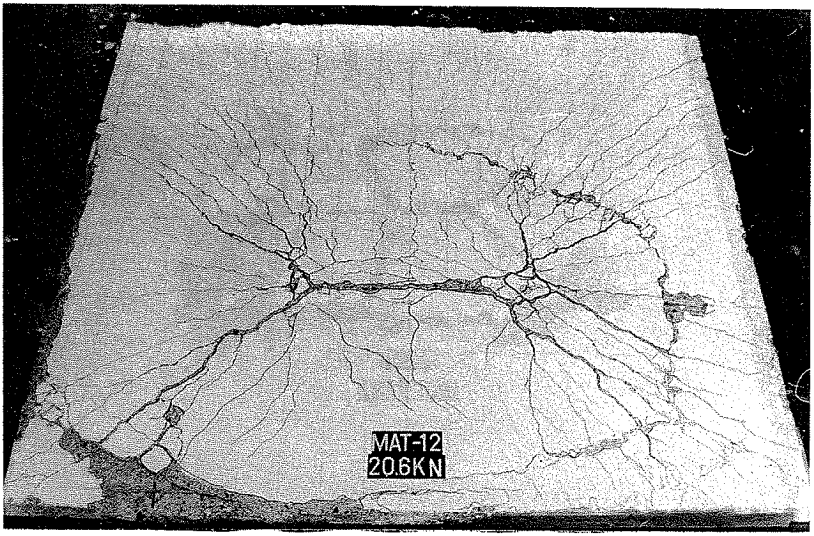

Figure 7.32 (Continued).

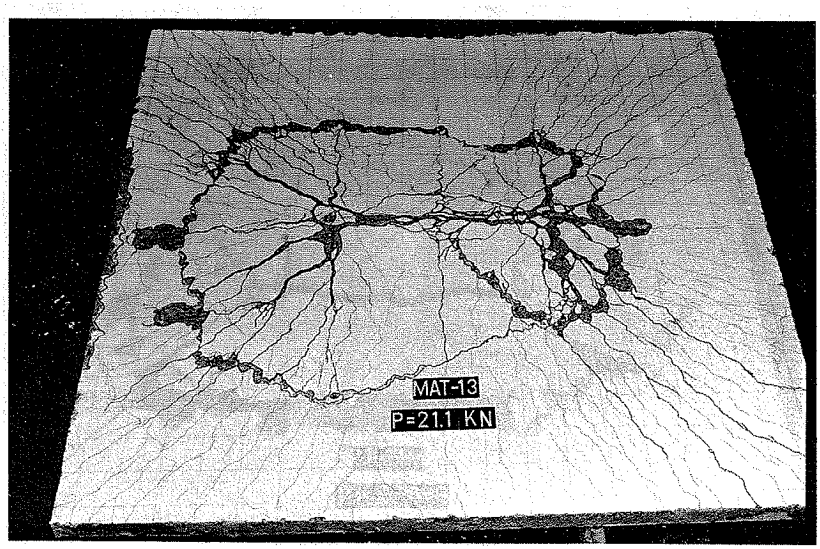

Figure 7.33 (Continued).

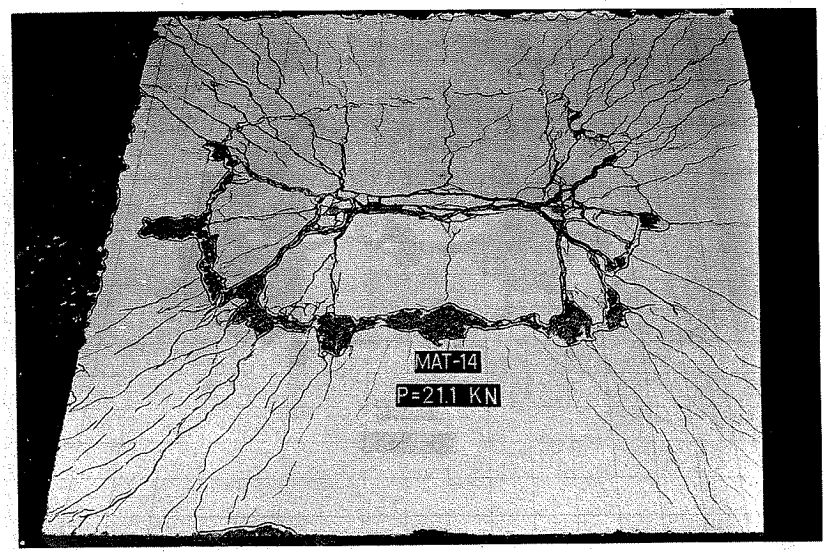

Figure 7.34 (Continued).

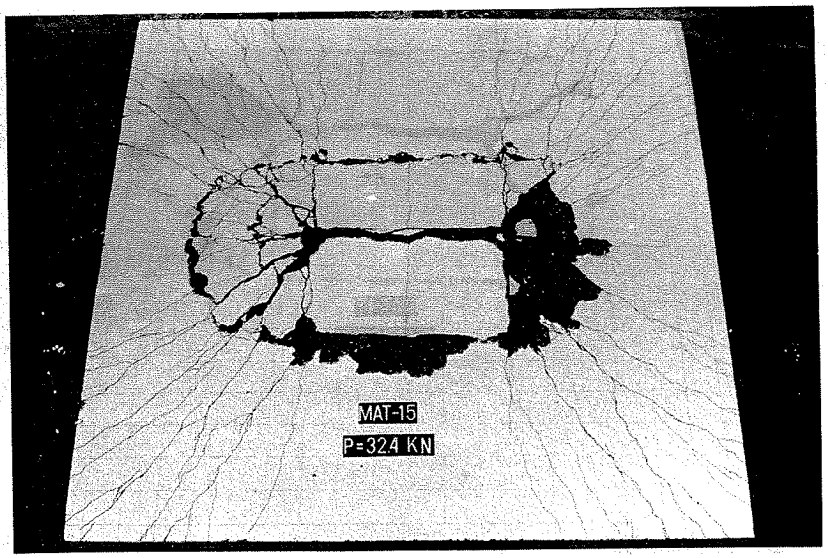

Figure 7.35 (Continued).

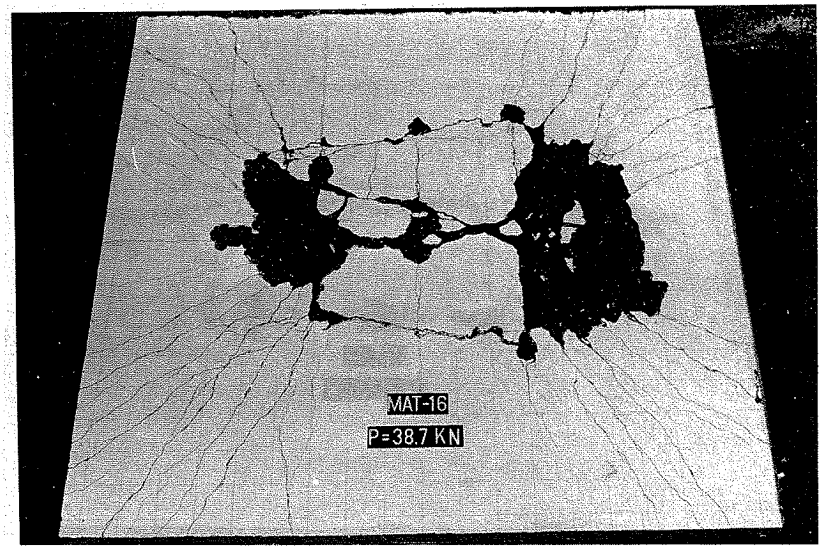

Figure 7.36 (Continued).

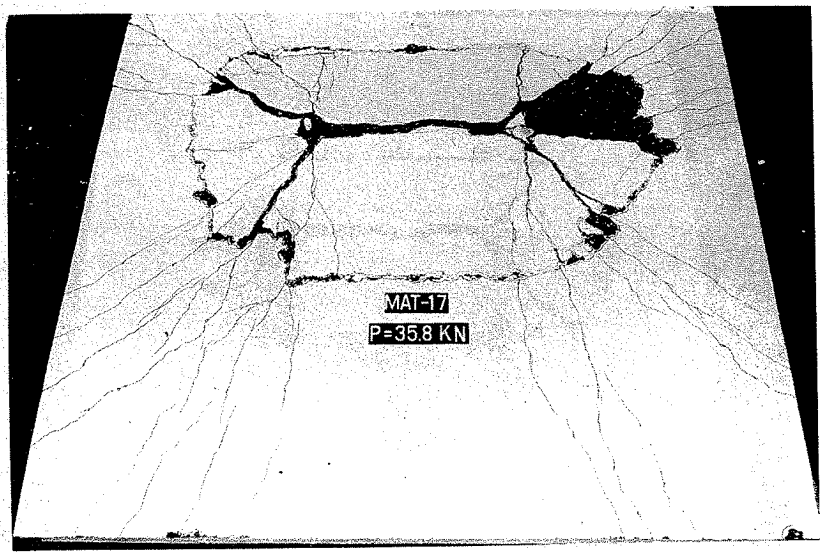

Figure 7.37 (Continued).

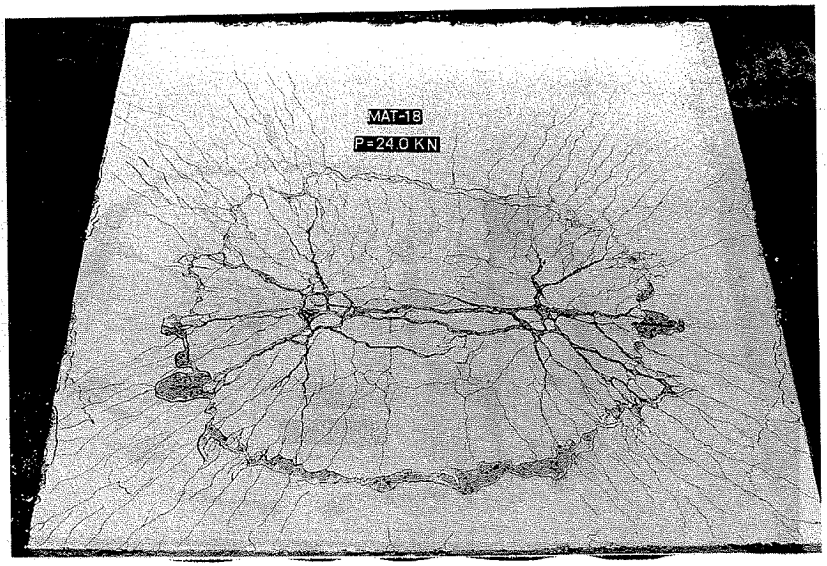

Figure 7.38 (Continued).

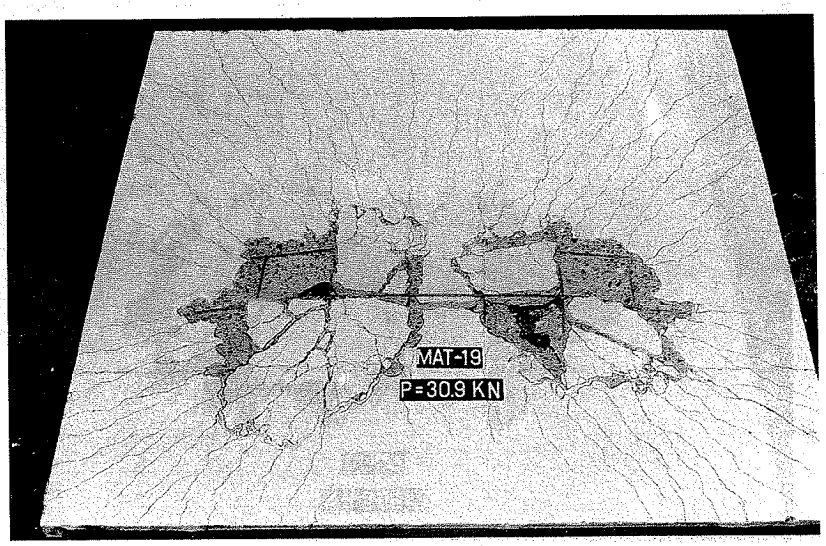

Figure 7.39 (Continued).

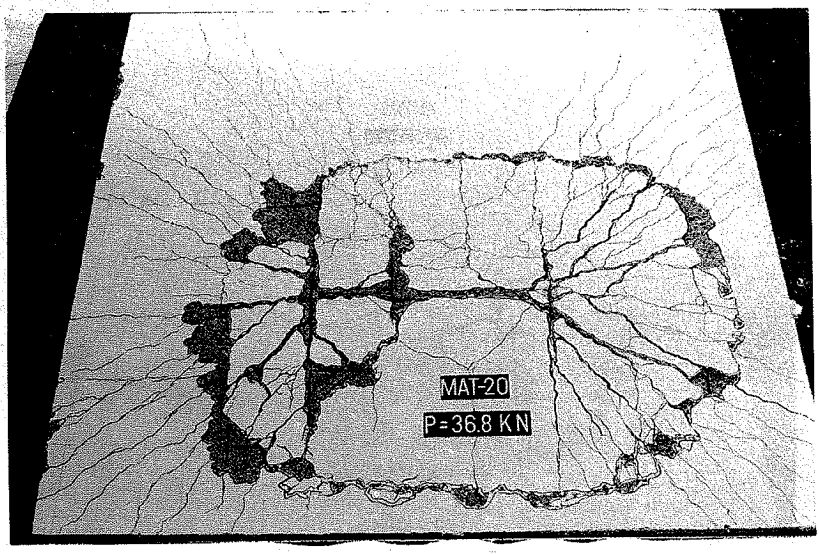

Figure 7.40 (Continued).

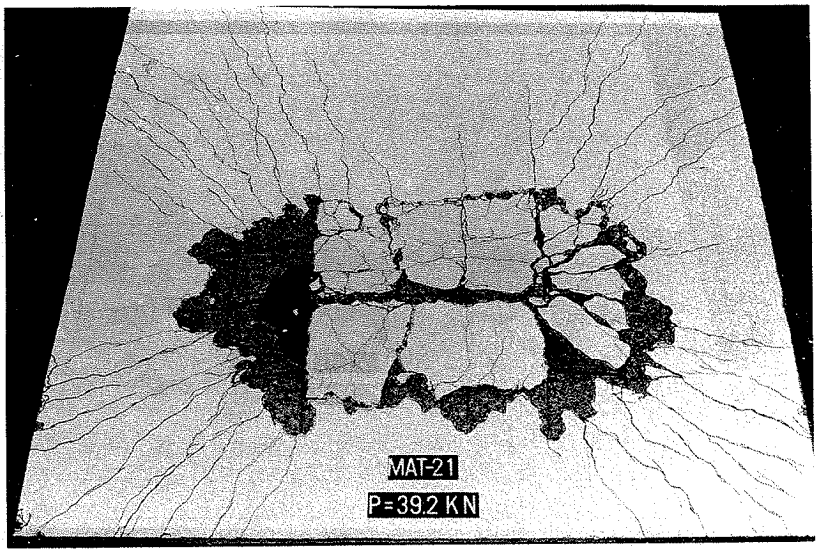

Figure 7.41 (Continued).

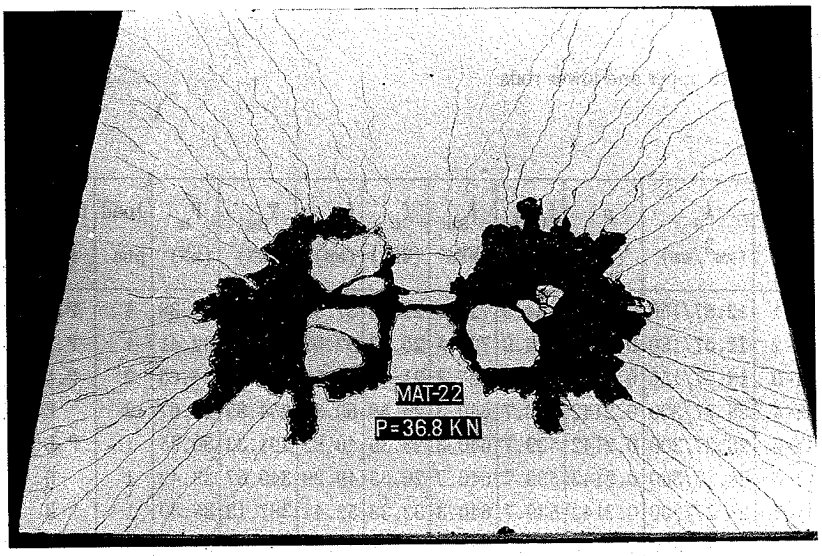

Figure 7.42 (Continued).

Chapter 8. Test Results

The most important results obtained from the tests are described in this chapter. The amount of reinforcement, the mechanical properties of the materials and the main test results are listed in Table 8.1.

In table 8.1, the maximum net deflection of the slab at ultimate load f_{umax} is the difference between the deflection in the middle point of the line connecting two loading centres and the average translation of the supports measured in the middle of the four supporting sides.

The total membrane forces T_{um} are the sum of the tensile forces of the 8 connecting steel rods at failure. In all the tests, the resultant tensile forces in E–W direction were larger than those in S–N direction. In each direction, the lower connecting steel rods were subjected to larger tensile forces than those in the upper ones. In load pattern 1, the symmetry only existed in S–N direction. In E–W direction, the connecting steel rods in the South took larger membrane forces than those in the North, which was

valid for both upper and lower rods.

Test No.	A_s (mm^2/mm)	ρ (%)	$f_{0.2}$ (MPa)	f_{su} (MPa)	f_c (MPa)	f_{umax} (mm)	T_{um} (kN)	P_u (kN)	load ptn	failure type*
MAT-1	12.57/150	0.1822	684.9	727.7	22.83	37.90	283.52	32.38	1	P.L.B
MAT-2	12.57/150	0.1822	684.9	727.7	26.83	32.02	246.02	32.41	1	P.L.B
MAT-3	12.57/150	0.1822	684.9	727.7	21.93	26.51	189.76	24.65	2	P.L.B
MAT-4	28.27/300	0.2142	539.7	640.3	25.58	60.89	354.89	29.67	2	B.
MAT-5	28.27/300	0.2142	539.7	640.3	23.36	40.82	291.32	30.35	1	P.L.B
MAT-6	28.27/300	0.2142	539.7	640.3	26.35	49.29	349.67	33.42	1	B.
MAT-7	28.27/300	0.2142	539.7	640.3	32.38	52.44	387.13	35.30	1	B.
MAT-8	28.27/300	0.2142	539.7	640.3	27.97	56.42	360.03	32.42	2	B
MAT-9	28.27/300	0.2142	539.7	640.3	36.75	47.82	359.31	34.83	2	B.
MAT-10	28.27/300	0.2142	539.7	640.3	33.98	47.34	351.04	34.33	2	P.L.B.
MAT-11	28.27/300	0.2142	539.7	640.3	36.69	44.20	343.41	35.33	1	B.
MAT-12	28.27/300	0.2142	539.7	640.3	8.41	56.56	231.65	20.63	1	B.
MAT-13	28.27/300	0.2142	539.7	640.3	8.92	61.73	236.59	21.13	2	P.L.B.
MAT-14	28.27/300	0.2142	539.7	640.3	10.95	70.25	212.25	21.17	2	B.
MAT-15	28.27/300	0.2142	539.7	640.3	43.47	60.77	362.75	32.44	2	B.
MAT-16	28.27/300	0.2142	539.7	640.3	49.24	52.90	409.38	38.82	2	P.L.B.
MAT-17	28.27/300	0.2142	539.7	640.3	48.41	48.15	371.15	35.86	1	B.
MAT-18	28.27/200	0.3213	539.7	640.3	8.98	74.22	222.68	24.5	1	B.
MAT-19	28.27/200	0.3213	539.7	640.3	21.82	52.19	269.57	30.99	1	P.L.B.
MAT-20	28.27/200	0.3213	539.7	640.3	31.66	44.55	310.76	36.78	1	P.L.B.
MAT-21	28.27/200	0.3213	539.7	640.3	38.16	47.87	305.10	39.33	1	P.L.B.
MAT-22	28.27/200	0.3213	539.7	640.3	32.61	55.69	308.43	36.90	1	P.L.B.

Table 8.1 Test Results

*P.L.B.: punching like–bending
B: bending
ptn: pattern

The loading–maximum deflection curves, the relationships between loading and corresponding membrane forces and the membrane forces – maximum deflection curves are shown in Fig. 8.1 , Fig. 8.2 and Fig. 8.3 respectively.

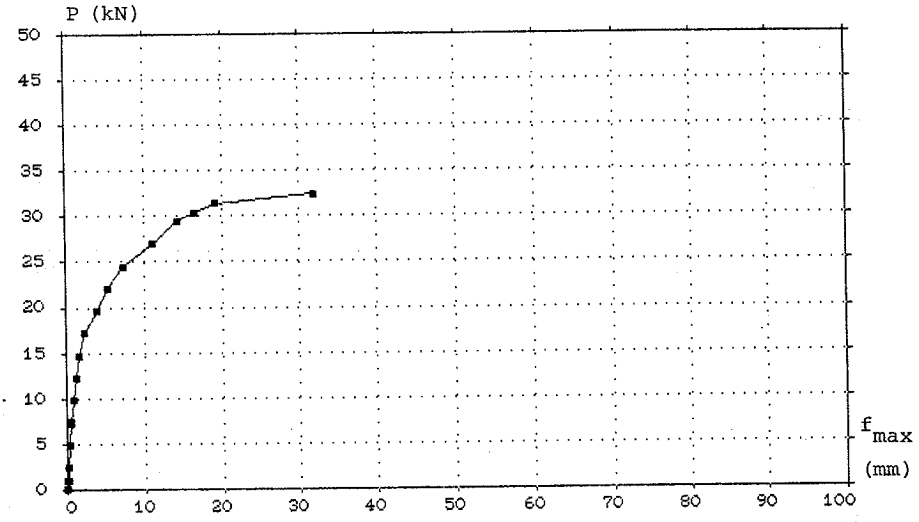

Figure 8.1 MAT–2.

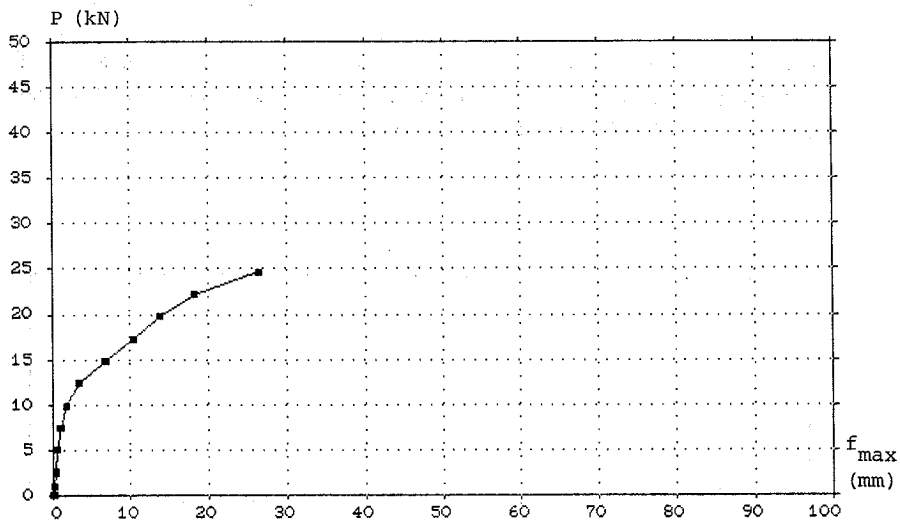

Figure 8.2 MAT–3.

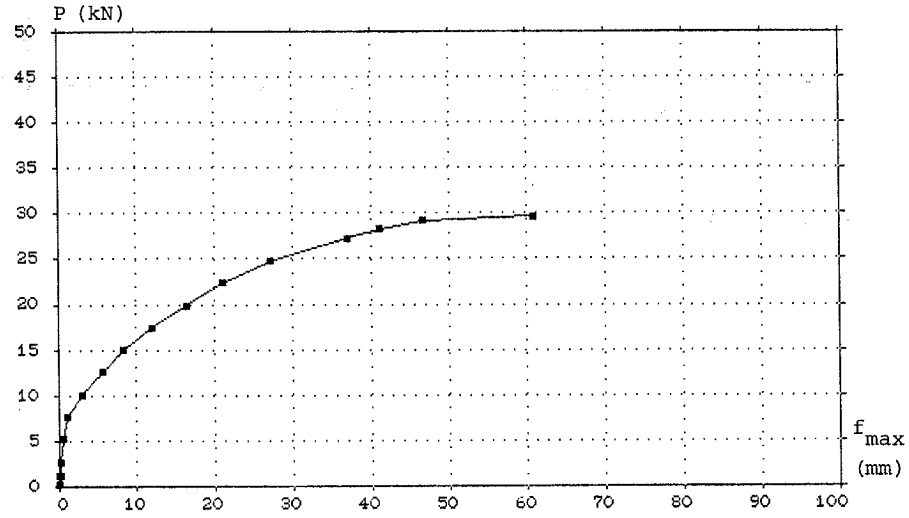

Figure 8.3 MAT–4.

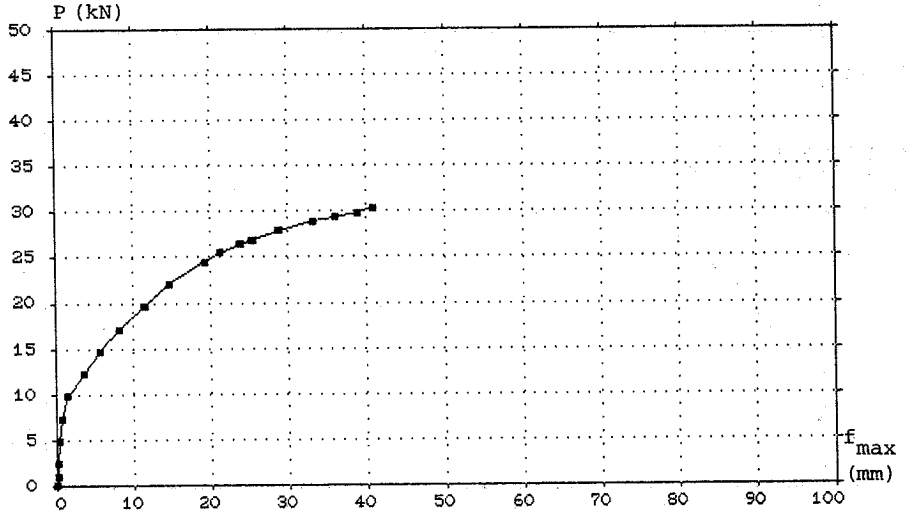

Figure 8.4 MAT–5.

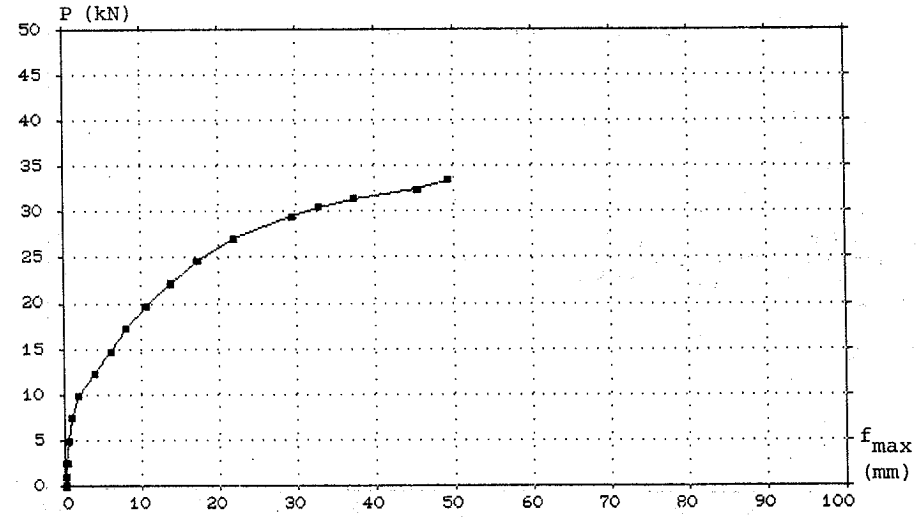

Figure 8.5 MAT–6.

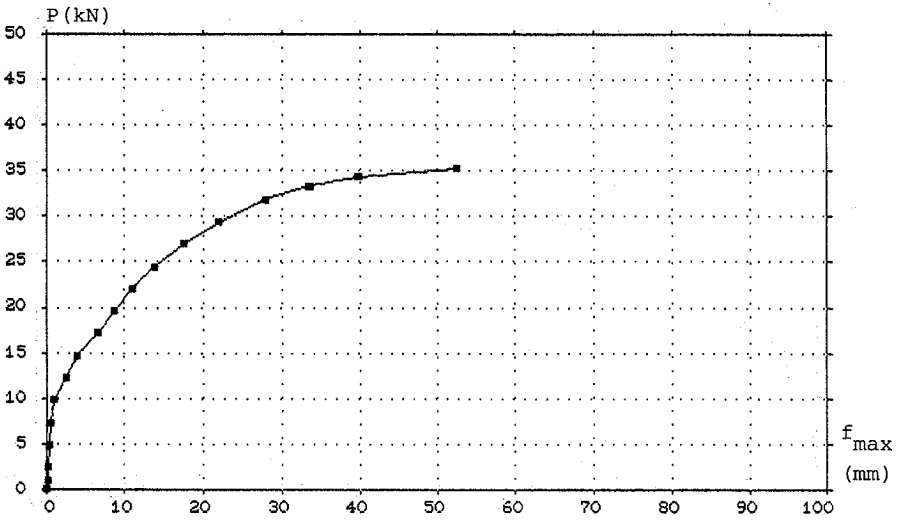

Figure 8.6 MAT–7.

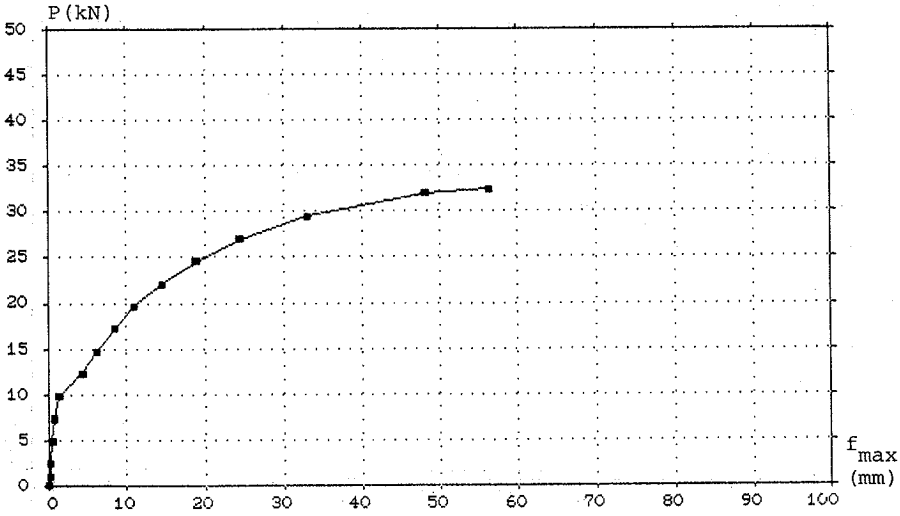

Figure 8.7 MAT–8.

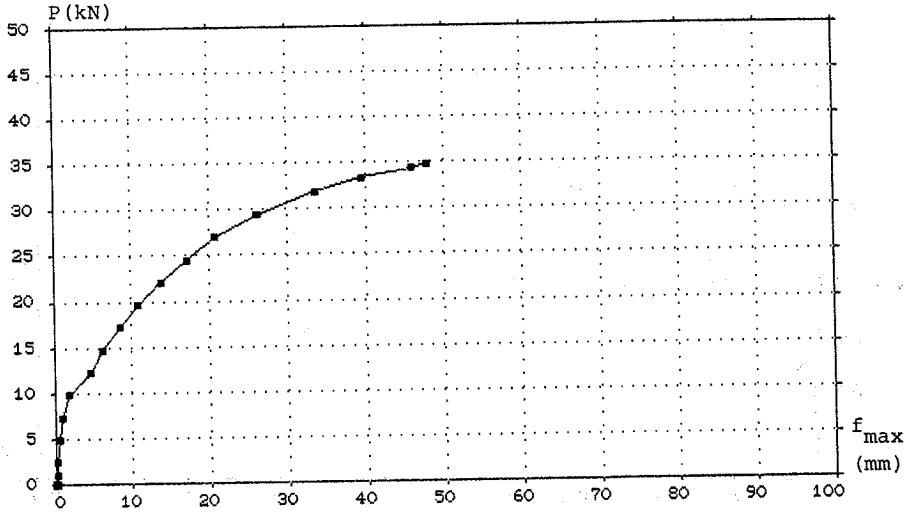

Figure 8.8 MAT–9.

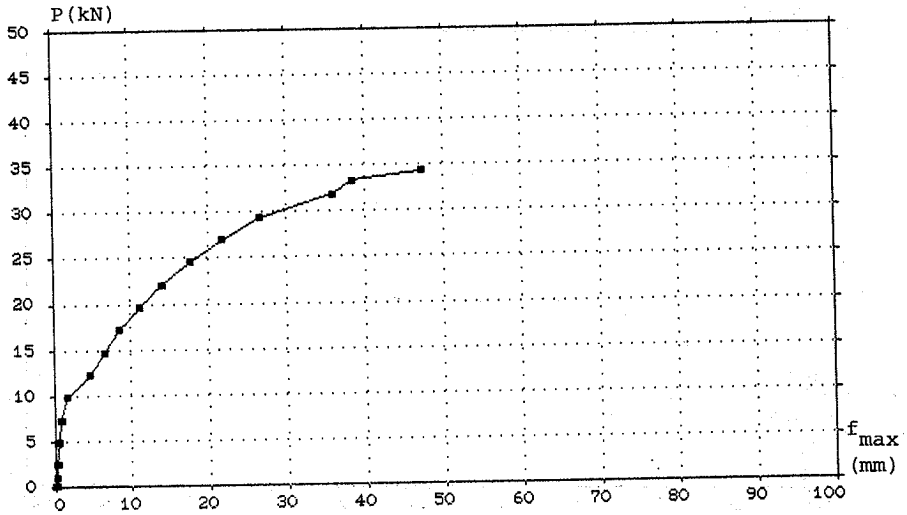

Figure 8.9 MAT–10.

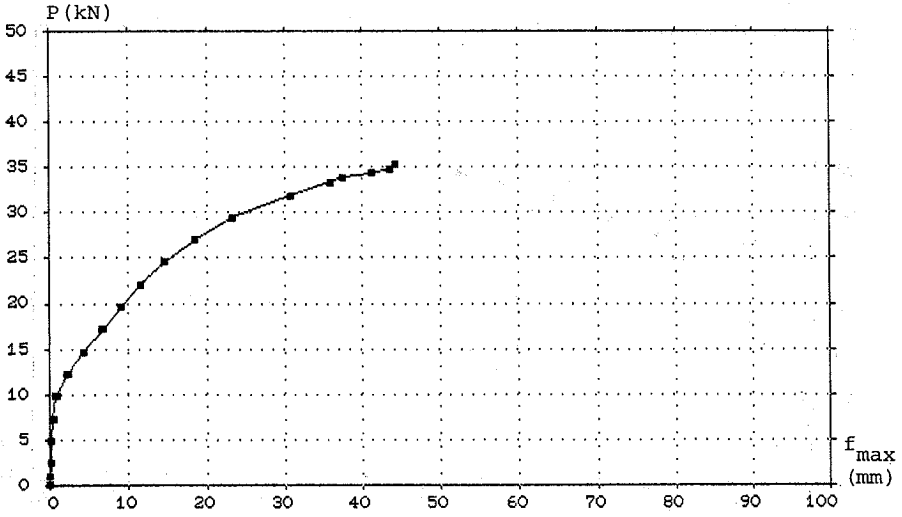

Figure 8.10 MAT–11.

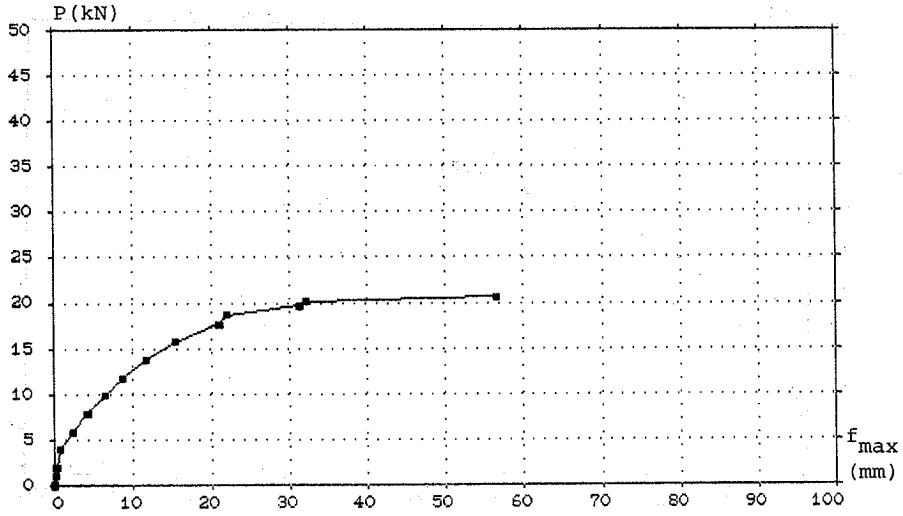

Figure 8.11 MAT–12.

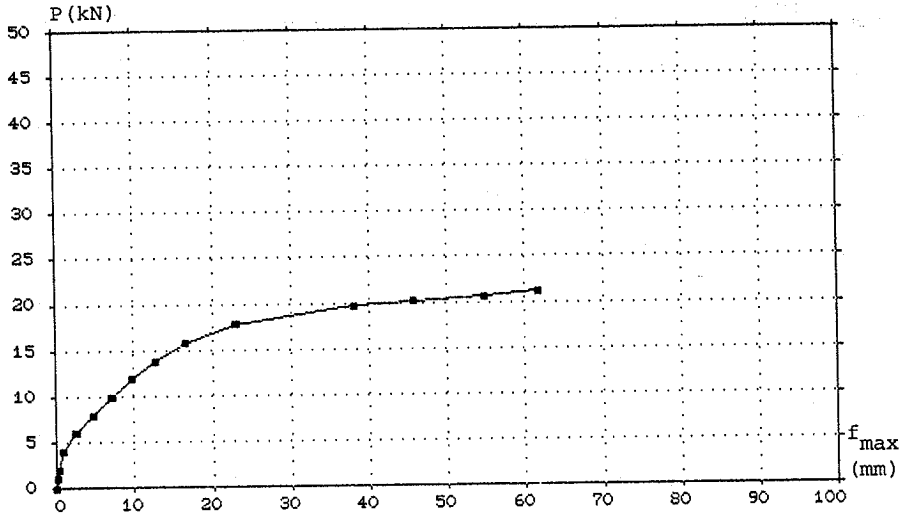

Figure 8.12 MAT–13.

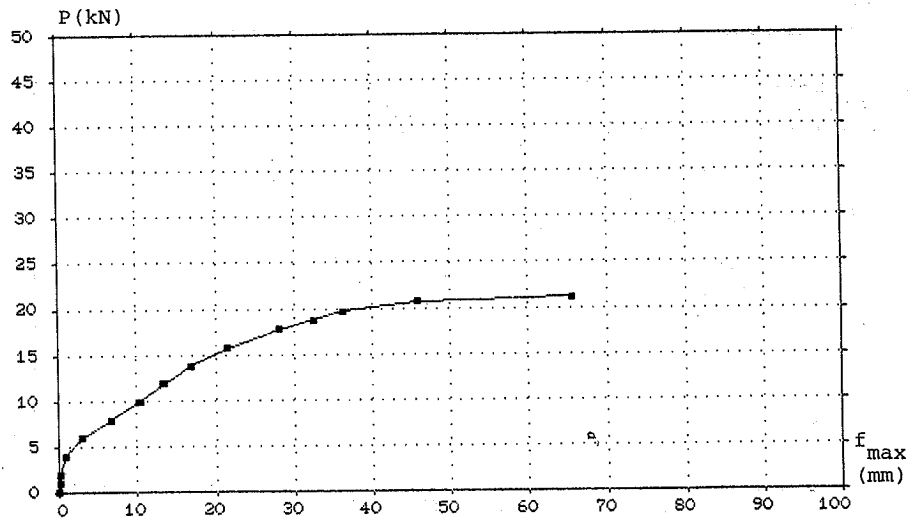

Figure 8.13 MAT–14.

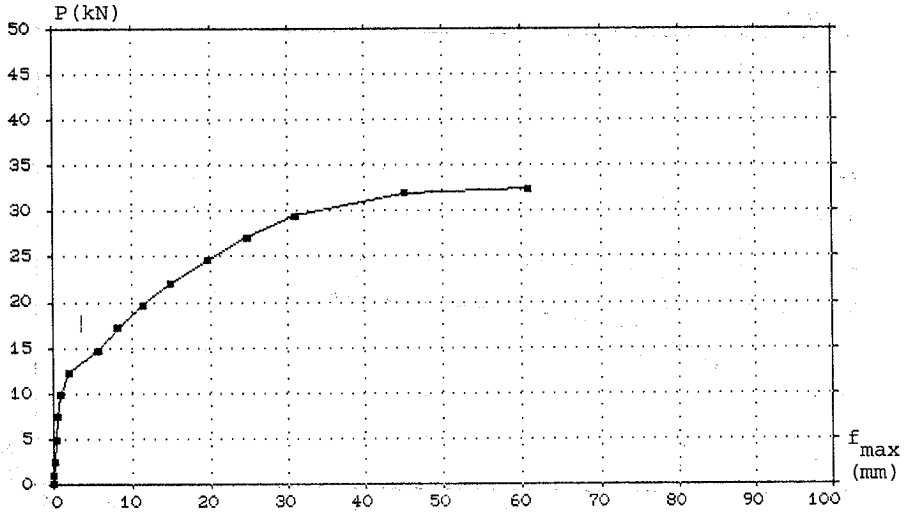

Figure 8.14 MAT–15.

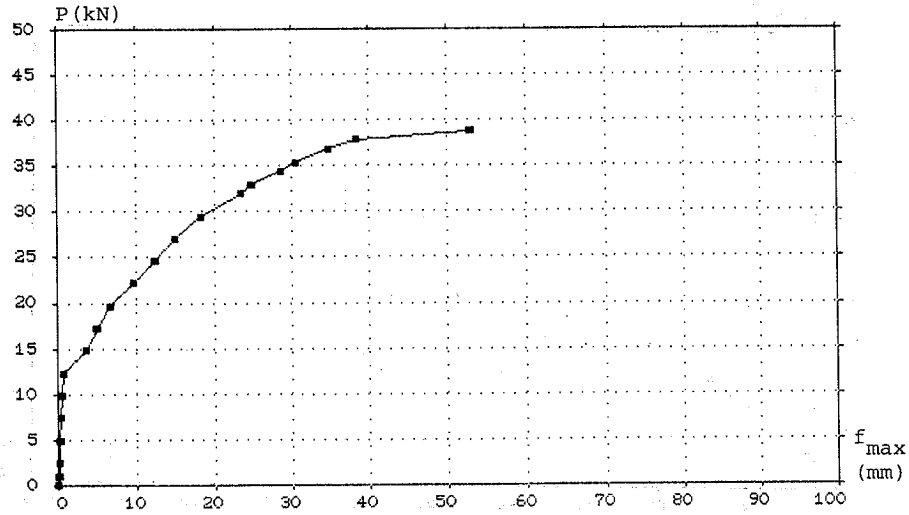

Figure 8.15 MAT–16.

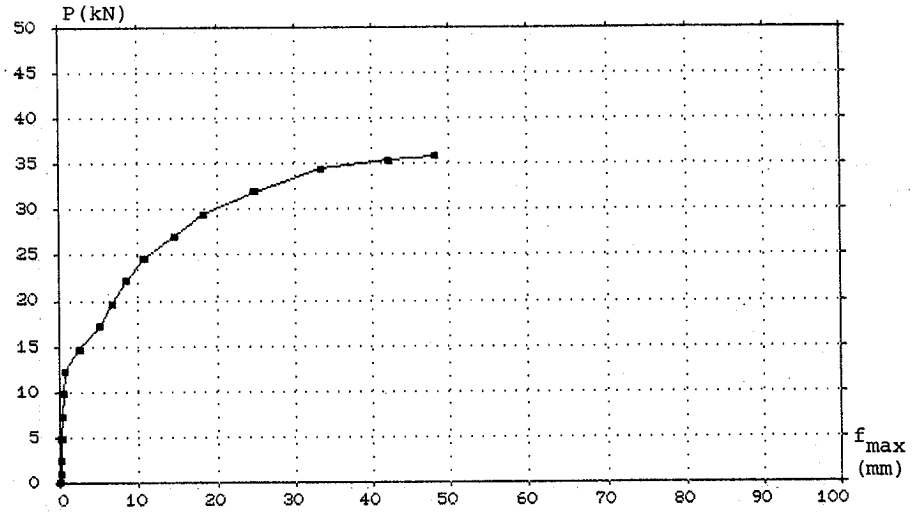

Figure 8.16 MAT–17.

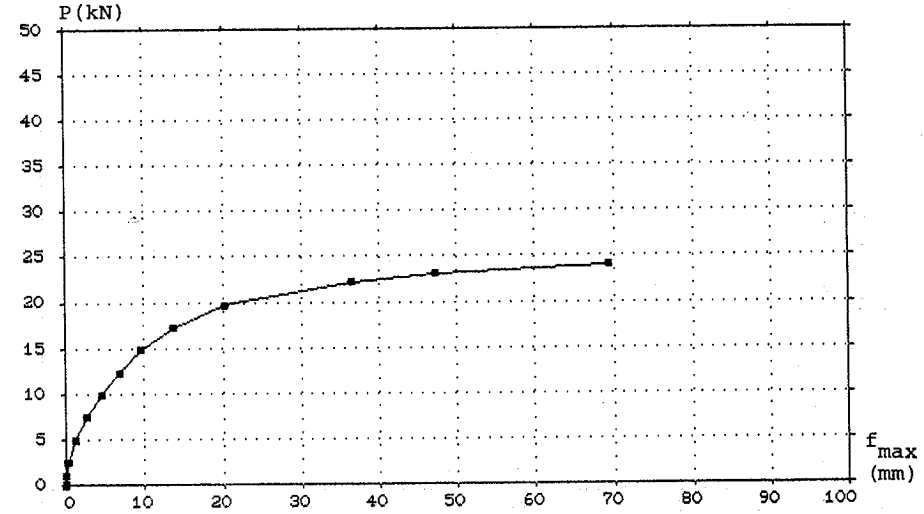

Figure 8.17 MAT–18.

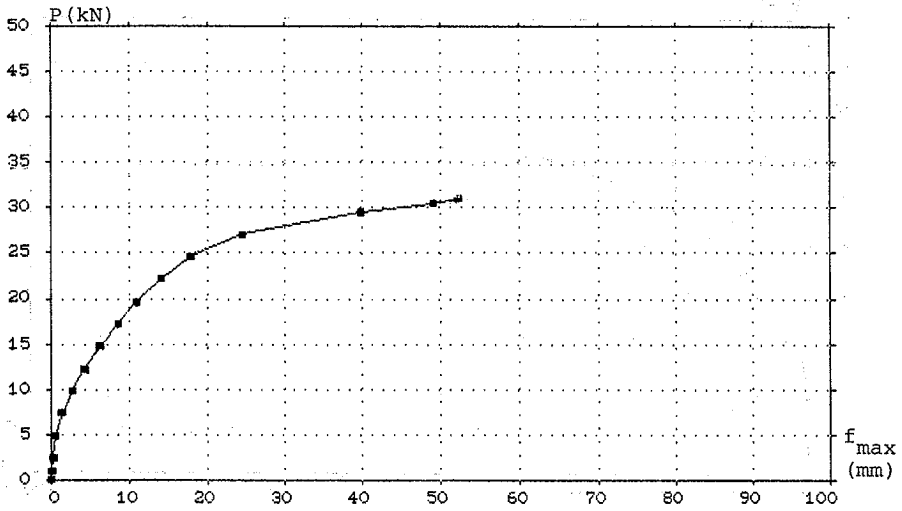

Figure 8.18 MAT–19.

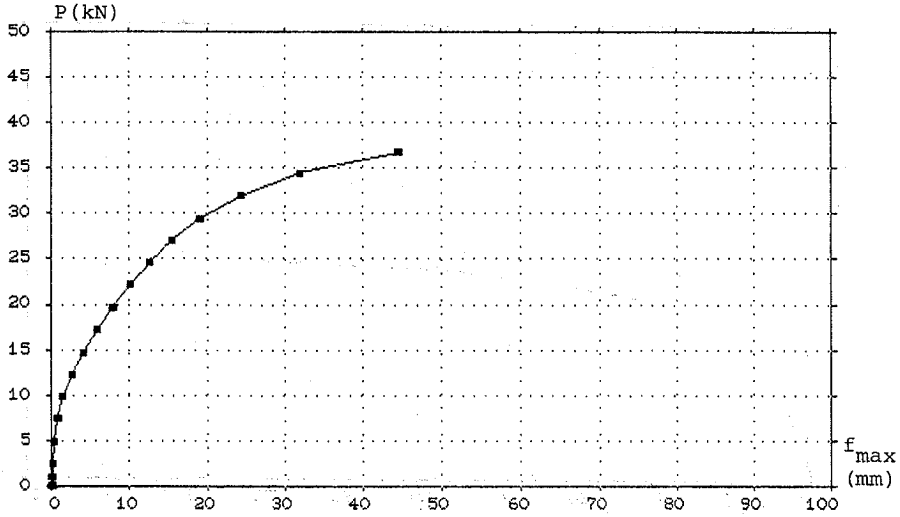

Figure 8.19 MAT–20.

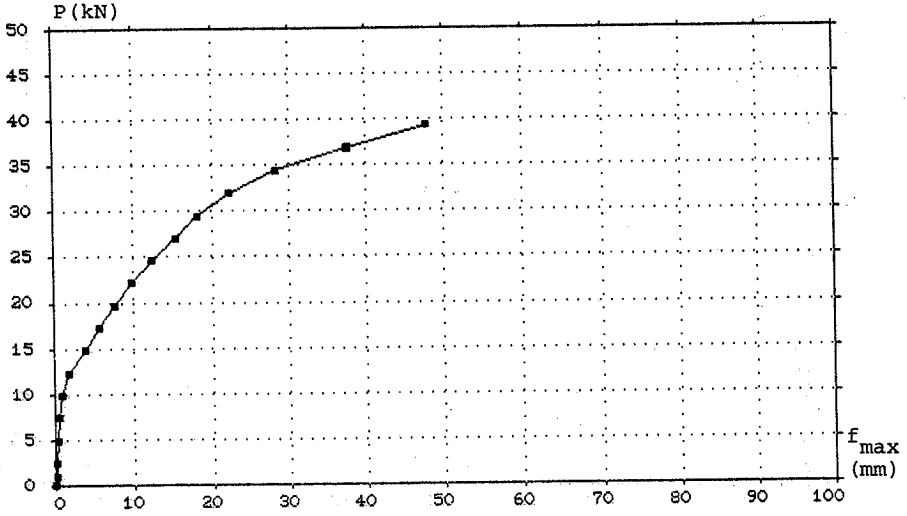

Figure 8.20 MAT–21.

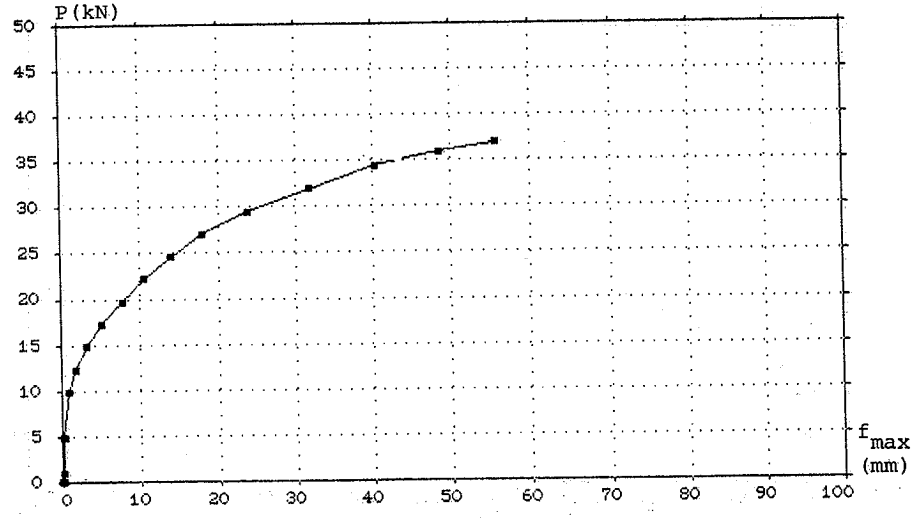

Figure 8.21 MAT–22.

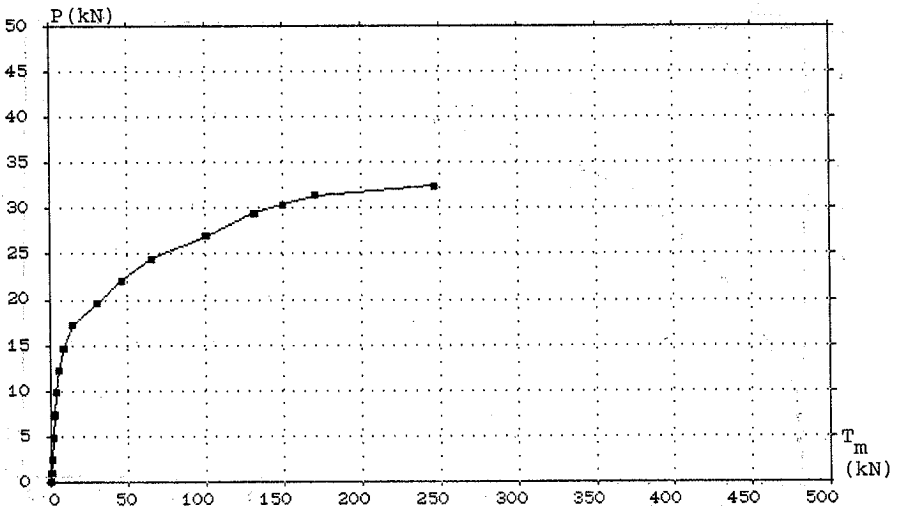

Figure 8.22 MAT–2.

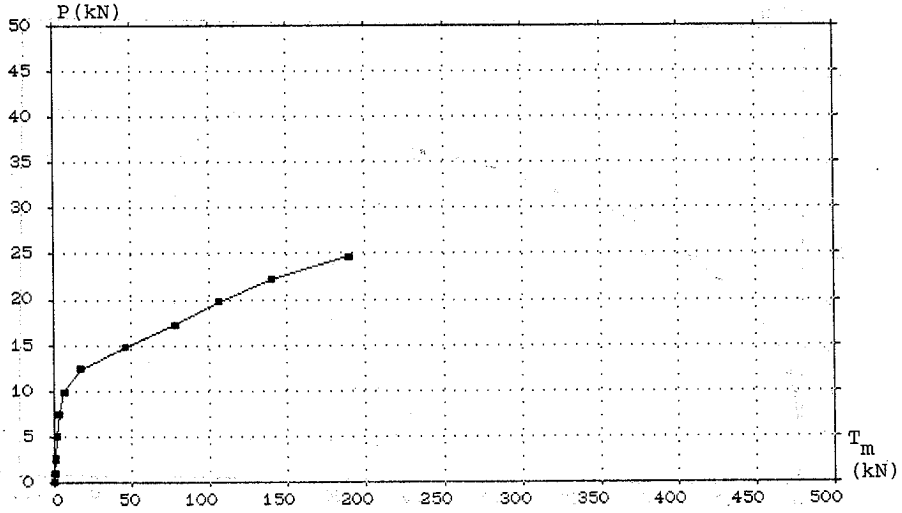

Figure 8.23 MAT–3.

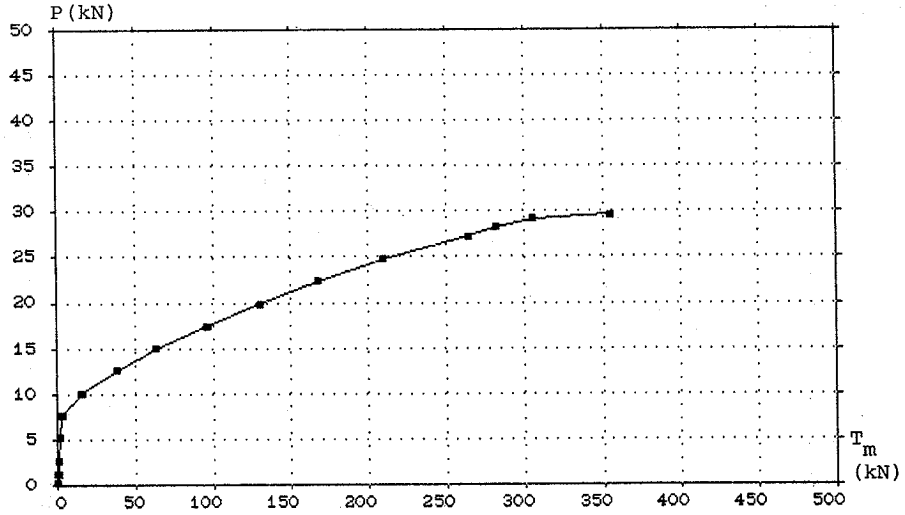

Figure 8.24 MAT–4.

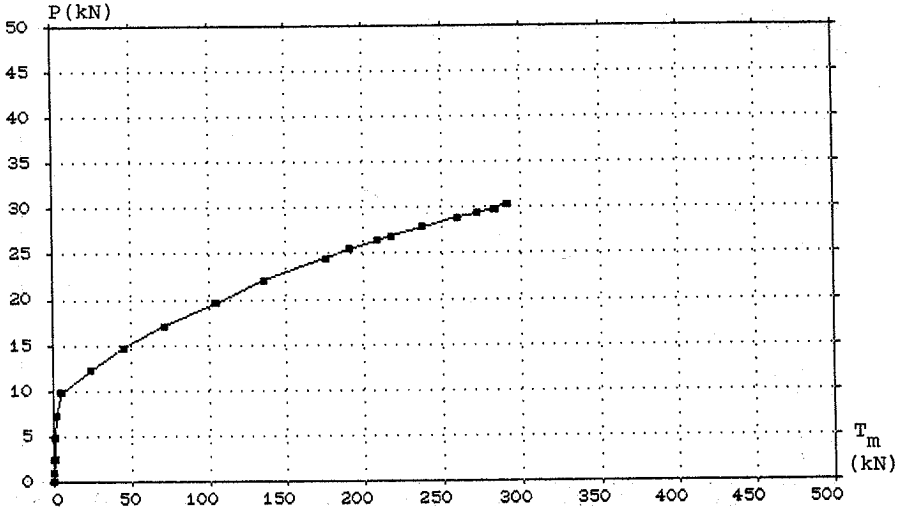

Figure 8.25 MAT–5.

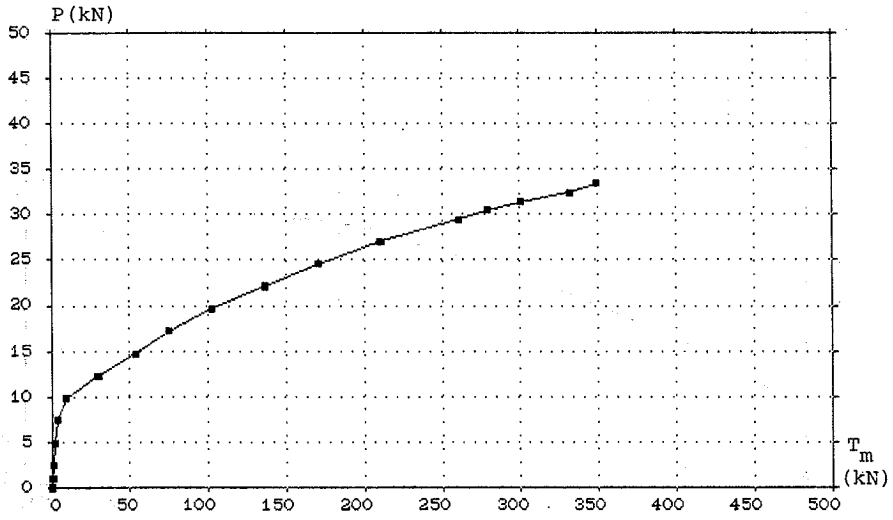

Figure 8.26 MAT–6.

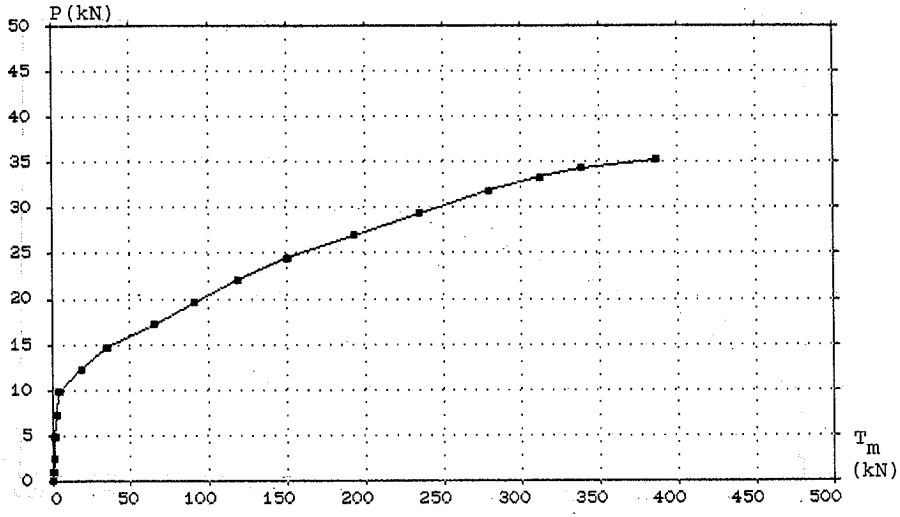

Figure 8.27 MAT–7.

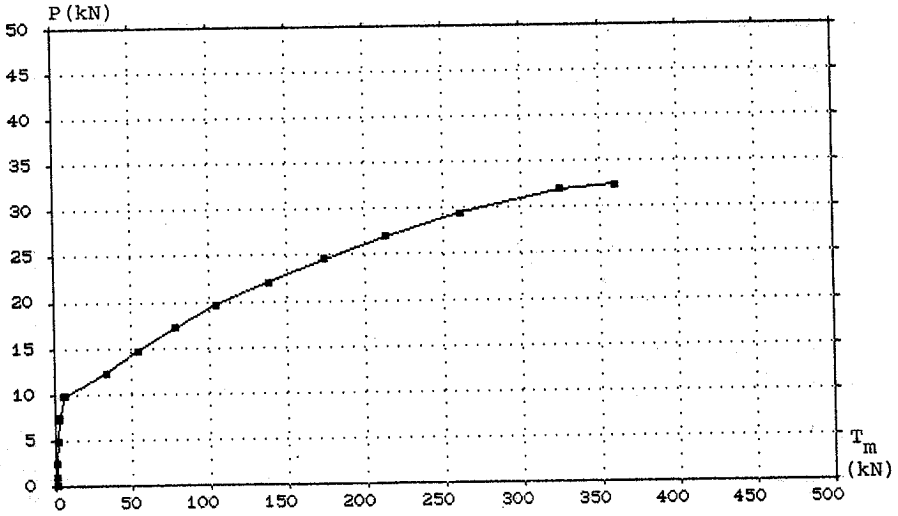

Figure 8.28 MAT–8.

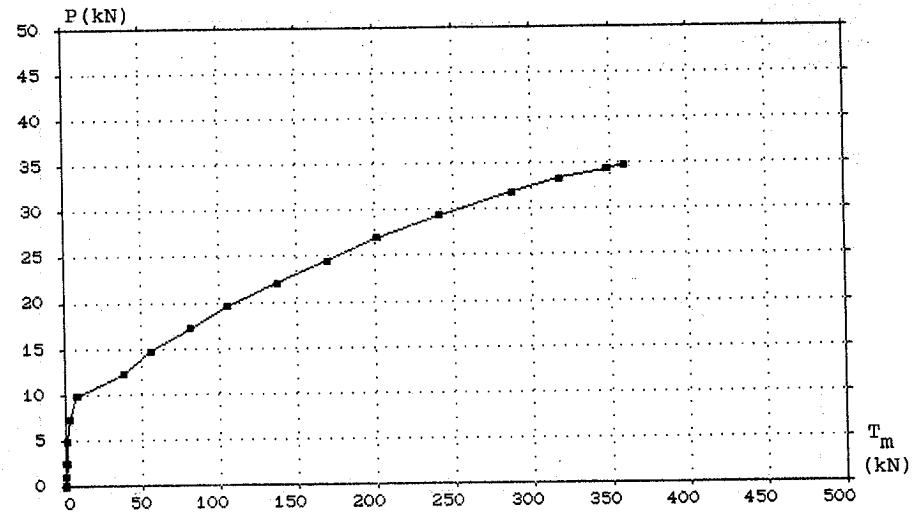

Figure 8.29 MAT–9.

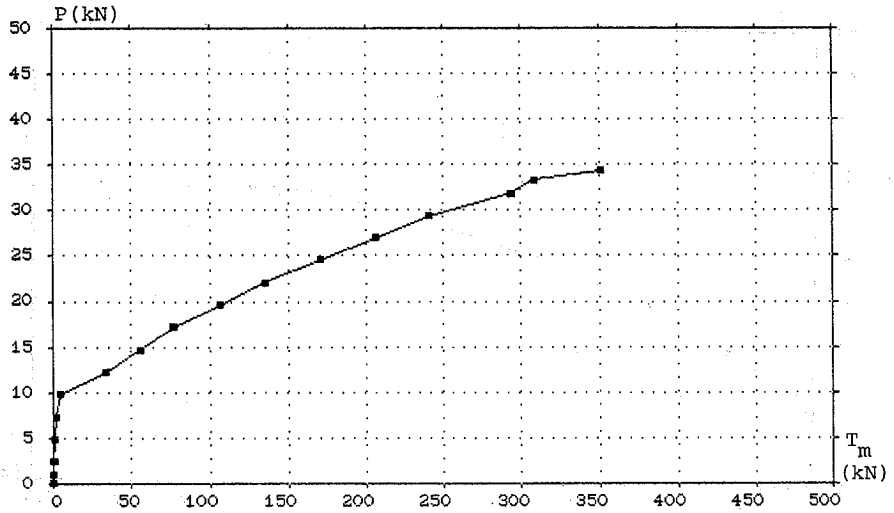

Figure 8.30 MAT–10.

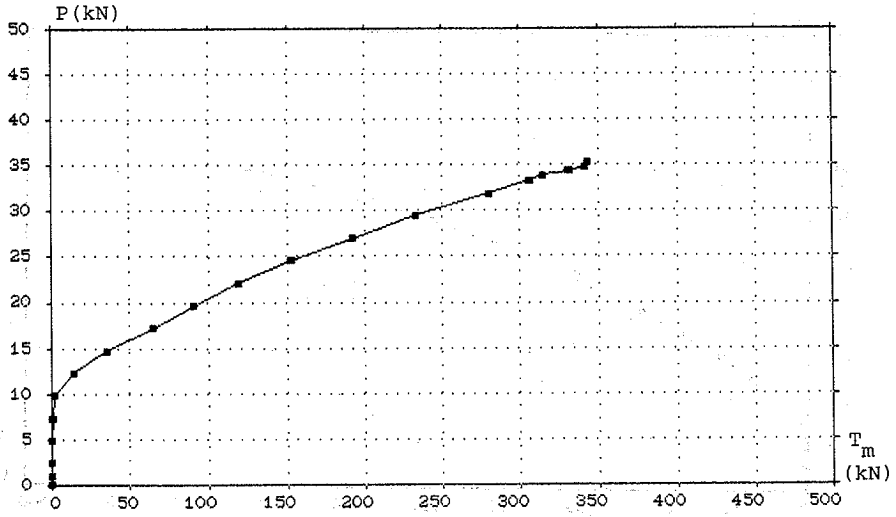

Figure 8.31 MAT–11.

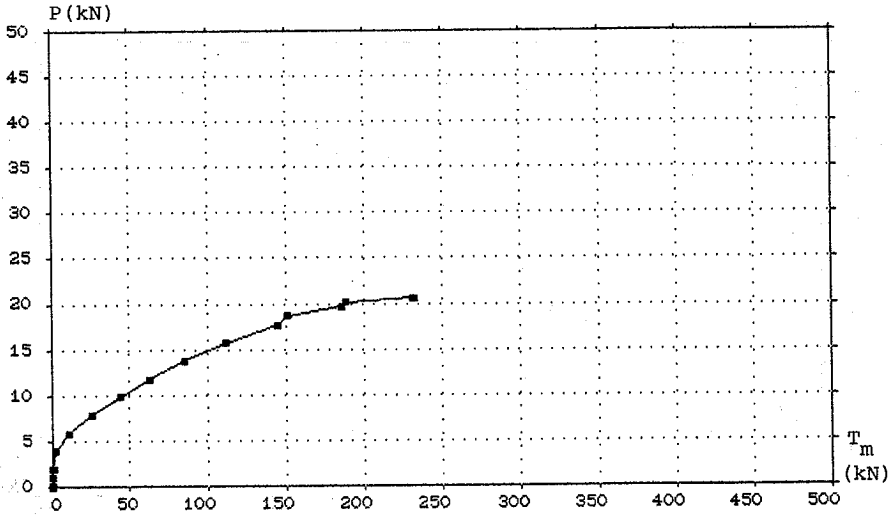

Figure 8.32 MAT–12.

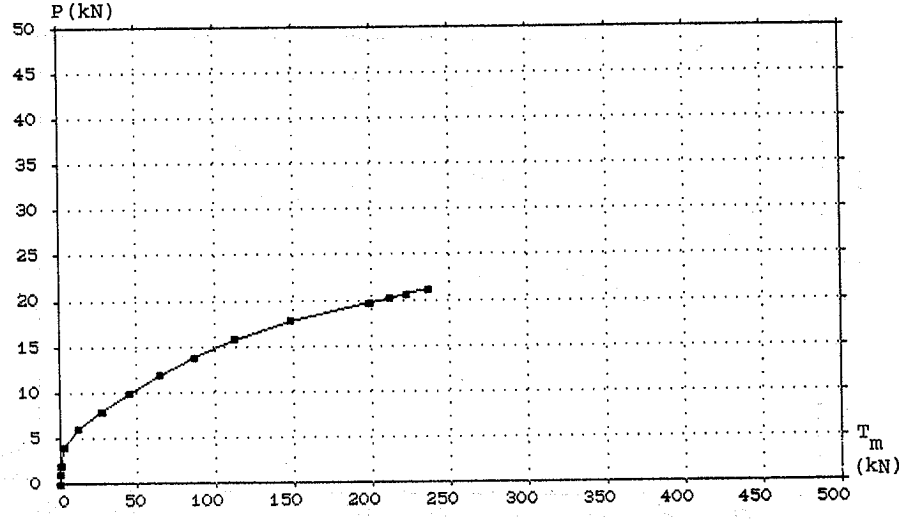

Figure 8.33 MAT–13.

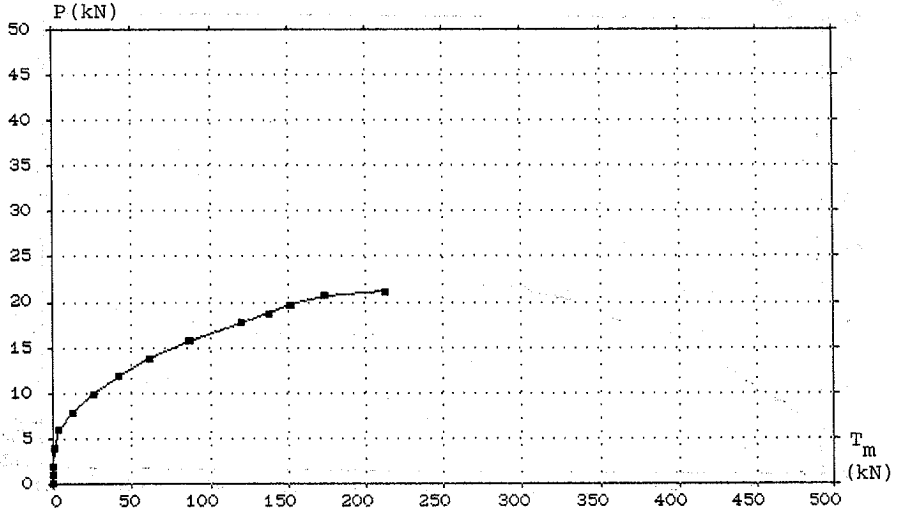

Figure 8.34 MAT–14.

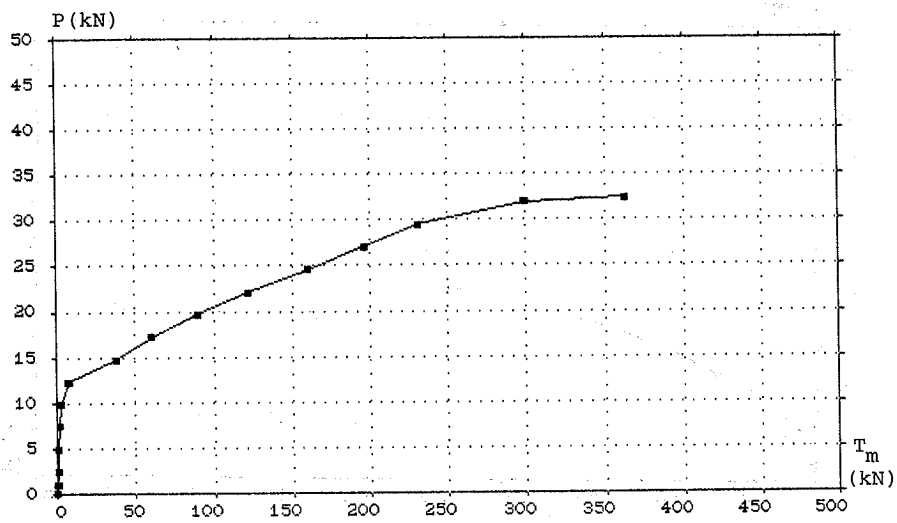

Figure 35 MAT–15.

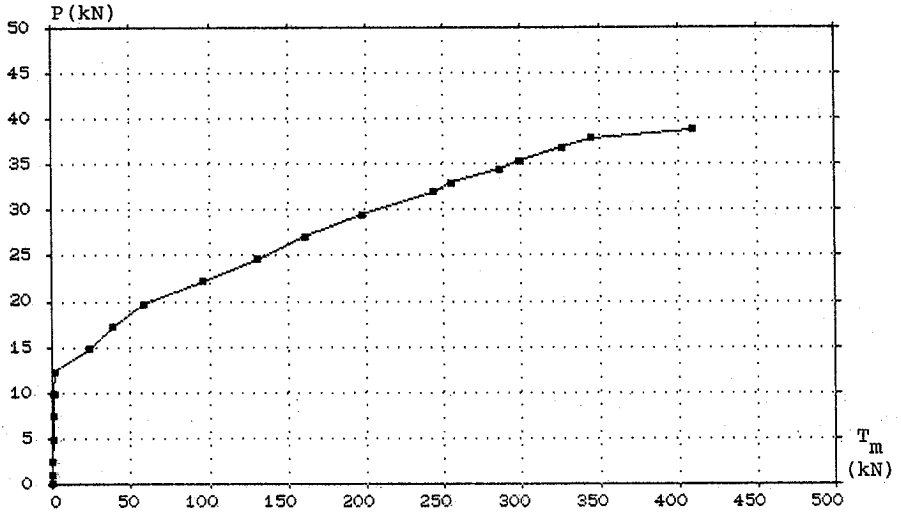

Figure 8.36 MAT–16.

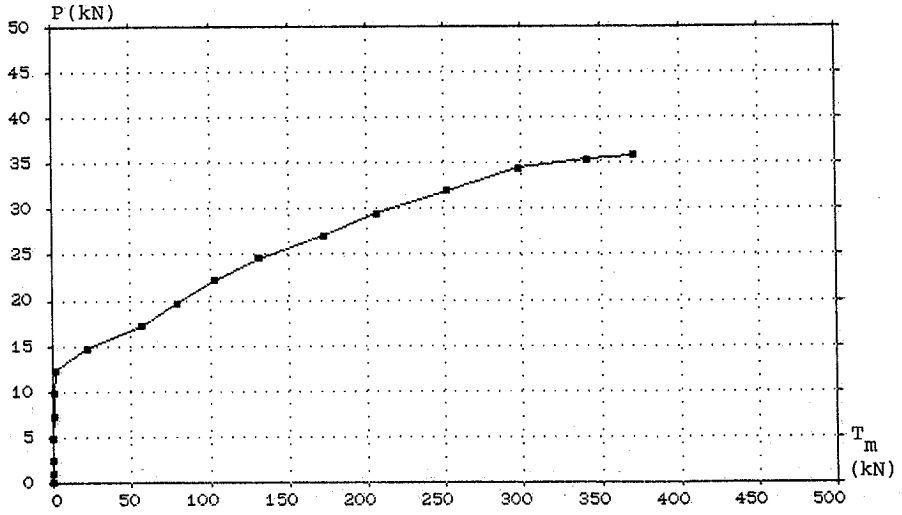

Figure 8.37 MAT–17.

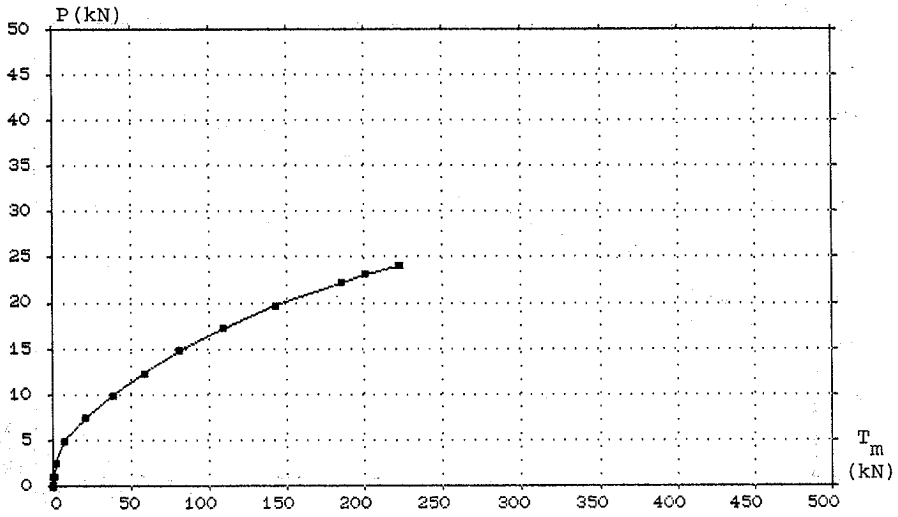

Figure 8.38 MAT–18.

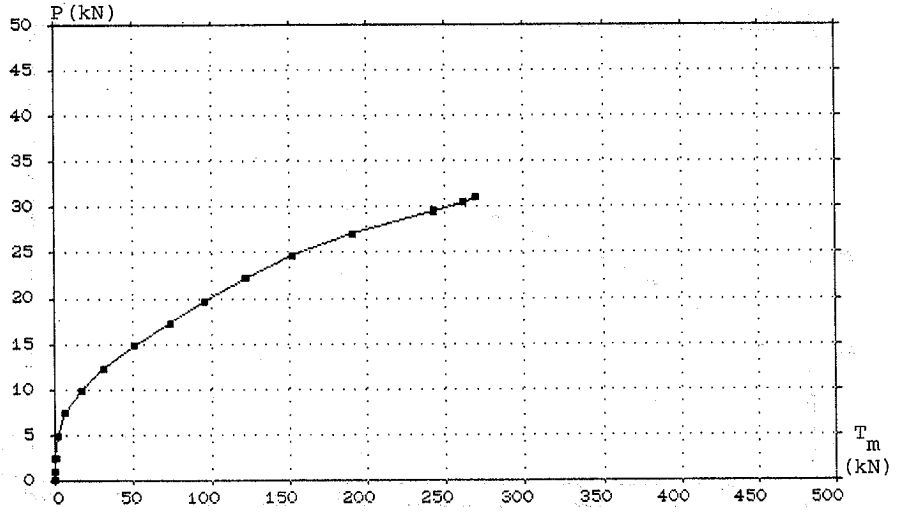

Figure 8.39 MAT–19.

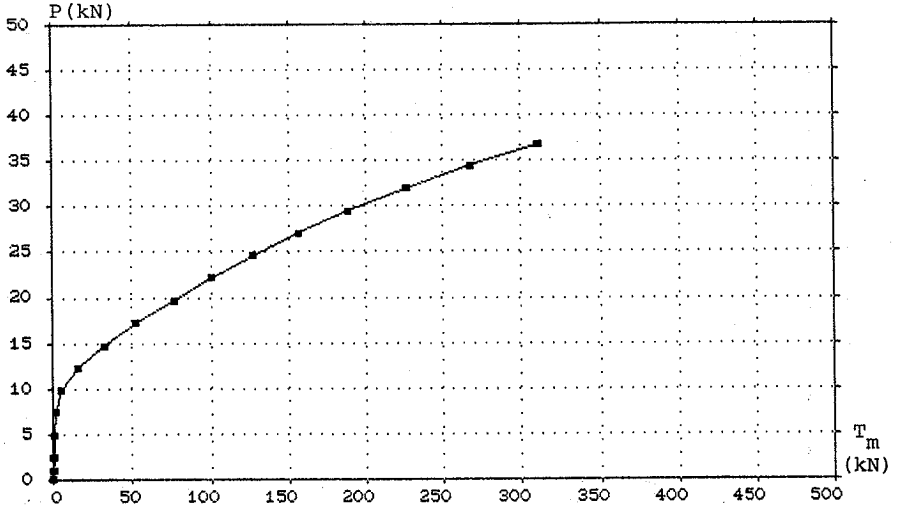

Figure 8.40 MAT–20.

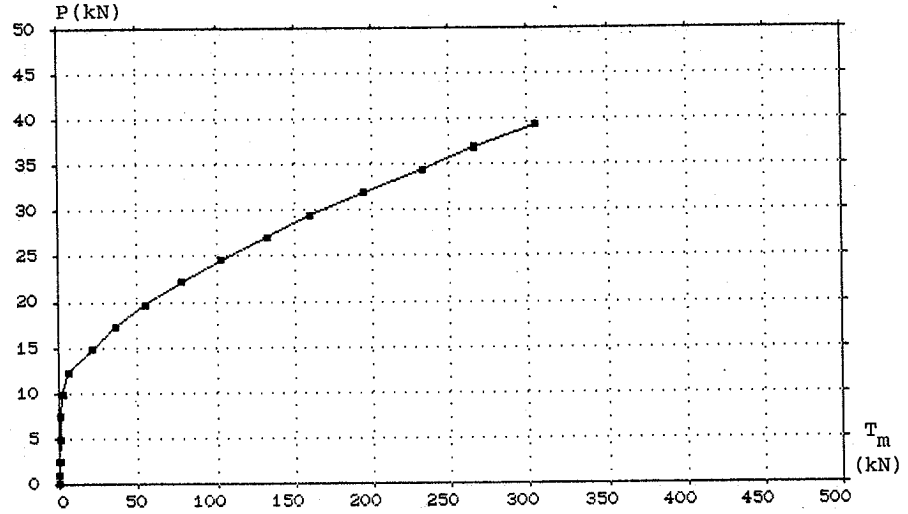

Figure 8.41 MAT–21.

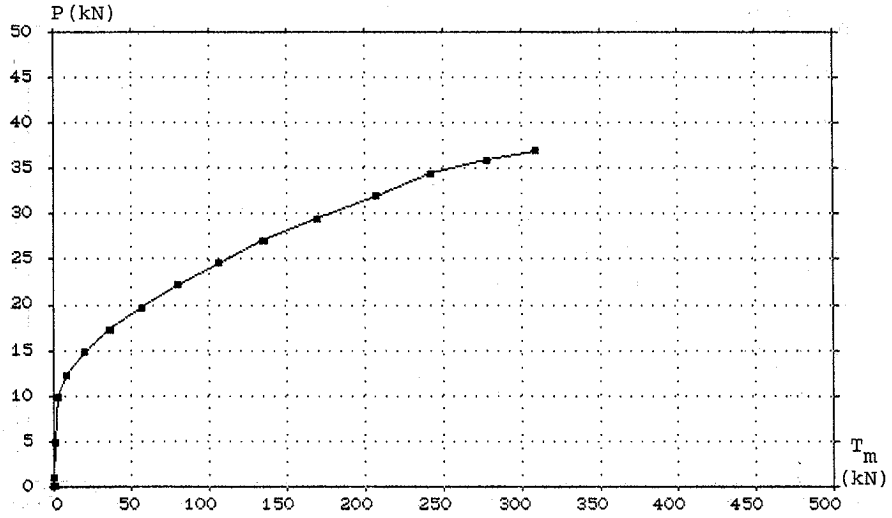

Figure 8.42 MAT–22.

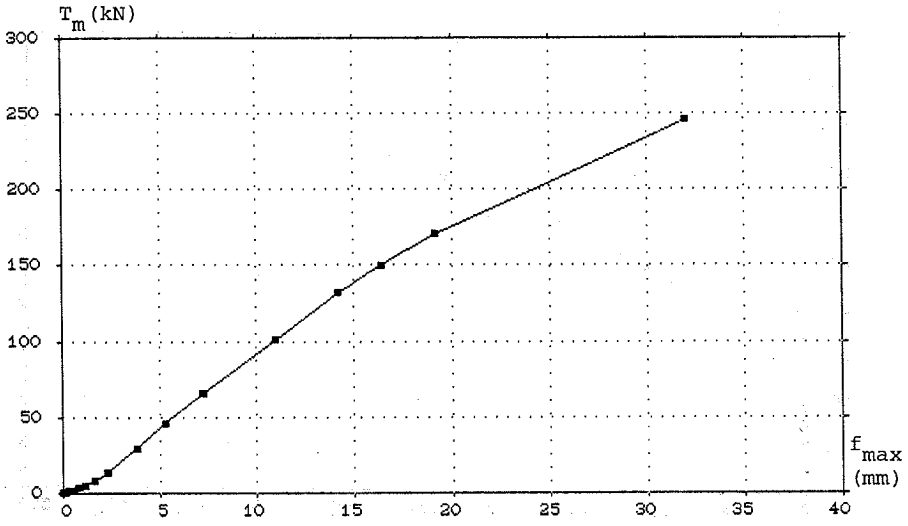

Figure 8.43 MAT–2.

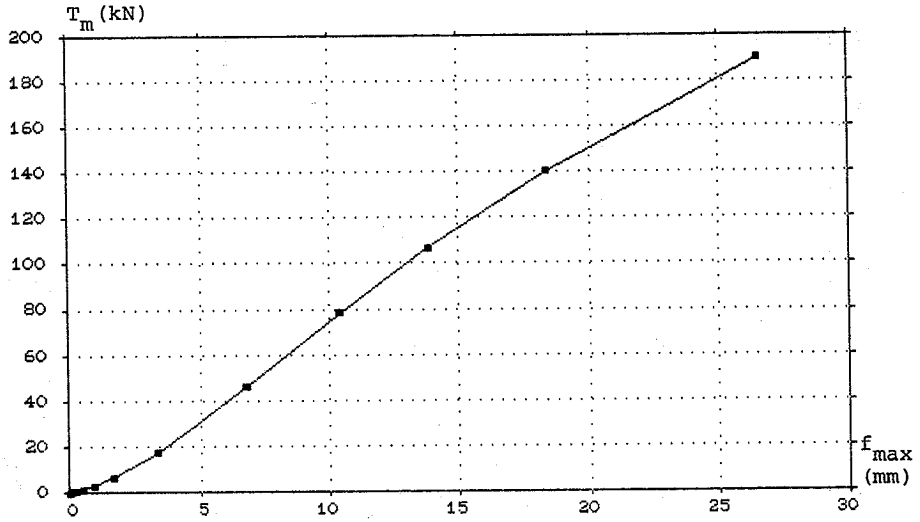

Figure 8.44 MAT–3.

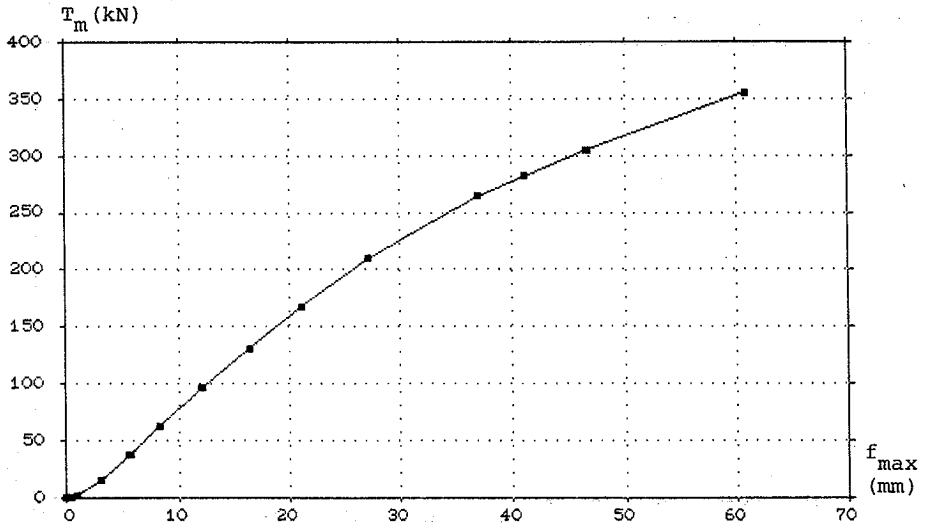

Figure 8.45 MAT–4.

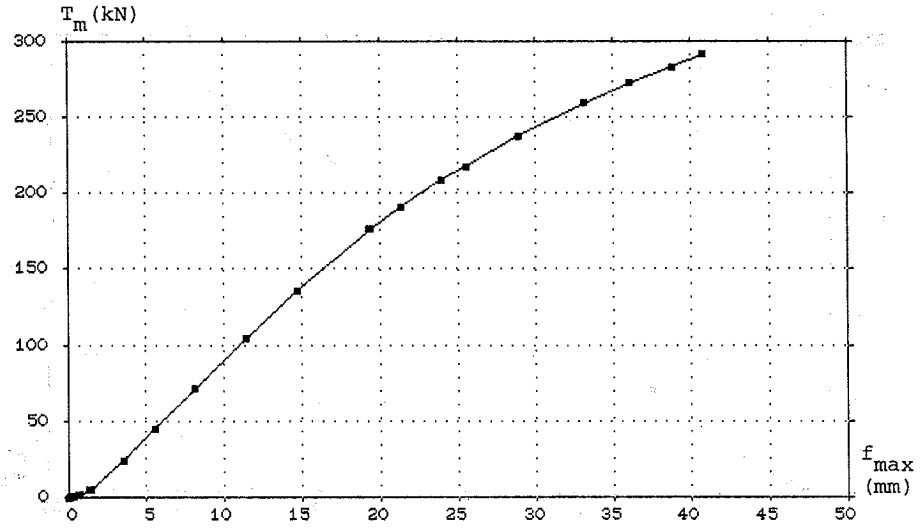

Figure 8.46 MAT–5.

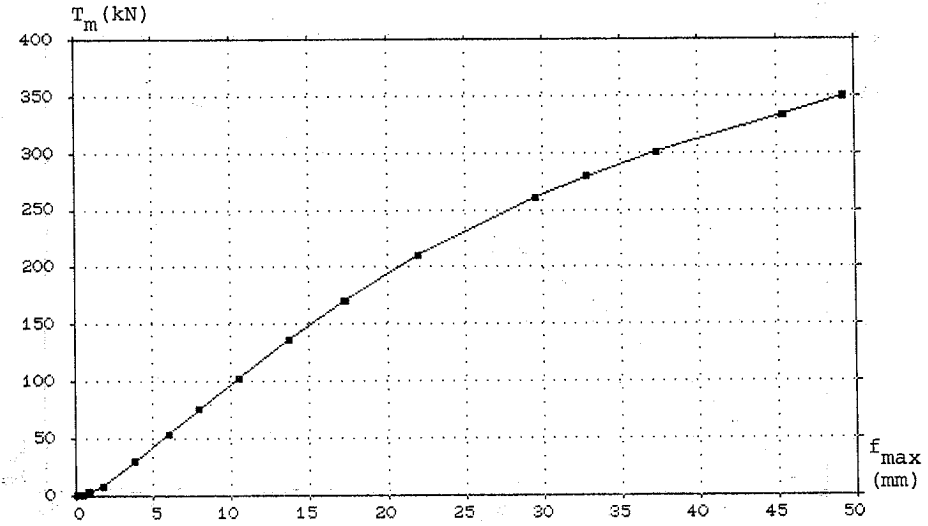

Figure 8.47 MAT–6.

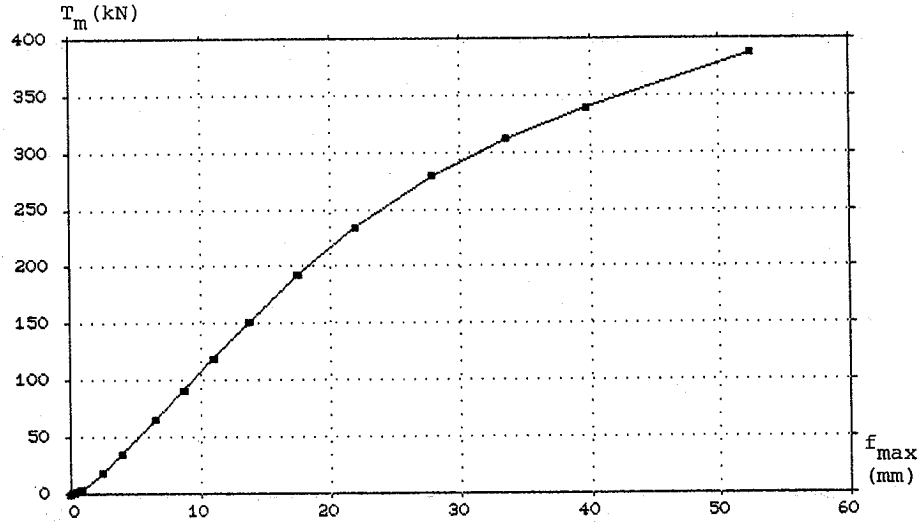

Figure 8.48 MAT–7.

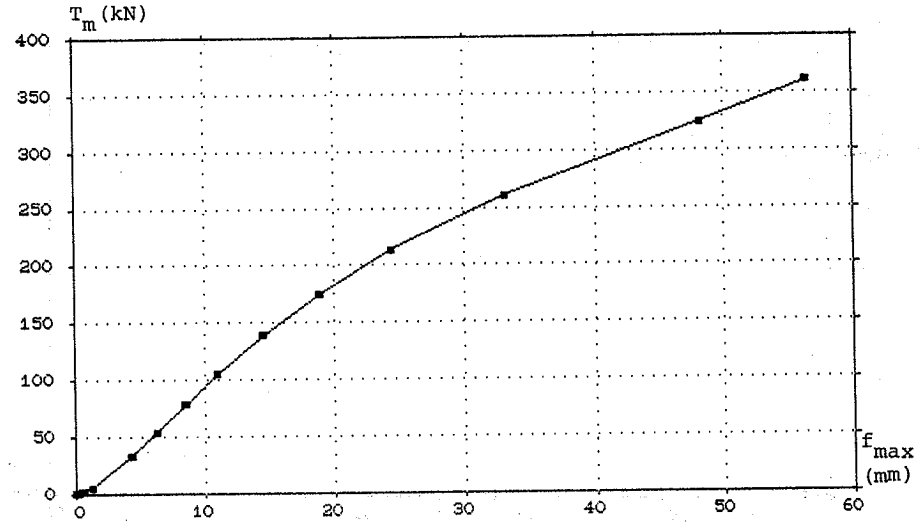

Figure 8.49 MAT–8.

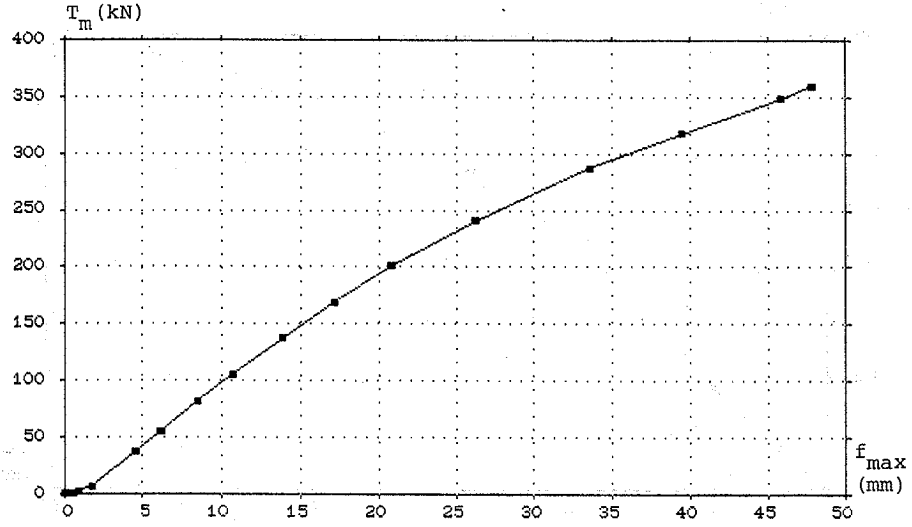

Figure 8.50 MAT–9.

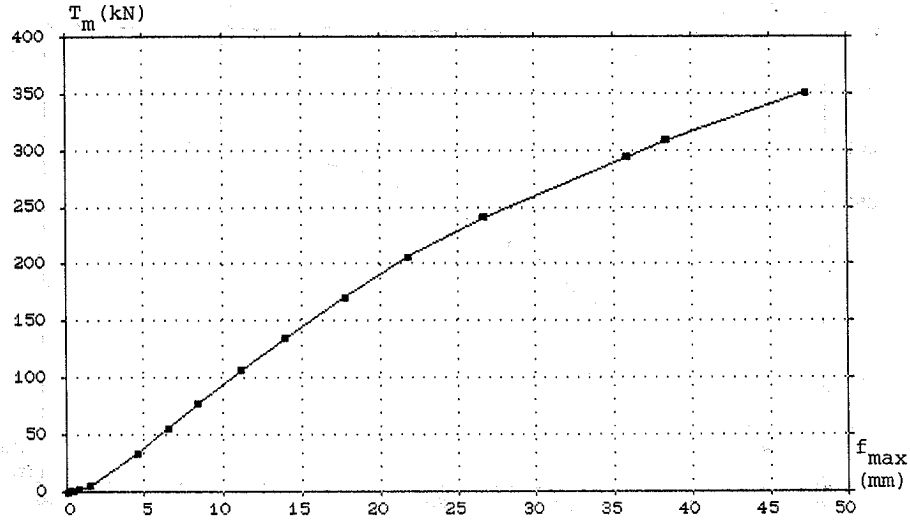

Figure 8.51 MAT–10.

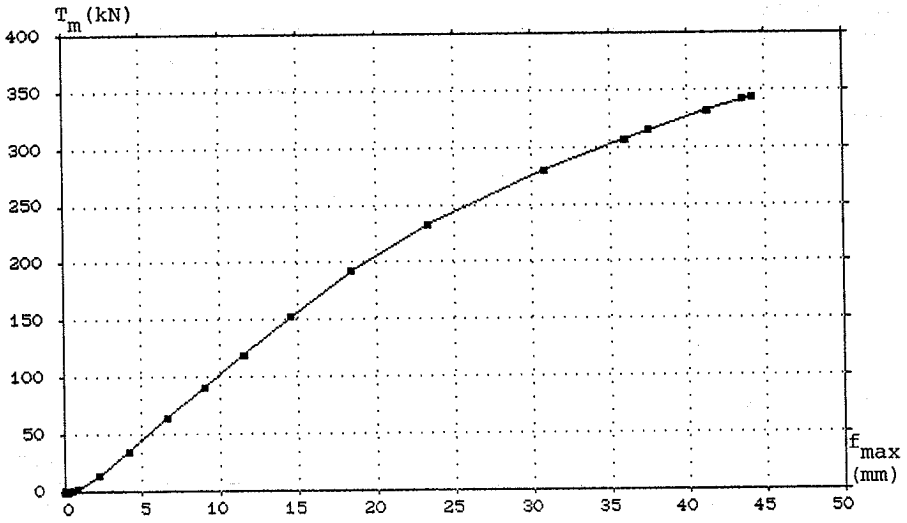

Figure 8.52 MAT–11.

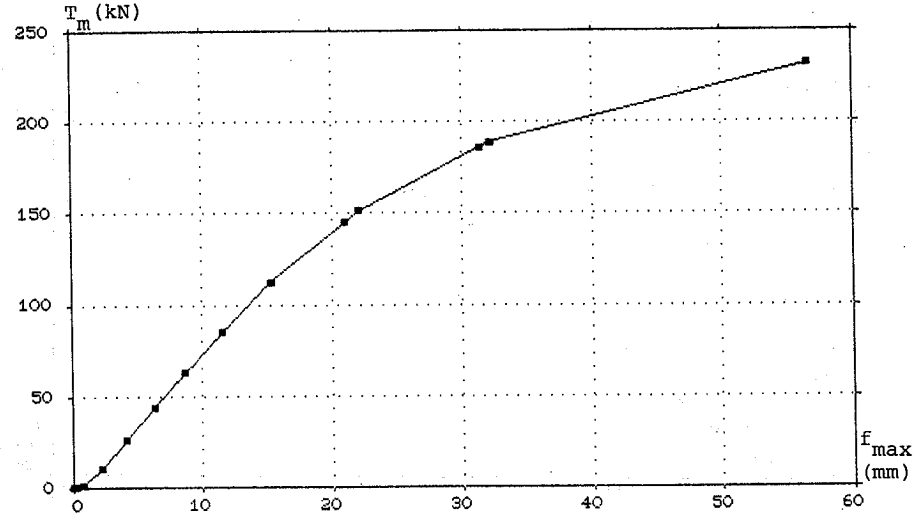

Figure 8.53 MAT–12.

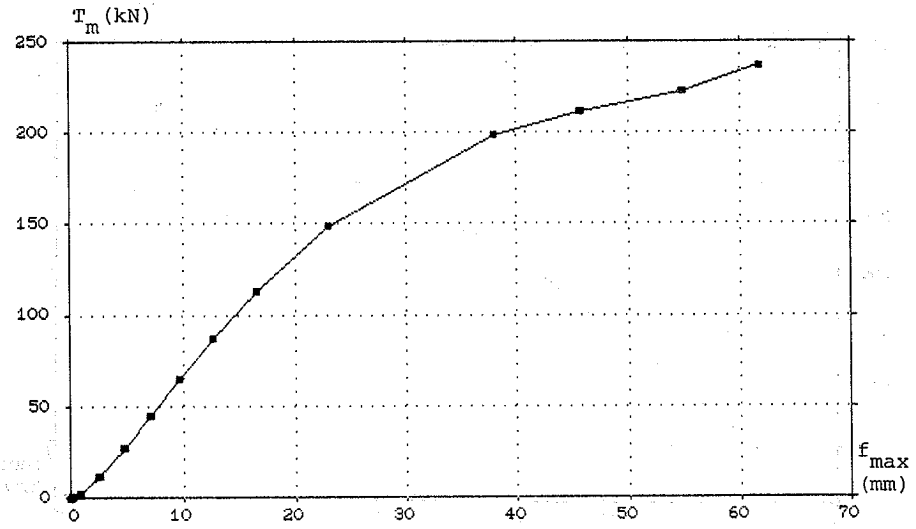

Figure 8.54 MAT–13.

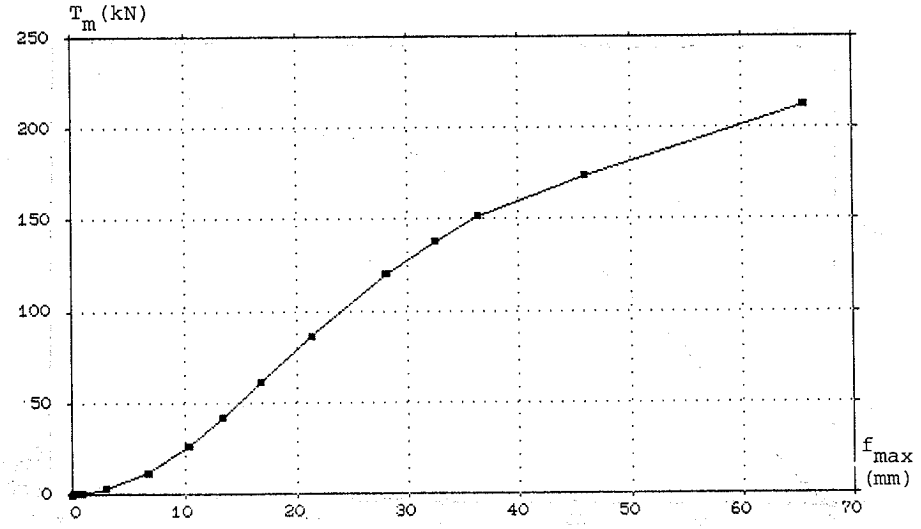

Figure 8.55 MAT–14.

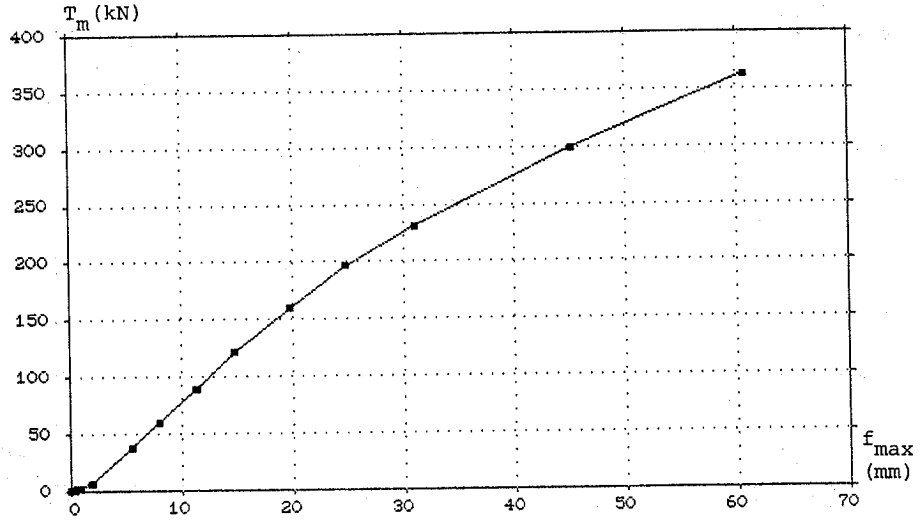

Figure 8.56 MAT–15.

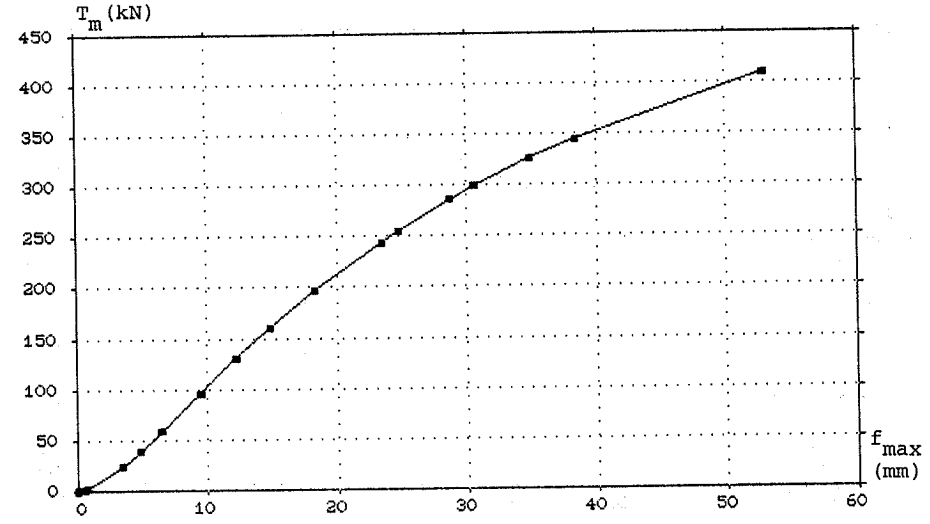

Figure 8.57 MAT–16.

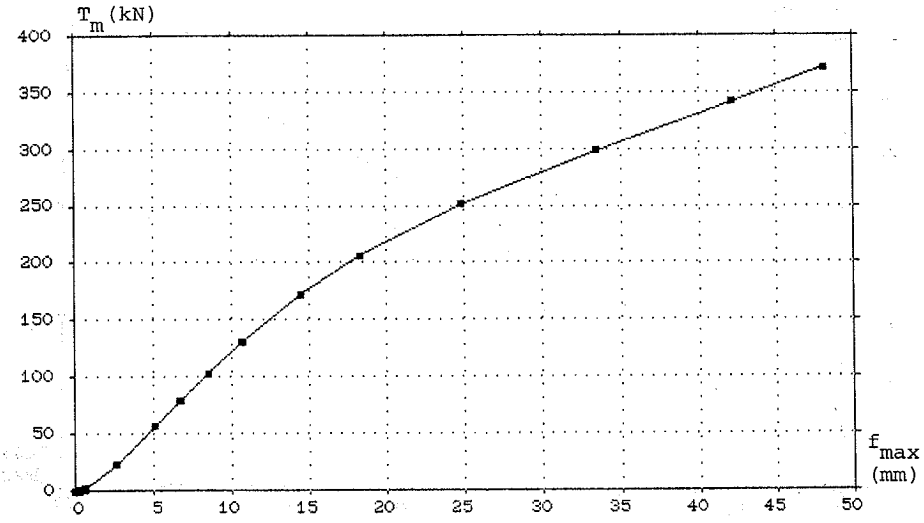

Figure 8.58 MAT–17.

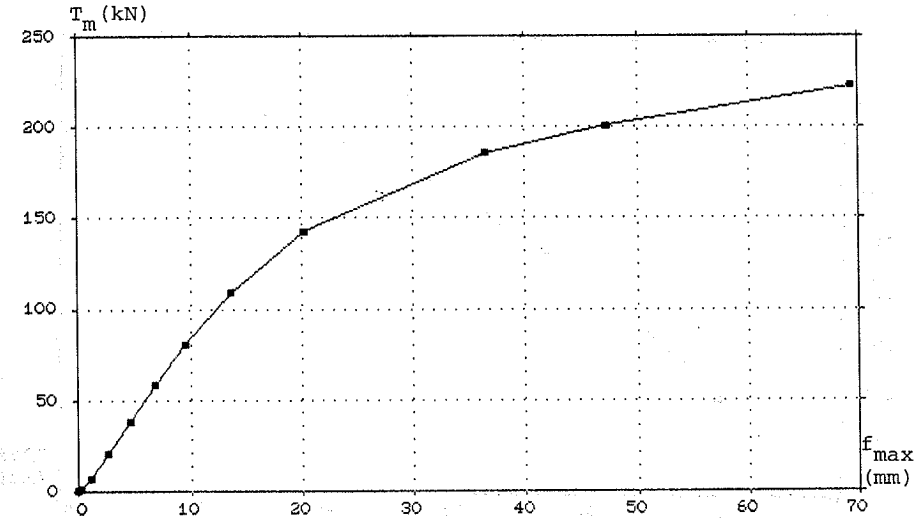

Figure 8.59 MAT–18.

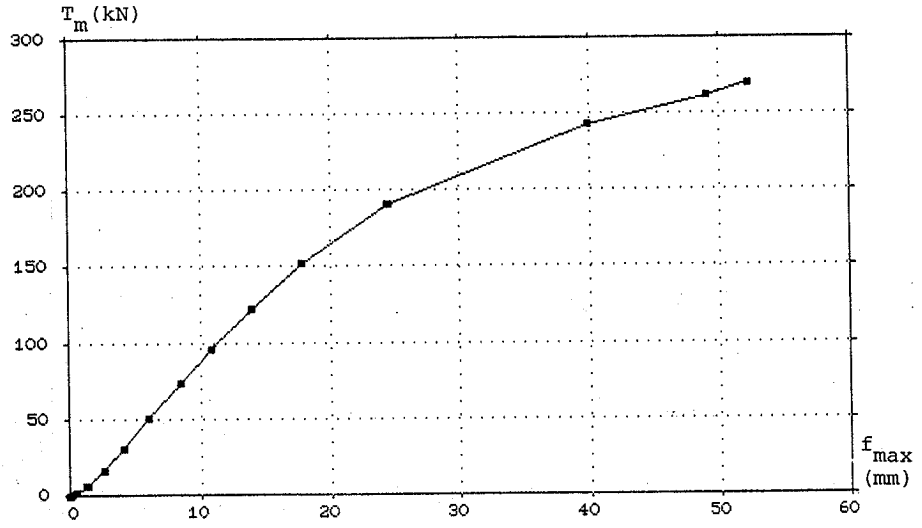

Figure 8.60 MAT–19.

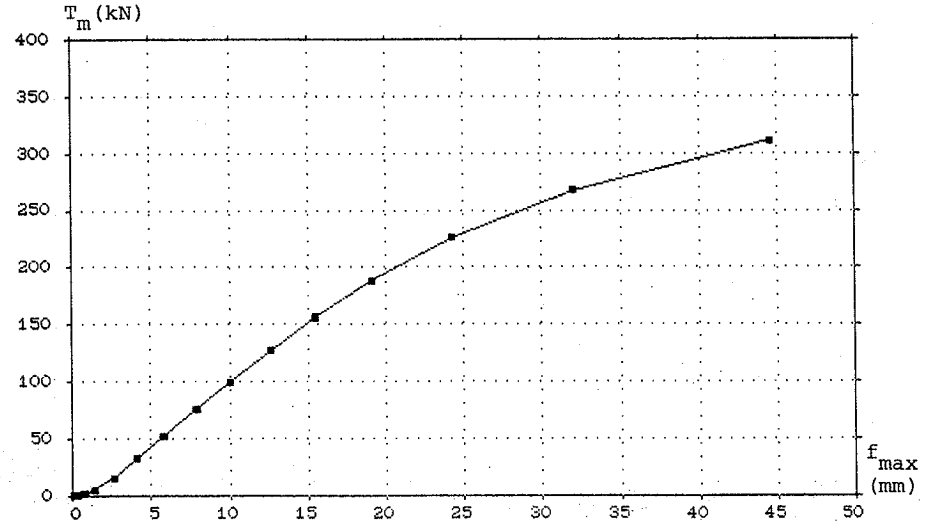

Figure 8.61 MAT–20.

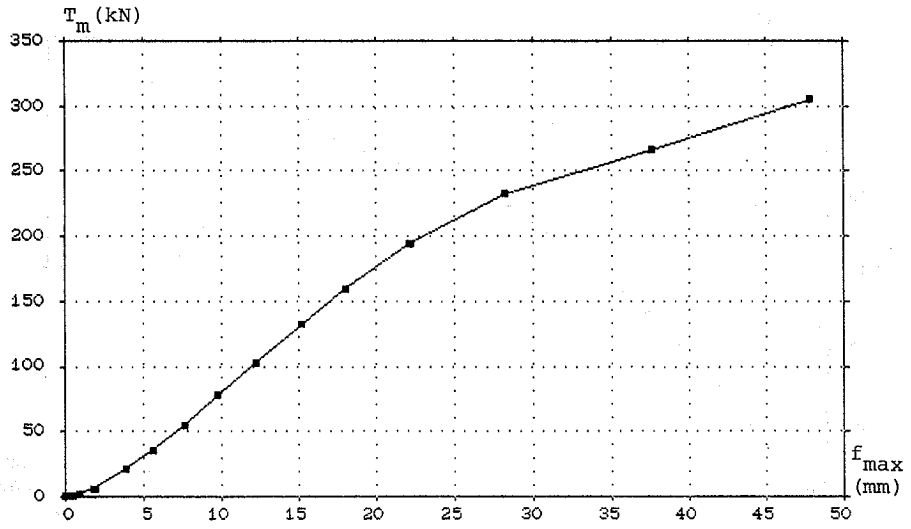

Figure 8.62 MAT–21.

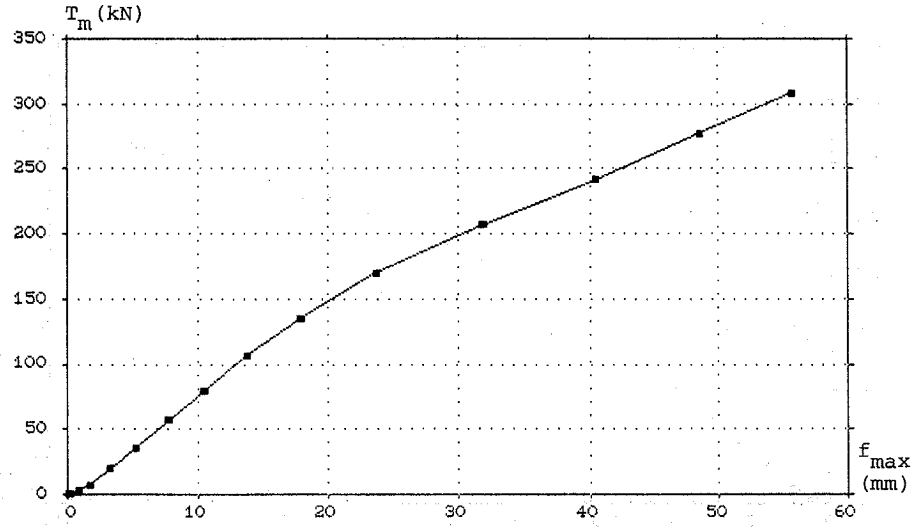

Figure 8.63 MAT–22.

The load and geometrical factor κ for these tests are

$$\kappa = \frac{\pi}{\pi + 1} \tag{9.1}$$

The theoretical load carrying capacity then can be written as

$$P_{cal} = C \cdot (M_j + M_m) \tag{9.2}$$

Here, C is a constant = (π+1), M_j and M_m are calculated according to equations (1.26), (1.27) and ν_b, ν_m from (1.29) and (1.30).

Table 9.1 and Fig. 9.1 show the comparison of test results with theoretical calculations.

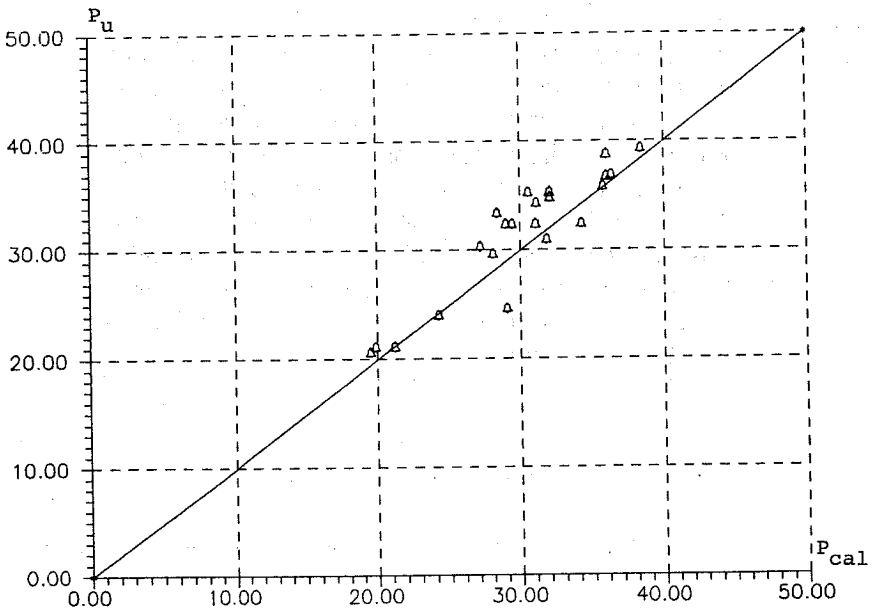

Figure 9.1 The comparison between tests and theoretical calculations.

SLAB No.	f_c MPa	ϕ^*	M_j kN	M_m kN	M_t kN	P_{cal} kN	P_u kN	P_u/P_{cal}
MAT-1	22.83	0.0554	3.322	3.784	7.106	29.43	32.38	1.1002
MAT-2	26.83	0.0479	3.401	4.102	7.504	31.08	32.41	1.0429
MAT-3	21.93	0.0574	3.303	3.709	7.012	29.04	24.65	0.8488
MAT-4	25.58	0.0427	2.773	4.006	6.779	28.07	29.67	1.0568
MAT-5	23.36	0.0463	2.739	3.828	6.567	27.20	30.35	1.1160
MAT-6	26.35	0.0415	2.785	4.066	6.850	28.37	33.42	1.1780
MAT-7	32.38	0.0347	2.874	4.507	7.381	30.57	35.30	1.1548
MAT-8	27.97	0.0394	2.809	4.189	6.997	28.98	32.42	1.1187
MAT-9	36.75	0.0312	2.939	4.801	7.740	32.06	34.83	1.0865
MAT-10	33.98	0.0333	2.898	4.617	7.515	31.12	34.33	1.1031
MAT-11	36.69	0.0312	2.938	4.797	7.735	32.04	35.33	1.1028
MAT-12	8.41	0.1208	2.418	2.297	4.715	19.53	20.63	1.0565
MAT-13	8.92	0.1142	2.437	2.365	4.803	19.89	21.13	1.0623
MAT-14	10.95	0.0938	2.501	2.621	5.121	21.21	21.17	0.9981
MAT-15	43.47	0.0272	3.040	5.222	8.261	34.22	32.44	0.9481
MAT-16	49.24	0.0247	3.129	5.558	8.687	35.98	38.82	1.0790
MAT-17	48.41	0.0250	3.116	5.511	8.626	35.73	35.86	1.0037
MAT-18	8.98	0.1701	3.471	2.373	5.845	24.21	24.05	0.9935
MAT-19	21.82	0.0738	3.981	3.700	7.681	31.81	30.99	0.9742
MAT-20	31.66	0.0531	4.225	4.456	8.681	35.95	36.78	1.0230
MAT-21	38.16	0.0453	4.376	4.892	9.268	38.38	39.33	1.0246
MAT-22	32.61	0.0518	4.247	4.523	8.770	36.32	36.90	1.0160

n	$\bar{x}$	σ	c_v
22	1.0494	0.0720	0.0687

Table 9.1 The test results compared with the theoretical load carrying capacity.

References

[68.1] **Calladine, C. R.** : Simple Ideas in the Large–Deflection Plastic Theory of Plates and Slabs, Engineering Plasticity, **Heyman and Leckie**, eds., Cambridge University Press, Cambridge, England, 1968, pp. 93–127.

[83.1] **Christiansen, K. P. and Frederiksen, V. T.** : Experimental Investigation of Rectangular Concrete Slabs with Horizontal Restraints, Materials and Structures, Vol.16, No.93, May–June 1983, pp. 179–192.

[84.1] **Nielsen, M. P.** : Limit Analysis and Concrete Plasticity, Prentice–Hall, Inc., Englewood Cliffs, New Jersey, 1984.

[86.1] **Andreasen, B. S. and Nielsen, M. P.** : Dome Effect in Reinforced Concrete Slabs. Department of Structural Engineering, Technical University of Denmark, Serie R, No. 212, 1986.

[88.1] **Nielsen, M.P., Andreasen, B. S., and Chen Ganwei** : Dome Effect in Reinforced Concrete Slabs, 11th ACMSM, University of Auckland, 1988.

Appendix A

The recipes for the different grades of concrete

Contents / Item (f_c / kg/m^3)	10 MPa	15-20 MPa	30 MPa	40 MPa	50 MPa
Rapid Cement	140	170	245	280	261
Flyash	-	-	-	-	105
Super Plastic.	-	-	-	-	14
Sand (0-4)	846	959	982	844	900
Gravel (4-8)	469	414	424	469	392
Stone (8-16)	564	508	521	561	581
Water	190	170	160	155	109
Density	2209	2221	2332	2309	2362

AFDELINGEN FOR BÆRENDE KONSTRUKTIONER
DANMARKS TEKNISKE HØJSKOLE

Department of Structural Engineering
Technical University of Denmark, DK–2800 Lyngby

SERIE R
(Tidligere: Rapporter)

Abonnement 1.7.1991 – 30.6.1992 kr. 130,–
Subscription rate 1.7.1991 – 30.6.1992 D.Kr. 130.–.

Hvis De ikke allerede modtager Afdelingens resumeoversigt ved udgivelsen, kan Afdelingen tilbyde at tilsende næste års resumeoversigt, når den udgives, dersom De udfylder og returnerer nedenstående kupon.

Returneres til
Afdelingen for Bærende Konstruktioner
Danmarks tekniske Højskole
Bygning 118
2800 Lyngby

Fremtidig tilsendelse af resumeoversigter udbedes af
(bedes udfyldt med blokbogstaver):

Stilling og navn: .....

Adresse: .....

Postnr. og -distrikt: .....

The Department has pleasure in offering to send you a next year's list of summaries, free of charge. If you do not already receive it upon publication, kindly complete and return the coupon below.

To be returned to:
Department of Structural Engineering
Technical University of Denmark
Building 118
DK-2800 Lyngby, Denmark.

The undersigned wishes to receive the Department's
List of Summaries:
(Please complete in block letters)

Title and name .....

Address.....

Postal No. and district.....

Country.....